



EXPLOITING HIGH PRESSURE ADVANTAGES IN CATALYTIC HYDROGENATION OF CARBON DIOXIDE TO METHANOL

Atul Baban Bansode

Dipòsit Legal: T 950-2014

ADVERTIMENT. L'accés als continguts d'aquesta tesi doctoral i la seva utilització ha de respectar els drets de la persona autora. Pot ser utilitzada per a consulta o estudi personal, així com en activitats o materials d'investigació i docència en els termes establerts a l'art. 32 del Text Refós de la Llei de Propietat Intel·lectual (RDL 1/1996). Per altres utilitzacions es requereix l'autorització prèvia i expressa de la persona autora. En qualsevol cas, en la utilització dels seus continguts caldrà indicar de forma clara el nom i cognoms de la persona autora i el títol de la tesi doctoral. No s'autoritza la seva reproducció o altres formes d'explotació efectuades amb finalitats de lucre ni la seva comunicació pública des d'un lloc aliè al servei TDX. Tampoc s'autoritza la presentació del seu contingut en una finestra o marc aliè a TDX (framing). Aquesta reserva de drets afecta tant als continguts de la tesi com als seus resums i índexs.

ADVERTENCIA. El acceso a los contenidos de esta tesis doctoral y su utilización debe respetar los derechos de la persona autora. Puede ser utilizada para consulta o estudio personal, así como en actividades o materiales de investigación y docencia en los términos establecidos en el art. 32 del Texto Refundido de la Ley de Propiedad Intelectual (RDL 1/1996). Para otros usos se requiere la autorización previa y expresa de la persona autora. En cualquier caso, en la utilización de sus contenidos se deberá indicar de forma clara el nombre y apellidos de la persona autora y el título de la tesis doctoral. No se autoriza su reproducción u otras formas de explotación efectuadas con fines lucrativos ni su comunicación pública desde un sitio ajeno al servicio TDR. Tampoco se autoriza la presentación de su contenido en una ventana o marco ajeno a TDR (framing). Esta reserva de derechos afecta tanto al contenido de la tesis como a sus resúmenes e índices.

WARNING. Access to the contents of this doctoral thesis and its use must respect the rights of the author. It can be used for reference or private study, as well as research and learning activities or materials in the terms established by the 32nd article of the Spanish Consolidated Copyright Act (RDL 1/1996). Express and previous authorization of the author is required for any other uses. In any case, when using its content, full name of the author and title of the thesis must be clearly indicated. Reproduction or other forms of for profit use or public communication from outside TDX service is not allowed. Presentation of its content in a window or frame external to TDX (framing) is not authorized either. These rights affect both the content of the thesis and its abstracts and indexes.

ATUL BABAN BANSODE

**EXPLOITING HIGH PRESSURE ADVANTAGES IN
CATALYTIC HYDROGENATION OF
CARBON DIOXIDE TO METHANOL**

DOCTORAL THESIS

SUPERVISED BY:

Dr. ATSUSHI URAKAWA

ICIQ-URV



UNIVERSITAT ROVIRA I VIRGILI

TARRAGONA, 2014

Dr. Atsushi Urakawa
Group Leader
Institute of Chemical Research of Catalonia (ICIQ)
Av Països Catalans 16
43007 Tarragona, Spain

CERTIFY THAT:

The present work, entitled “Exploiting High Pressure Advantages in Catalytic Hydrogenation of Carbon Dioxide to Methanol” by Atul Baban Bansode for the award of the degree of doctor, has been carried out under my supervision at Institute of Chemical Research of Catalonia (ICIQ), and that it fulfils all the requirements to obtain the degree of Doctor in Chemical Science and Technology.

Tarragona, 7th February 2014

Dr. Atsushi Urakawa



UNIVERSITAT ROVIRA I VIRGILI

*“Knowledge can only be got in one way, the way of experience;
there is no other way to know.”*

Swami Vivekanand

Acknowledgement

First and foremost, I would like to express my sincere gratitude towards my thesis supervisor, Dr. Atsushi Urakawa, for giving me the opportunity to pursue my doctoral studies in his research group. I will be remaining ever grateful to him for his expert guidance, unending support, research freedom and encouragement throughout my endeavour to write this thesis. I take this opportunity to express my intense reverence towards him for his friendship, wonderful personality and great assistance in my professional as well as in personal life. My deepest personal regards are due to you forever and thanks for all the trust you had in me.

I am grateful to all the scientific and non-scientific staff from ICIQ for their help and cooperation given to me during my research work. I am very much thankful to Dr. Miguel Gonzalez from Heterogeneous Catalysis Unit for allowing me to use almost all the instruments in his lab, as well as for his valuable help numerous times. I owe my special thanks to Jose Luis Leon from the Mechanical Workshop and Xavier Asensio from Glass Blowing Workshop for bringing my crazy ideas into reality. I also thank Aurora and Ingrid, for their valuable assistance in all the administrative as well as bureaucratic processes throughout my stay in Tarragona.

I am grateful to our collaborators; Dr. Gemma Guilera, Dr. Vera Cuartero, Dr. Laura Simonelli and Dr. Marta Avila for extending me all the possible support during the EXAFS measurements at ALBA Synchrotron Light Facility, Barcelona. I am equally thankful to Dr. Bruno Tidona from ETH, Zurich for fruitful scientific collaboration for the past three years.

It gives me a great pleasure to express my deep sense of gratitude and indebtedness to my mentors, friends and former colleagues from Dow Chemicals. Moving from a well settled industry job to the studies was not an easy decision to make and without all your support it would have never been possible. My heartfelt thanks are due to Dr. P. Manikandan for his guidance, constant inspiration and the incredible support which I have received over the past six years. I am highly indebted to Dr. Paul Davis, Dr. B. P. Kiran, Sanjay Thorat for being true friends, from whom I have received invaluable help, encouragement and moral support in difficult times.

I would like to express my appreciation to all the former/current members of Urakawa research group, Bertram, Noelia, Sven, Sergio, Luis, Dina, Reza and all the visiting members, who have not only provided assistance in the lab, but also made it such an enjoyable and interesting place to work. It gives me immense pleasure to thank my friends and colleagues, Jordi and Antonio (*aka* Chutonio) for their helpful hand; sympathetic ears and making the lab feel like a family for the past few years. The wonderful time we shared together in lab, at conferences and especially during synchrotron measurements, cannot be forgotten for my whole life. Their help, cooperativeness, immensely friendly attitude and compromising nature have made me learnt so much from them. I also thank them for enriching my Catalan, Italian and Spanish vocabulary every day, which they have shown to me in their own special way.

I must thank my old friends, Prashant, Satpal, Yogesh, Sachin, Amol, Sachin Kulkarni, from whom I have received timely help and support during many years of studies.

This thesis could not have been completed without the endless love, support and blessings from my parents and sisters. Their faith in my capability has always made me an optimist in any unknown areas I had ventured. No words of admiration can be adequate to express my feelings towards my dear wife, Aparna, for her love, respect, patience and believe in me during last years. I must mention that if I have seen the life other than lab, computer and home then it's only because of you. Thanks for being with me in all those years. Your presence has brought a great deal of happiness to my life.

I would like to acknowledge, ICIQ foundation, Ministry of Economy and Competitiveness (MINECO), Spain for the financial support and AGAUR (FI), Generalitat de Catalunya for providing me a research fellowship.



Generalitat de Catalunya
**Departament d'Economia
i Coneixement**



GOBIERNO
DE ESPAÑA

MINISTERIO
DE ECONOMIA
Y COMPETITIVIDAD



Table of Contents

1 Introduction and Overview	1
1.1 Energetic Issues and Carbon Dioxide Problem	1
1.2 Carbon Dioxide Mitigation Strategies	3
1.3 Methanol: History and Current Status	6
1.4 Methanol Synthesis Catalysts	9
1.4.1 Nature of Active Site	11
1.4.2 Catalyst Preparation Methods	13
1.4.2.1 Coprecipitation Method	13
1.4.2.2 Impregnation Method.....	14
1.5 High Pressure CO ₂ Hydrogenation to Methanol.....	15
1.6 Aim and overview of the Thesis	18
References.....	20
2 High Pressure (400 bar) CO₂ Hydrogenation Reactor Setup	25
2.1 Introduction.....	25
2.2 Reactor Design and Setup.....	26
2.2.1 H ₂ Compression and Flow Control.....	28
2.2.2 Liquid and Gas CO ₂ Flow Control	29
2.2.3 The Reactor System; Temperature and Pressure Control.....	29
2.2.4 Analytical System and Reactor Automation.....	31
2.2.4.1 Analytical System	31
2.2.4.2 Reactor Automation.....	33
2.3 Reactor Operation and Catalytic Activity Testing.....	37
2.4 Conclusions.....	43
References.....	44

3. Impact of K And Ba Promoters on CO₂ Hydrogenation Over Cu/Al₂O₃ Catalysts at High Pressure	45
3.1 Introduction.....	45
3.2 Experimental.....	46
3.2.1 Catalyst Preparation.....	46
3.2.2 Catalyst Characterization Methods.....	46
3.3 Results and Discussion.....	49
3.3.1 XRD.....	49
3.3.2 Textural Properties.....	51
3.3.3 H ₂ -TPR.....	52
3.3.4 CO ₂ -TPD.....	54
3.3.5 CO ₂ Hydrogenation.....	57
3.3.5.1 Unpromoted Cu/Al ₂ O ₃	57
3.3.5.2 Potassium and Barium Promoted Cu/Al ₂ O ₃	59
3.3.6 <i>In Situ</i> DRIFTS Study.....	63
3.3.7 Impact of K and Ba Promoters and Possible Reaction Mechanisms.....	68
3.4 Conclusions.....	73
References.....	74
4 High Pressure CO₂ Hydrogenation Over Co-precipitated Cu/ZnO/Al₂O₃ Catalysts	77
4.1 Introduction.....	77
4.2 Methods.....	78
4.1 Catalyst Synthesis.....	78
4.2 Catalyst Characterization.....	79
4.3 Thermodynamic Calculation.....	80
4.3 Results and Discussion.....	81
4.3.1 Physicochemical Characterization.....	81
4.3.2 CO ₂ Hydrogenation.....	82
4.3.2.1 Feed Ratio Study.....	82
4.3.2.2 Temperature Study.....	84
4.3.2.3 GHSV Study.....	89

4.3.2.4 Effect of Zinc Addition and Synthesis Method	91
4.3.2.5 Catalyst Stability Test	93
4.3.2.6 Comparing Thermodynamic Calculations and Experimental Results	94
4.4 Conclusions	96
References	97
5 Synthesis of Dimethyl Ether and Hydrocarbons via High Pressure CO₂ Hydrogenation	99
5.1 Introduction	99
5.2 Methods	100
5.2.1 Catalyst Synthesis	100
5.2.2 Catalytic Testing	101
5.3 Results and Discussion	101
5.3.1 DME Synthesis	101
5.3.2 Hydrocarbon Synthesis	103
5.4 Conclusions	105
References	106
6 High Pressure Capillary Cell for <i>Operando</i> X-Ray Absorption Spectroscopy Studies of CO₂ Hydrogenation Reaction	107
6.1 Introduction	107
6.2 Experimental	108
6.2.1 XAFS Measurements:	108
6.2.2 Catalyst synthesis	109
6.2.3 Capillary Cell Design and Setup	109
6.2.3.1 Coiled Heater System	109
6.2.3.2 Gas Blower Heating System	111
6.2.4 CO ₂ Hydrogenation Setup	113
6.2.4 Raman Spectroscopy	114
6.3 Results and Discussion	114
6.3.1 Capillary Testing	114

6.3.2 <i>In Situ</i> XAFS Spectroscopy	115
6.3.3 Testing of the Capillary Reactor as a Fixed Bed Micro-Reactor.....	117
6.3.4 Raman Study.....	119
6.3.5 Effect of heating mode on EXAFS signal.....	121
6.4 Conclusions.....	127
References.....	128
7 Summary and Outlook	131
7.1 Summary	131
7.2 Outlook	135
Appendix A Supplementary Information of Chapter 3	143
Table A.1 CO ₂ hydrogenation over Cu/Al ₂ O ₃ catalyst.....	143
Table A.2 CO ₂ hydrogenation over Cu-K/Al ₂ O ₃ catalyst.....	144
Table A.3 CO ₂ hydrogenation over Cu-Ba/Al ₂ O ₃ catalyst	145
Appendix B Supplementary Information of Chapter 4.....	147
Table B.1 Feed ratio effect on CO ₂ conversion	147
Figure B.2 Effect of temperature on CO ₂ conversion.....	148
List of Publications	151
Curriculum Vitae.....	153

1

Introduction and Overview

1.1 Energetic Issues and Carbon Dioxide Problem

The continuing advancements in the field of science and technology have brought human race to a convenient and modern lifestyle. The industrialization over past few centuries has led us to remarkable discoveries and cutting-edge technologies which touch our daily lives in a myriad of ways. This human strive towards the best living quality has also brought us many severe problems such as pollution and emissions from factories, vehicles, and chemical and power plants. The modern society is built on energy, every aspect of modern life is made from, powered or affected by energy. As of 2010, world total primary energy supply (Figure 1.1) has three major energy sources; oil (32.4 %), coal (27.3 %) and natural gas (21.4 %) with a combined fuel share of 81.1 % (1). It is clear that our energy supply heavily depends on fossil fuels which are finite and non-renewable energy sources. This means that on the human time-scale they cannot be naturally regenerated and are only available in a finite amount on the earth. According to the International Energy Outlook 2013 (2) (IEO2013), with society's current level of energy consumption and high standards of living, world total energy consumption is estimated to grow by 56 %, from 524 quadrillion Btu (British thermal unit) in 2010 to 820 quadrillion Btu, by year 2040. It is projected that most of the growth in energy consumption occurs in non-OECD (Organisation for Economic Co-operation and Development) countries, where demand is driven by strong, long-term economic growth and expanding populations. Therefore, the development of new

energy strategy that could be economically and environmentally sustainable as well as that meets the demands for wide range of services (industry, transportation, household) is an imperative task.

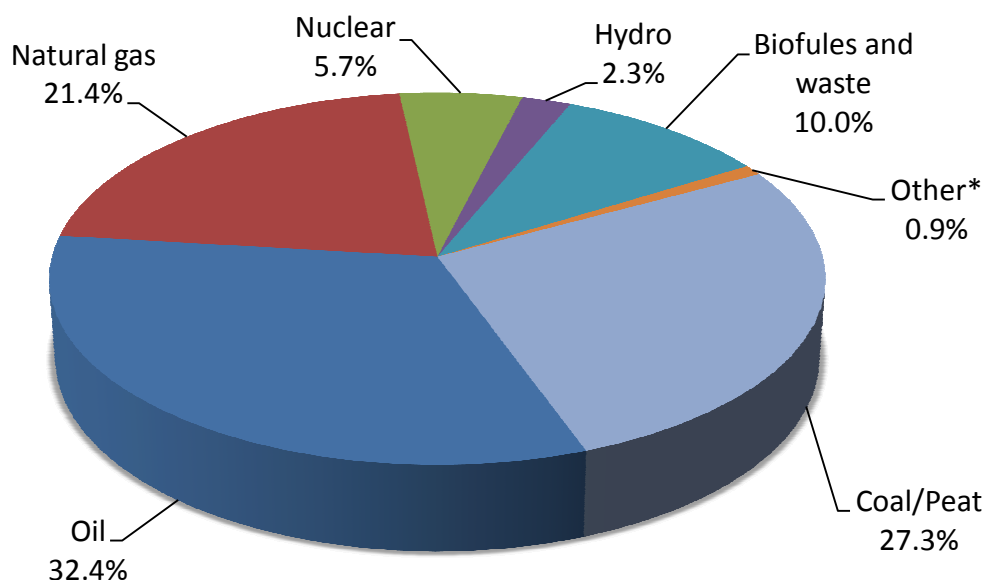


Figure 1.1 2010 fuel shares of total primary energy supply. (* Geothermal, solar, wind etc.) (1)

The challenge to deal with the finite resources of fossil fuels is accompanied by a major environmental threat which our planet is facing now, called global warming induced by the greenhouse gas effect. Carbon dioxide (CO_2) is the most common waste from burning fossil fuels and the main greenhouse gas, considered to be largely responsible for global warming. It is the fourth abundant gas naturally present in the atmosphere of the earth. The concentration of CO_2 in the atmosphere is rising gradually and today there is an excess of 1 teraton of carbon dioxide in the atmosphere. There is continuous addition of 24 gigaton of carbon dioxide into atmosphere annually, which is man-made and unlikely to reduce significantly in the next decades (3). Current research shows that there is an excess of approximately 3.9 % CO_2 with respect to the natural “carbon cycle”. The natural carbon cycle is the carbon-flow between the atmosphere

and oceans and the fixation of CO₂ by plants and microorganisms, which is balanced by emission of CO₂ from plants, animals and volcanoes. Such excess of carbon dioxide is not balanced over the period of time and, as a result, the concentration of CO₂ in the atmosphere has kept steadily increasing in the last 200 years. Since the industrial revolution, the concentration of CO₂ has been increased by 40 % (4). Furthermore, as atmospheric CO₂ increases, the global mean temperature increases, causing a more intense water evaporation into the atmosphere. Water vapour is also a very effective greenhouse gas and the effect of global warming by CO₂ could be further amplified by excess of water vapour (5). The IPCC (Intergovernmental Panel on Climate Change) predicts that, by the year 2100, the atmosphere may contain up to 570 ppm of CO₂, causing a rise of mean global temperature of around 1.9 °C. Furthermore, it is predicted that this will give an increase in mean sea level of up to 38 cm, increased desert formation and the extinction of species (6).

1.2 Carbon Dioxide Mitigation Strategies

In the past few decades, there has been growing scientific consensus to devise the strategy for CO₂ capture, fixation, and recycling technologies to level off the atmospheric CO₂ concentration. Nature has its own CO₂ fixation process which is extraordinarily selective in converting CO₂ into organic compounds. However, natural chemical transformation of CO₂ is not simply fast enough to cope with the ever increasing CO₂ emission rate of the industrialized world. Three major strategies or technological options for CO₂ mitigation available nowadays are (i) minimize/zero emissions, (ii) capture and storage and (iii) usage of CO₂ as chemical feedstock by chemical transformation.

The first strategy can be addressed by producing energy with higher efficiency or a change in the primary energy source to decrease the amount of CO₂ emitted.

Increasing efficiencies of conversion and end use, conservation of energy, and recycling of the products could also form the part of this strategy. One could also choose energy sources that are CO₂ free such as hydro, wind, geothermal or solar. The second strategy involves the development of new technologies for capture and sequestration of CO₂. The capture of carbon dioxide from the flue gases of coal-, oil-, or gas-fired power plants and from industrial processes is a well established and commercially available technology. The captured and separated CO₂ can be confined in natural sites such as: aquifers, deep geological cavities, spent oil- or gas-fields, coal-mines or the ocean (7, 8). And the third strategy, which deserves our attention, is to use it as a source in the synthesis of chemicals, fuels, intermediates and/or fine chemicals. The chemical transformation of CO₂ is not only about mitigating the global warming; rather it is about recycling of the carbon, irreversibly relocated in the form of CO₂ from the ground by burning fossil fuels. In the light of the finite availability of fossil fuels, the production of commercially valuable chemicals and fuels from CO₂ is a promising strategy to simultaneously tackle the two major problems of the century, namely the global warming and fossil fuel depletion, for sustainable development. CO₂ is thermodynamically stable molecule, but there are several pathways for its activation and conversion to useful chemicals, and often requires the use of highly active homogeneous or heterogeneous catalysis.

The term “Catalysis” was first introduced by J.J. Berzelius in 1835, which comes from the Greek word *loosen*. It was used to describe the property of substances that facilitate chemical reactions without being consumed or reacted during the reaction. Catalysis can be classified into two types depending on the state of catalyst and reactants and products. Homogeneous catalysis involves catalyst in the same phase as reactants and products, usually liquid, while in heterogeneous catalysis the catalysts are

present in a different phase, usually solid. Among two, heterogeneous catalysis is an important part of the technology which has remarkable impact on industrially developed societies. Production of transportation fuel, petrochemical products, pollution control, production of low-cost and high-quality raw materials, speciality chemicals are just some of the areas where heterogeneous catalysis is practiced extensively. Heterogeneous catalytic processes facilitate convenient, continuous production of desired products by means of a flow-through operation using a fixed or fluidized bed reactor. More importantly, it avoids the separation of catalysts from the reactants or products, whereas it is the case for homogenous catalysis.

Proper choice of catalysts allows conversion of CO₂ to useful chemicals by its hydrogenation reaction. Among various possible reaction paths, synthesis of methanol holds a key position since it is a primary feedstock for many organic compounds as well as a vital intermediate for various chemicals used in daily life products such as silicone, paint, and plastics. Of course, the required hydrogen must be available on a large scale and its production must be achieved without or negligible CO₂ emissions. With our diminishing resources of fossil fuels, there exists a need to develop feasible, new and safe ways to store and distribute the energy as well as to produce efficiently manmade hydrocarbons. The approach that was proposed and has received widespread attention is generation of hydrogen and its use as a clean fuel source; the so-called “hydrogen economy”. This scenario considers that in the future, when the fossil fuel resources diminished, hydrogen would be the main energy carrier. Hydrogen is a clean-burning fuel which produces only water as by-product and does not produce CO₂ or other pollutants as in case of fossil fuels burning. Actively investigated hydrogen production by photocatalytic or electrocatalytic water splitting powered by renewable (e.g. solar and wind) energies can be regarded as future sources of hydrogen (9, 10). Despite this,

hydrogen is not convenient either as a means to store energy or for its subsequent use as a fuel due to its potentially explosive nature and necessitates special conditions such as high pressure, use of special materials to minimize diffusion and leakage, and extensive safety precautions. Due to the serious limitations of the hydrogen economy, a promising alternative has been proposed and named as “methanol economy”(11). Therein, CO₂ captured from the atmosphere or from the industrial sources could be hydrogenated to methanol and methanol-derived chemicals using hydrogen obtained from renewable energy sources as photolytic water splitting (Figure 1.3). This approach will help to achieve two goals; recycling of carbon which is “lost” in CO₂ and converting volatile hydrogen gas to a convenient, safe liquid, easy to handle and transport.

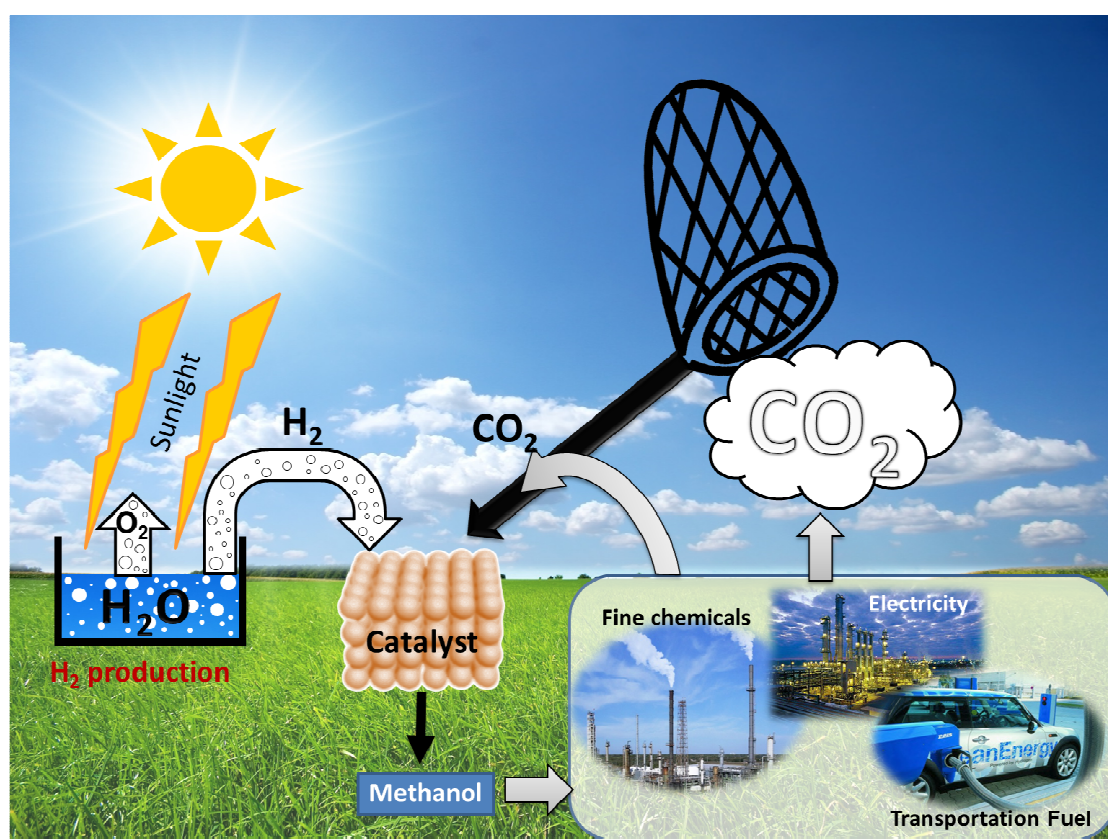


Figure 1.2 Methanol economy; CO₂ hydrogenation to methanol and applications.

1.3 Methanol: History and Current Status

Methanol also called as “wood alcohol”, a colourless, water soluble liquid with mild alcoholic odour, in its pure form was first isolated in 1661 by Robert Boyle (12). He named the new compound as “*adiaphorus spiritus lignorum*” meaning “spirit of box” since he produced it through the distillation of boxwood. There was no written history or record of its use for any purpose, either domestic or industrial, before the 19th century. The chemical or molecular identity of methanol was first established independently by J. B. A. Dumas and J. von Liebig in 1834. The term “methyl” was introduced in chemistry in 1835 on the basis of their work. From ca. 1830 to 1923 the “wood alcohol” was obtained by the dry distillation of wood, which was the only source of methanol. In 1913 A. Mittasch and co-workers at BASF (Baden Aniline and Soda Factory) successfully produced organic oxygen compounds including methanol, from syngas during the developmental work on the ammonia synthesis. The decisive step in the large-scale industrial production of methanol was made by M. Pier and co-workers in the early 1920s. First commercial methanol synthesis plant was developed in 1923 by BASF chemists with sulphur resistant zinc-chromite catalysts having typical operating conditions of 320-450 °C and 250-350 bar (13). For over the next 40 years these processes defined the methanol production from syngas. In the 1960s, changing feedstock from coal to naphtha or natural gas led to less impurities in the synthesis gas. This resulted the introduction of highly selective copper/zinc oxide/alumina catalyst in 1966 by ICI (Imperial Chemical Industries). Due to its enhanced activity, the ternary catalyst required significantly milder reaction conditions, i.e. at pressures between 50 and 100 bar and temperatures between 240 and 260 °C (14, 15).

Today, methanol is one of the most celebrated and widely suggested alternative for chemical energy carrier. Most importantly, in its liquid form, methanol presents an

excellent way to store and transport energy conveniently and safely (11, 16, 17). The use of methanol in fuel cells as a direct reagent or indirectly as the source of hydrogen by a reforming reaction is well documented. In addition, fundamental chemical products like olefins can be produced via a methanol-to-olefin (MTO) process (18) and various organic compounds like dimethyl ether (DME), that is a potential substitute of diesel oil for its better combustion performance (19). Figure 1.3 gives an overview of methanol demand by end use in 2011. Worldwide, formaldehyde (an important precursor for organic synthesis) production is the largest consumer of methanol, accounting for almost 32 % of world methanol demand. Further major products are methyl-tert-butyl-ether (MTBE) and acetic acid. Almost 22 % methanol produced is used for direct fuel (DME and gasoline/fuel) applications. It is anticipated that methanol to olefins (MTO) and methanol to propylene (MTP) to become a high growth sector by 2016 (20).

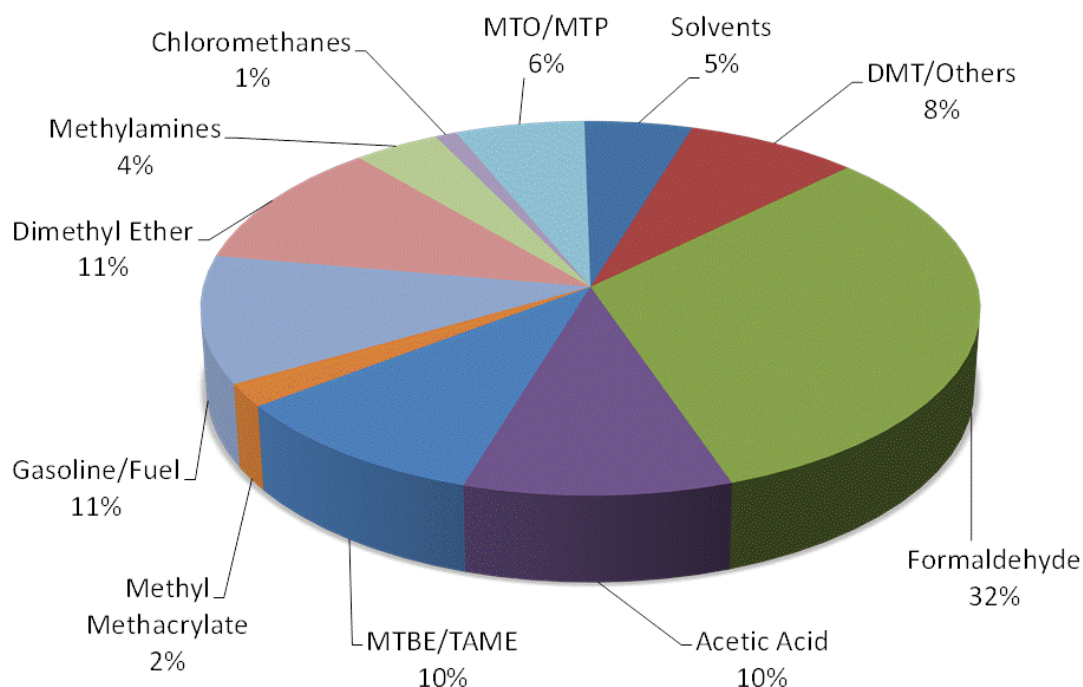


Figure 1.3 Distribution of global methanol consumption in 2011 (20)

Currently worldwide, over 90 methanol plants have a combined production capacity of about 100 million metric tons and each day more than 100,000 tons of methanol is used as a chemical feedstock or as a transportation fuel. It was estimated that in 2013 the global methanol demand expected to reach 65 million metric tons (21). By volume, methanol is one of the top 5 chemical commodities shipped around the world each year. It should be noted that most of the methanol production facilities use syngas blended with CO₂ as a starting material.

1.4 Methanol Synthesis Catalysts

The catalysts which were originally developed for the syngas based methanol synthesis process are also active for CO₂ hydrogenation towards methanol. Mostly, the catalysts for CO/CO₂ hydrogenation contained Cu as a main component together with different promoters such as Zn, Zr, Si, Al, B, Cr, Ce, Ga, V, and Ti (22-27). Along with main component, an appropriate support is crucial to improve the catalytic activity. An appropriate support has strong effect on the formation and stabilization of the active phase of the catalyst. Furthermore, it plays crucial role in tuning the interactions between the major component and the promoter. Metal oxides are the commonly used supports for the preparation of a methanol synthesis catalyst. It was observed that ZnO when used as support can improve the dispersion and stabilization of copper (28, 29). ZnO is a wurtzite, n-type semiconductor and possesses lattice oxygen vacancies, consisting of an electron pair in the lattice, which may serve as an active site for methanol synthesis (30). The synergy between the metal component and the support has been reported to enhance the catalytic performance of Cu/ZnO for methanol synthesis from CO₂ (31). Zirconia can also be considered as a promising catalyst support or promoter due to its high stability under reducing or oxidising atmospheres (25). However, the activity of methanol formation using zirconia as a support is slightly

lower than that of ZnO. Silica as catalyst support, possesses predominant properties, such as acid-base nature, porosity texture and thermal stability. However, copper supported on high-purity silica was found to be nearly inactive in methanol synthesis reaction (32, 33). Most of the catalysts prepared using silica as the support needed addition of promoters to improve the catalytic performance (34, 35).

Cu/ZnO catalyst has been reported to be active for the methanol synthesis, however to improve the catalytic activity, multicomponent catalysts were developed (36, 37). It is well-known that Al₂O₃ is the widely used third component in a Cu-based catalyst due to its good promoting activity. Doping of Cu/ZnO catalyst with trivalent metal ions such as Al³⁺, Sc³⁺, and Cr³⁺ assists the formation of monovalent cationic defects on the crystal surface of ZnO, which might accelerate both enrichment and stabilization of monovalent Cu on the surface during reduction and reaction (38). Ga₂O₃ showed a strong promoting effect on the activity and stability of Cu/ZnO multicomponent catalysts (39). It was found that the promoting effect of Ga₂O₃ in Cu/ZnO catalyst is associated with Ga₂O₃ particle size. Small Ga₂O₃ particles favour the formation of an intermediate state of copper between Cu⁰ and Cu²⁺, probably Cu⁺, which lead to the higher catalytic activity (40). As mentioned earlier ZrO₂ acts as a favourable promoter in methanol synthesis reaction. Yang et al. (41) studied the properties of the ZrO₂-doped Cu/ZnO catalyst prepared by precipitation method. The presence of ZrO₂ led to a high copper dispersion, which was distinctive from Cu/ZnO. Though the activity for carbon monoxide hydrogenation was little lower than that of Cu/ZnO catalyst, ZrO₂-doped Cu/ZnO catalyst showed much higher activity and selectivity in CO₂ hydrogenation. Other elements such as B, Cr, Mg and V were also used as promoters in copper-based catalysts which can modify the physical-chemical properties just like mentioned above (24, 42, 43).

In addition to Cu-based catalysts, several noble-metal based catalysts were studied for methanol synthesis in CO₂ hydrogenation. Edwin et al. investigated the effect of the supports such as SiO₂, Al₂O₃, ThO₂, La₂O₃ on the catalytic performance of the supported Pd catalysts (44). It was observed that high methanol selectivity can be obtained when Pd was supported on La₂O₃ support, whereas acidic support has negative influence on methanol selectivity and favours the methane (CH₄) formation. Liang et al. developed a type of Pd/ZnO catalyst, supported on multi-walled carbon nanotubes, which could reversibly adsorb a greater amount of hydrogen forming higher concentration of adsorbed H species on the surface, which enhanced the rate of surface hydrogenation reactions (45). Use of multi-walled carbon nanotubes led to an increase of surface concentration of Pd⁰-species in the form of PdZn alloys, a kind of kinetically active Pd⁰-species closely associated with methanol generation, thus superior in catalytic activity than activated carbon and γ-Al₂O₃. Ag and Au-based catalysts supported on ZnO/ZrO₂ shown good methanol selectivity at high metal content, however the CO₂ conversion was found to be much lower as compared to supported Cu catalyst (46). Interestingly, Lee et al. reported that CO₂ hydrogenation reaction over PtCu/SiO₂ catalyst led to formation of formaldehyde instead of methanol. This significant change in the product profile could be due to the adsorption of hydrogen on the Pt surface and subsequent migration to Cu which promotes the selective hydrogenation of CO₂ to produce formaldehyde (47).

Different transition metal carbides were also tested for CO₂ hydrogenation reaction, where Mo₂C and Fe₃C showed high CO₂ conversion and good methanol selectivity, while TaC and SiC were found to be almost inactive (48).

1.4.1 Nature of Active Site

Methanol synthesis is a highly surface sensitive reaction and the activity and selectivity strongly depends on the catalyst's surface structure and stability. Although the properties of the catalysts used in methanol synthesis have been extensively studied for many years, Cu still remains an important active catalyst component. Numerous reports suggested that methanol is formed on a metallic copper surface of a copper based catalyst, and the activity of the catalyst is directly proportional to the surface area of metallic copper (49-53). Chinchén et al. found that copper metal crystallites in Cu/ZnO/Al₂O₃ catalyst are in partially oxidised state (54, 55). In their experiments it was found that in presence of CO₂ and with a large fraction of the metallic copper surface covered by oxygen-containing species, the catalytic activity towards methanol synthesis was independent of the Cu⁰ surface area. Herman et al. claimed that Cu⁺ sites are active sites in methanol synthesis (56). It was reported that the addition of alkali metals such as potassium or cesium could positively promote methanol synthesis from syngas on non-supported Cu catalysts (57). Sheffer et al. reported that, high activity to methanol synthesis from syngas is due to the stabilization of Cu⁺ species by potassium, probably in the form of CuKCO₃ (58). Studies on clean Cu(100) and oxidized Cu(100) by Szanyi and Goodman showed that Cu ion is an active site in methanol synthesis (59). Using mixtures of Cu/SiO₂ and ZnO/SiO₂ to examine the role of ZnO in Cu/ZnO methanol synthesis, Choi et al. concluded that ZnO was beneficial for stabilization of Cu⁺ sites on the Cu surface and it could control the Cu⁺/Cu⁰ ratio without affecting the Cu morphology (60). Burch et al. suggested that the high activity of conventional Cu/ZnO/Al₂O₃ catalysts may arise from a synergy between the Cu and ZnO phases (61, 62). It is proposed that ZnO can act as a reservoir for spillover hydrogen, and that reverse spillover may account for the higher rate of methanol synthesis on Cu when

ZnO is present in the catalyst (63). Recently Behrens et al. shown that the active site in industrial methanol synthesis consists of Cu steps decorated with Zn atoms, stabilized by a series of well-defined bulk defects and surface species (26).

It is clear that there are still controversies regarding the role of active site of catalyst in methanol synthesis. Still, synergy between the main catalyst component (Cu) and promoter or support do now seem to be a rather well-established phenomenon.

1.4.2 Catalyst Preparation Methods

Majority of methanol synthesis catalyst are prepared by mainly two types of preparation methods, co-precipitation and impregnation method. Several other methods such as deposition precipitation, sequential precipitation, ion-exchange have been also employed for the preparation of methanol synthesis catalyst. However, co-precipitation and impregnation methods are discussed in detail in the proceeding sections.

1.4.2.1 Co-precipitation Method

As stated earlier, methanol synthesis catalysts are structurally sensitive. The differences in preparation methods as well as pre-treatment conditions have remarkable influence on the structure of catalysts. Co-precipitation methods are most widely used to prepare copper-based catalysts. The co-precipitation technique requires the simultaneous formation of the support and active phase. In co-precipitation, an alkali solution is added to a solution of the desired metal salt concentration to precipitate and form catalyst precursors. Co-precipitation of catalysts may also include an aging step after precipitation or washing of the catalyst. Factors such as concentration, temperature, pH of solution, precipitating agent plays an important role in determining the activity of final catalyst.

Li et al. studied the effect of pH and temperature during the precipitation for methanol synthesis catalysts (64). It was observed that at pH= 7.0, the precipitate mainly consisted of the malachite-like phase and the catalysts therefrom were more active in methanol synthesis. Precipitation at $\text{pH} \leq 6$ favored the formation of hydroxynitrate, which led to less active catalysts. It was suggested that to obtain an ideal composition of the precursors and a high activity and selectivity of the catalysts, the precipitation step should be performed at a constant pH of 7.0 and a temperature of 70 °C. Baltes et al. reported that, catalysts obtained from precursors precipitated in the pH range of 6–8 at 70 °C shown good catalytic activity (65). Koepfel et al. reported that catalysts prepared using ammonium carbonate as a precipitating agent showed lower activity than the catalyst made from sodium hydroxide as precipitating agent (66). Use of oxalate as precipitating agent resulted a homogenous Cu and Zn distribution over spherical particles was obtained, whereas irregular Cu aggregates on the surface of catalyst were found for conventional carbonate.

1.4.2.2 Impregnation Method

In addition, the most common way to prepare metal supported catalysts, the impregnation technique, can also be used to synthesize methanol synthesis catalysts. Impregnation is the simplest and most direct technique for catalyst preparation (67). Impregnated catalysts are prepared by mixing a metal salt solution with a pre-formed support, followed by drying to remove excess solvent. If the volume of the solution is equal to the pore volume of the support, the process is called incipient wetness impregnation. When using precious metals, the metal is well dispersed and there is no loss of material within the support phases. The advantage of this method is that catalyst support can be prepared separately, allowing for higher temperature treatments than

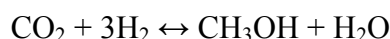
would be possible if the active metal was already incorporated on the support. The distribution of the active species on the support can vary, depending on the reaction conditions. Various factors such as type and concentration of precursor salt, solvent, temperature, type of support and contact time with support could be controlled to obtain optimum distribution of active species. This method has been employed quite often in catalyst preparation for methanol synthesis reaction, however the performance of the catalyst prepared using this technique is not as good as its with co-precipitation method (66).

1.5 High Pressure CO₂ Hydrogenation to Methanol

Converting captured CO₂ into products such as valuable chemicals, fuels, building materials, and other commodities could form an important part of a solution for reducing CO₂ emissions in an economical and ecological way. Heterogeneous catalytic hydrogenation of CO₂ bears a strong potential to treat large amount of CO₂ in a short time, rendering it an important mean for CO₂ mitigation. In the past few decades conversion of CO₂ by means of catalytic hydrogenation has attracted considerable attention as one of the key processes for CO₂ fixation and as recycling of carbon source emitted as CO₂ (22). Numerous research works have been reported on converting CO₂ into basic chemicals such as methanol, hydrocarbons, esters, and ethers by means of CO₂ hydrogenation (23-25, 68).

CO₂ hydrogenation using methanol synthesis catalysts involves two important, competitive reactions. The first one is the targeted methanol synthesis (reaction 1) and the second one is reverse water-gas shift (RWGS) reaction (reaction 2). There is also a possibility that CO formed in reaction 2 undergoes further hydrogenation to give methanol (reaction 3). Despite existing controversies about the reaction pathways, i.e. methanol formation via CO or CO₂ hydrogenation, isotope labelling study by Chinch

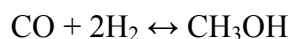
et al. suggested that CO₂ is the main carbon sources in methanol from CO/CO₂ hydrogenation reaction over Cu/ZnO/Al₂O₃ catalyst (69). Further recent modelling study by Grabow et al. showed that on Cu, both CO and CO₂ hydrogenation pathways are active under typical methanol synthesis conditions (70).



$$\Delta H_{298 \text{ K}, 5\text{MPa}} = -40.9 \text{ kJ/mol} \quad (1)$$



$$\Delta H_{298 \text{ K}, 5\text{MPa}} = 49.8 \text{ kJ/mol} \quad (2)$$



$$\Delta H_{298 \text{ K}, 5\text{MPa}} = -90.7 \text{ kJ/mol} \quad (3)$$

Formation of methanol is an exothermic reaction with reduction of reaction molecule number. According to Le Châtelier's principle, methanol conversion is favoured by increasing pressure and decreasing temperature. However, considering the reaction rate and the chemically inert nature of CO₂, increase in reaction temperature is useful to facilitate the CO₂ activation and its subsequent conversion to methanol. The RWGS reaction causes extra consumption of hydrogen and reduction in methanol formation, hence it is necessary to suppress the RWGS reaction in order to obtain high methanol yield. From both, methanol synthesis and the reverse water-gas shift reaction, large amount of water is produced as a by-product, which may have inhibitory effect on the active metal during the reaction, leading to the deactivation of the catalyst. Therefore, the catalysts for carbon dioxide hydrogenation to methanol should be able to overcome water intolerance, as well as improve activity, selectivity, and stability. In addition, other side products such as dimethyl ether, methyl formate and hydrocarbons such as methane are usually formed during CO₂ hydrogenation reaction. Considering all

this aspects, methanol synthesis from CO₂ hydrogenation desires a more selective catalyst to avoid the formation of undesired by-products/secondary products.

Besides catalyst composition and active site structure, an optimal reaction condition is also essential in maximizing the product yield, as well as the catalyst life time. The parameters like temperature, pressure, and space velocity play important role in determining the performance of the reaction. As mentioned earlier, methanol synthesis is an exothermic reaction with stoichiometric decrease in total number of molecules. Therefore, from the thermodynamic point of view high methanol yields are achieved at low temperature and high pressure.

Due to the high operating pressure range (up to 350 bar), in 1923 when BASF first commercialized the methanol synthesis process, it was essentially termed as *high-pressure methanol synthesis technology*. The era of low pressure (up to 100 bar) methanol synthesis began in 1963 with ICI's *low-pressure synthesis technology*, which become an industrial successor to high pressure synthesis. These methanol synthesis processes utilizes syngas blended with CO₂ as a starting material. Lowering the reaction pressure is generally favored because of the general perception of increased energy demands at high pressure operation. Ever since the efforts were made to lower the reaction pressure range as much as possible. Further the processes which were developed for conversion of pure CO₂ for methanol synthesis, also adopted the low reaction pressure approach. Therefore, numerous investigations about methanol synthesis from CO₂ and H₂ reports results from experiments conducted at pressures below 100 bar (22, 25, 39, 40, 66, 71). However, a recent investigation on energetic aspects of CO₂ hydrogenation to methanol shows that the energy efficiency of the whole process is almost pressure independent and the dominant process in energy demand is the electrolysis of water which was assumed as the source of hydrogen source (72). In

1945, Ipatieff and Monroe from UOP (Universal Oil Products) reported high pressure CO₂ hydrogenation and CO₂/CO hydrogenation over a copper/alumina catalyst at pressures between 117 and 410 atm. and 300 °C (73). In their study, Ipatieff and Monroe conducted the experiments in a flow type apparatus consisting mainly four parts: a high-pressure gas charger for hydrogen and hydrogen-carbon monoxide, high-pressure liquid charger for carbon dioxide, high-pressure vertical reaction tube (ID = 2.38 cm) and a pressure regulator attached to the exit end of the reaction tube. The results show a remarkable increase of CO₂ conversion to methanol with increasing pressure. Despite the thermodynamic benefit of conducting the reaction at high pressure, except the work mentioned above, the area of CO₂ hydrogenation i.e. above 250 bar remains largely unexplored due to expensive equipment and safety precautions. High pressure approaches can facilitate the reduction in reactor volume when reactants and/or products are compressive, reducing the plant area which consequently reduces capital costs, and possible improvements in handling dangerous chemicals such as hydrogen more safely when used in a small volume. As stated, the cost of installation and operation of high pressure reactions is mainly associated with the volume of reactor and required associated equipment. The use of micro-reactors can be advantageous for such type of reactions where the reactants can be in liquid phase above 200 bar and can use commercially available high pressure syringe pumps for the micro flow range up to 1300 bar. Moreover, due to high surface to volume ratios, heat/mass transfer in micro-reactors is much more enhanced compared to their macro scale counterpart. The fast heat removal is especially attractive for highly exothermic reactions leading to homogeneous temperature distributions and suppression of hot spot formation. Also, mass transfer limitations can be avoided when, due to an increase of pressure and temperature, the multiphase fluid is brought to a single supercritical phase system.

Above all, such approaches may result in shifting the equilibrium conversion and in the formation of unique phase and states of reaction mixture and catalysts, thus boosting catalytic activity (74).

1.6 Aim and Overview of the Thesis

The aim of this thesis is to develop a highly efficient CO₂ hydrogenation process towards methanol and methanol derived products, by use of micro-reactors and high pressure approach. The main objective is to design and construction of a high pressure lab scale micro-reactor setup for the continuous catalytic hydrogenation of CO₂ at pressures up to 400 bar. The thesis also concerns with development of a high pressure capillary based transparent micro-reactor for *in situ* spectroscopic investigation by Raman and XAS techniques.

Chapter 2 describes the design and construction of high pressure lab scale plant developed during the thesis to conduct CO₂ hydrogenation up to 400 bar. In house LabVIEW program was developed to control the critical components of the plant in order to control and monitor the reaction parameters remotely. The functioning of reactor together with online analytical system is described in detail.

Chapter 3 shows high pressure CO₂ hydrogenation reaction over impregnated copper/alumina catalysts. The impact of pressure and of K and Ba promoter is discussed in detail. Further, chapter 3 shows also the *in situ* DRIFTS observation of intermediate species during the reaction at ambient pressure over the prepared catalysts. High pressure CO₂ hydrogenation over coprecipitated Cu/ZnO/Al₂O₃ is described in chapter 4. The optimization of reaction parameters such as pressure, temperature and feed ratio of reactant gas were studied in detail.

Chapter 4 shows some of the outstanding results ever reported in CO₂ hydrogenation to methanol reaction over commercial methanol catalyst. Chapter 5 is

focused on direct hydrogenation of CO₂ to methanol derived products such as dimethyl ether and hydrocarbons. It deals with various combinations of catalyst bed position and influence of pressure on it. The design, construction and operation of high pressure capillary based transparent micro-reactor for in situ spectroscopic studies are discussed in chapter 6. In addition to in situ Raman and XAS studies, a comparison of capillary reactor to the lab scale micro-reactor is made. Chapter 7 concludes the thesis by summarising the main results and giving an outlook to the high pressure process.

References

1. IEA, “Key World Energy Statistics 2012” (International Energy Agency, Paris, 2012).
2. J. Conti *et al.* (The U.S. Energy Information Administration (EIA), U.S. Department of Energy, Washington DC, 2013), pp. 1-338.
3. M. Mikkelsen, M. Jorgensen, F. C. Krebs, *Energ. Environ. Sci.* **3**, 43 (2010).
4. D. Luthi *et al.*, *Nature* **453**, 379 (2008).
5. E. Wilson, *Chem. Eng. News* **87**, 10 (2009).
6. H. Audus, P. Freund, A. Smith, *Global warming damage and the benefits of mitigation - [report]*. H. Audus, P. Freund, A. Smith, Eds., (IEA Greenhouse gas R&D programme, 1995).
7. H. Yang *et al.*, *J. Environ. Sci.* **20**, 14 (2008).
8. Xu, J. A. Moulijn, *Energy Fuels* **10**, 305 (1996).
9. R. M. Navarro, F. del Valle, J. A. Villoria de la Mano, M. C. Álvarez-Galván, J. L. G. Fierro, in *Advances in Chemical Engineering*, I. d. L. Hugo, R. Benito Serrano, Eds. (Academic Press, 2009), Volume 36, pp. 111-143.
10. M. G. Walter *et al.*, *Chem. Rev.* **110**, 6446 (2010).
11. G. A. Olah, *Catal. Lett.* **93**, 1 (2004).
12. E. Fiedler, G. Grossmann, D. B. Kersebohm, G. Weiss, C. Witte, in *Ullmann's Encyclopedia of Industrial Chemistry*. (Wiley-VCH Verlag GmbH & Co. KGaA, 2000).
13. BASF. (German Patents 415686, 441433, 462837, 1923).

14. L. Sunggyu, in *Handbook of Alternative Fuel Technologies*. (CRC Press, 2007), pp. 297-321.
15. J. B. Hansen, P. E. Højlund Nielsen, in *Handbook of Heterogeneous Catalysis*. (Wiley-VCH Verlag GmbH & Co. KGaA, 2008).
16. G. A. Olah, A. Goepfert, G. K. S. Prakash, *J. Org. Chem.* **74**, 487 (2008).
17. G. A. Olah, *Angew. Chem. Int. Edit.* **44**, 2636 (2005).
18. M. Stöcker, *Microporous Mesoporous Mater.* **29**, 3 (1999).
19. S. C. Sorenson, *J. Eng. Gas Turb. Power* **123**, 652 (2001).
20. D. Johnson. (IHS Inc., 2012).
21. www.methanol.org.
22. Y. Nitta, O. Suwata, Y. Ikeda, Y. Okamoto, T. Imanaka, *Catal. Lett.* **26**, 345 (1994).
23. M. Saito, K. Murata, *Catal. Surv. Asia.* **8**, 285 (2004).
24. B. J. Liaw, Y. Z. Chen, *Appl. Catal. A-Gen.* **206**, 245 (2001).
25. F. Arena *et al.*, *J. Catal.* **249**, 185 (2007).
26. M. Behrens *et al.*, *Science* **336**, 893 (2012).
27. I. Nakamura, T. Fujitani, T. Uchijima, J. Nakamura, *J. Vac. Sci. Technol., A* **14**, 1464 (1996).
28. J. Yoshihara, C. T. Campbell, *J. Catal.* **161**, 776 (1996).
29. C. V. Ovesen *et al.*, *J. Catal.* **168**, 133 (1997).
30. X.-M. Liu, G. Q. Lu, Z.-F. Yan, J. Beltramini, *Ind. Eng. Chem. Res.* **42**, 6518 (2003).
31. J. C. J. Bart, R. P. A. Sneed, *Catal. Today.* **2**, 1 (1987).
32. A. Gotti, R. Prins, *J. Catal.* **178**, 511 (1998).
33. S. Fujita, M. Usui, T. Hanada, N. Takezawa, *React. Kinet. Catal. L.* **56**, 15 (1995).
34. T. Fujitani, J. Nakamura, *Appl. Catal. A-Gen.* **191**, 111 (2000).
35. I. A. Fisher, A. T. Bell, *J. Catal.* **172**, 222 (1997).
36. M. Saito *et al.*, *Energ. Convers. Manage.* **38**, Supplement, S403 (1997).
37. J. Toyir *et al.*, *Phys. Procedia.* **2**, 1075 (2009).
38. H.-B. Chen *et al.*, *Appl. Surf. Sci.* **147**, 85 (1999).
39. J. Toyir, P. R. de la Piscina, J. L. G. Fierro, N. Homs, *Appl. Catal. B-Environ.* **34**, 255 (2001).

40. J. Toyir, P. R. de la Piscina, J. L. G. Fierro, N. Homs, *Appl. Catal. B-Environ.* **29**, 207 (2001).
41. C. Yang *et al.*, *Catal. Today.* **115**, 222 (2006).
42. Y. Zhang, J. Fei, Y. Yu, X. Zheng, *J. Nat. Gas Chem.* **16**, 12 (2007).
43. M. Kilo *et al.*, *J. Mol. Catal. A: Chem* **126**, 169 (1997).
44. E. Ramarosan, R. Kieffer, A. Kiennemann, *J. Chem. Soc., Chem. Commun.*, 645 (1982).
45. X.-L. Liang, X. Dong, G.-D. Lin, H.-B. Zhang, *Appl. Catal. B-Environ.* **88**, 315 (2009).
46. J. Słoczyński *et al.*, *Appl. Catal. A-Gen.* **278**, 11 (2004).
47. D.-K. Lee, D.-S. Kim, S.-W. Kim, *Appl. Organomet. Chem.* **15**, 148 (2001).
48. J.-L. Dubois, K. Sayama, H. Arakawa, *Chem. Lett.* **21**, 5 (1992).
49. W. X. Pan, R. Cao, D. L. Roberts, G. L. Griffin, *J. Catal.* **114**, 440 (1988).
50. P. B. Rasmussen *et al.*, *Catal. Lett.* **26**, 373 (1994).
51. P. B. Rasmussen, M. Kazuta, I. Chorkendorff, *Surf. Sci.* **318**, 267 (1994).
52. T. S. Askgaard, J. K. Norskov, C. V. Ovesen, P. Stoltze, *J. Catal.* **156**, 229 (1995).
53. D. Jingfa, S. Qi, Z. Yulong, C. Songying, W. Dong, *Appl. Catal. A-Gen.* **139**, 75 (1996).
54. G. C. Chinchin, K. C. Waugh, D. A. Whan, *Appl. Catal.* **25**, 101 (1986).
55. G. C. Chinchin, M. S. Spencer, K. C. Waugh, D. A. Whan, *J. Chem. Soc. Farad. T. 1* **83**, 2193 (1987).
56. R. G. Herman *et al.*, *J. Catal.* **56**, 407 (1979).
57. G. R. Sheffer, T. S. King, *J. Catal.* **116**, 488 (1989).
58. G. R. Sheffer, T. S. King, *J. Catal.* **115**, 376 (1989).
59. J. Szanyi, D. W. Goodman, *Catal. Lett.* **10**, 383 (1991).
60. Y. Choi, K. Futagami, T. Fujitani, J. Nakamura, *Appl. Catal. A-Gen.* **208**, 163 (2001).
61. R. Burch, R. J. Chappell, *Appl. Catal.* **45**, 131 (1988).
62. R. Burch, R. J. Chappell, S. E. Golunski, *J. Chem. Soc. Farad. T. 1* **85**, 3569 (1989).
63. R. Burch, R. J. Chappell, S. E. Golunski, *Catal. Lett.* **1**, 439 (1988).
64. J. L. Li, T. Inui, *Appl. Catal. A-Gen.* **137**, 105 (1996).

65. C. Baltes, S. Vukojević, F. Schüth, *J. Catal.* **258**, 334 (2008).
66. R. A. Koepfel, A. Baiker, A. Wokaun, *Appl. Catal. A-Gen.* **84**, 77 (1992).
67. J. T. Richardson, *Principles of Catalysts Development. Fundamental and Applied Catalysis*. M. V. Twigg, M. S. Spencer, Eds., (Plenum Press, New York, 1989).
68. W. Wang, S. Wang, X. Ma, J. Gong, *Chem. Soc. Rev.* **40**, 3703 (2011).
69. G. C. Chinen, P. J. Denny, D. G. Parker, M. S. Spencer, D. A. Whan, *Appl. Catal.* **30**, 333 (1987).
70. L. C. Grabow, M. Mavrikakis, *ACS Catal.* **1**, 365 (2011).
71. K. K. Bando, K. Sayama, H. Kusama, K. Okabe, H. Arakawa, *Appl. Catal. A-Gen.* **165**, 391 (1997).
72. B. Tidona, C. Koppold, A. Bansode, A. Urakawa, P. Rudolf von Rohr, *J. Supercrit. Fluids* **78**, 70 (2013).
73. V. N. Ipatieff, G. S. Monroe, *J. Am. Chem. Soc.* **67**, 2168 (1945).
74. J. G. v. Bennekom, J. G. M. Winkelman, R. H. Venderbosch, S. D. G. B. Nieland, H. J. Heeres, *Ind. Eng. Chem. Res.* **51**, 12233 (2012).

2

High Pressure (400 bar) CO₂ Hydrogenation Reactor Setup

2.1 Introduction

Heterogeneously catalysed reactions are widely studied under continuous flow conditions in stainless steel tube filled with packed catalyst beds. Tubular reactors are operated continuously, enabling reaction samples to be collected more quickly. Conventional lab-scale catalytic reactors consist of a reactor tube, having inner diameter in the range of sub-inches. Hence, the infrastructure, required area and amount of reactants and catalysts required for the operation of such a reactor are quite large. Often these lab scale reactors suffer from mass transfer and heat transfer limitations along with maximum operating pressure limitation due to the large dimensions of used reactor tube. Micro-reactors offer various advantages over traditional reactors. They excel in number of characteristics such as improved mass and heat transport, access to high pressure operation, increased space time yield, increased reaction selectivity and importantly the ability to handle dangerous chemicals with improved safety (1-5). These benefits have led micro-reactors to get preferred over traditional techniques. Most benefits of micro-reactor originate from the small sizes inherent to micro-reactor technology. Efficient mass transfer by fast mixing and diffusion can be achieved in micro-reactors thanks to reduced characteristic length scales. The maximum operating pressure of a reactor is a function of both, the material properties and the reactors design. By reducing internal volume, less force is exerted on the reactor wall, enabling

higher pressure operation. This reduction of force reduces the required thickness of the wall and also reduces the risk associated with catastrophic failures of the reaction system operated at high pressure. Furthermore, reduced wall thickness allows improved isothermal operation or quick heat removal for exothermic reactions thereby minimizing the heat transfer limitations.

As previously stated (Chapter 1, section 1.6), one of the objectives of this thesis is to design and construct a high pressure lab scale micro-reactor setup for the continuous catalytic hydrogenation of CO₂ at pressures up to 400 bar. This chapter describes the design and construction of a fully automated micro-reactor setup together with an analytical system in detail. It also discusses the reactor operation, difficulties arisen during the commissioning of the reactor setup, and our solutions in practice.

2.2 Reactor Design and Setup

The schematic representation of the high pressure plant constructed and used in this work for studying the CO₂ hydrogenation reaction up to 400 bar is shown in Figure 2.1. The reactor setup can be broadly divided into four sections *viz.*

1. H₂ compression and flow control
2. Liquid and gas CO₂ flow control
3. The reactor system; temperature and pressure control
4. Analytical system and reactor automation

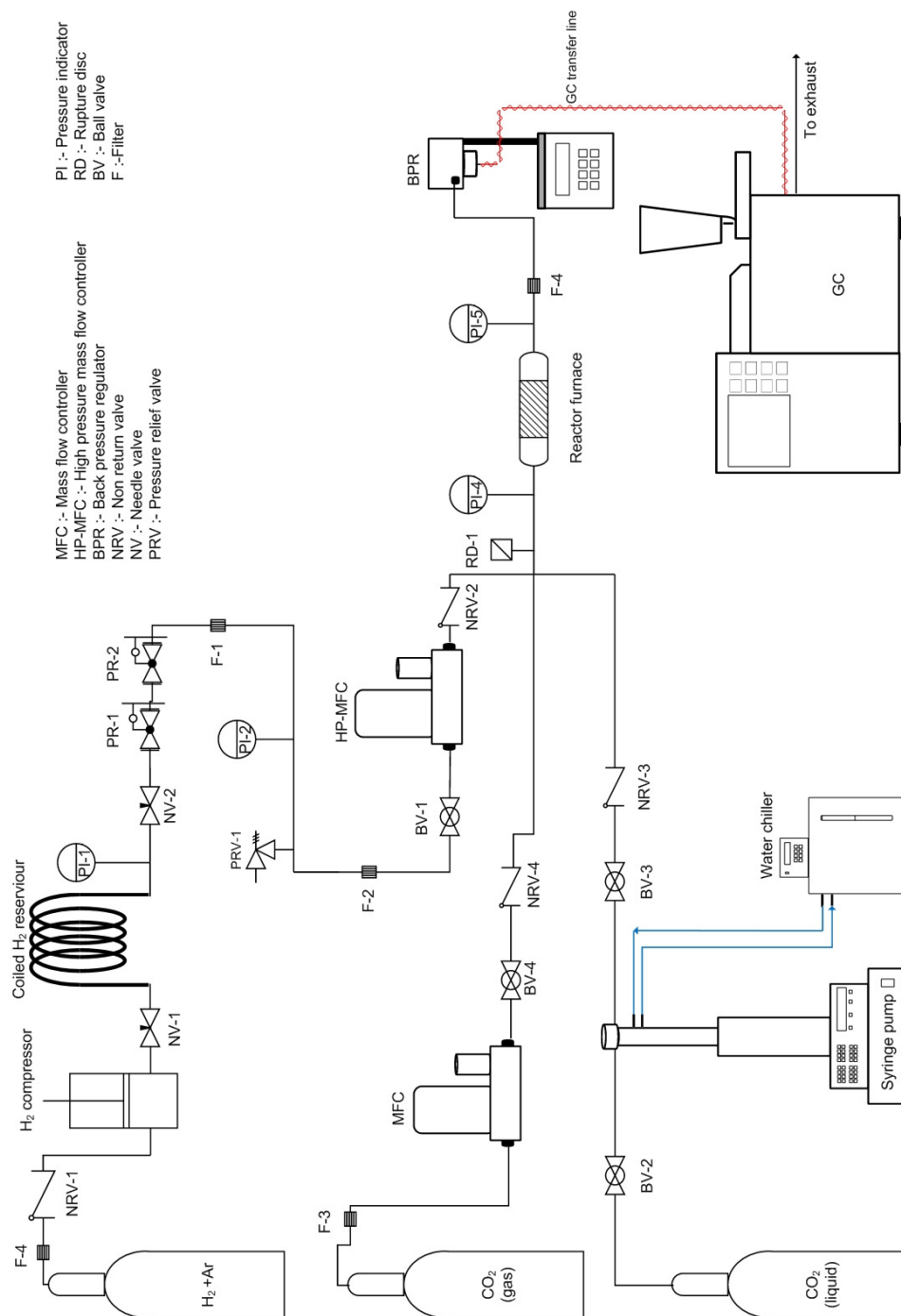


Figure 2.1 Schematic flow diagram of high pressure plant

2.2.1 H₂ Compression and Flow Control

H₂ compression and flow control section consists of many critical components and it is one of the most crucial section of this reactor setup. Commercially available hydrogen in regular laboratory gas cylinders can only be obtained up to 200 bar pressure. To achieve the pressure up to 400 bar a hydrogen gas booster was used. As it can be seen in the Figure 2.1, a hydrogen cylinder is connected to air driven hydrogen gas booster (Haskel) using 1/8" SS tubing (Sandvik, ID 1.75 mm). A non return valve (also called check valve) is connected in between the booster and cylinder to ensure one directional flow. The outlet of gas booster is connected to a H₂ gas reservoir which is made up of by coiling 6 meters of 1/4" SS tubing (Sandvik, ID 4.7 mm). Due to the safety reasons, the hydrogen is stored in the coiled tube reservoir rather than a vessel. Two high pressure needle valves were connected at the inlet and outlet of H₂ reservoir in order to isolate the reservoir from the reactor system if required. As shown in Figure 2.1, pressure indicator PI-1 was used to measure the pressure in H₂ reservoir. Two pressure reducing regulators (Circor GO and TESCO) were connected in series to the system to remove the pressure pulsations caused by the boosting cycles of the gas booster. Pressure indicator PI-2 indicates the pressure after the pressure regulators. Followed by pressure regulators, a pressure relief valve avoids any overshoot of pressure above 400 bar. Two filters, 10 μm (F-1) and 2 μm (F-2) (VICI, Europe) were connected in series to ensure the removal of any debris or dust particles. A high pressure thermal mass flow controller (Bronkhorst, Hi-Tec) was used to control the flow of hydrogen to the reactor system. The outlet of this flow controller is connected to a cross (HiP) which is connected to the inlet of reactor system.

2.2.2 Liquid and Gas CO₂ Flow Control

To dispense the liquid CO₂, a high pressure syringe pump (Teledyne ISCO, 260 D) was used. The inlet of syringe pump was connected to a liquid CO₂ cylinder with dip pipe configuration via a high pressure ball valve BV-2 (HyLok, Europe). Since, the liquid CO₂ is sensitive to the density change caused by changes in the ambient temperature, a constant temperature covering jacket was attached to the cylinder of pump. The temperature of the cooling jacket was maintained at 20 °C by using a constant temperature water circulation bath. The outlet of syringe pump was connected to a ball valve BV-3 and finally to the cross which was connected to the reactor system. As depicted in Figure 2.1 a CO₂ mass flow controller (Bronkhorst, Hi-Tec) was used to carry out reactions at low pressure. The switching from high pressure to low pressure CO₂ feeding was achieved by closing BV-3 and opening BV-4 valve or vice versa from low pressure to high pressure.

2.2.3 The Reactor System; Temperature and Pressure Control

The micro-reactor system consists of a 1/8" stainless steel tube (Sandvik, Europe) with an inner diameter (ID) of 1.75 mm and ca. 18 cm in length, as shown in Figure 2.2 together with the heating system. The heating system consists of two stainless steel bodies having length of 15 cm. A mortise in the bottom SS body was machined to embed the reactor tube in it. Another L shape mortise, touching the reactor tube mortise was made for thermocouple (Type K, Watlow) embedment. A resistive heating cartridge with capacity of 750 W (Watlow) was inserted into the bottom body. The temperature control was achieved by a PID controller from Watlow (EZ-zone). The heating assembly was covered with ceramic insulation material. The ceramic insulation was wrapped in aluminium foil.

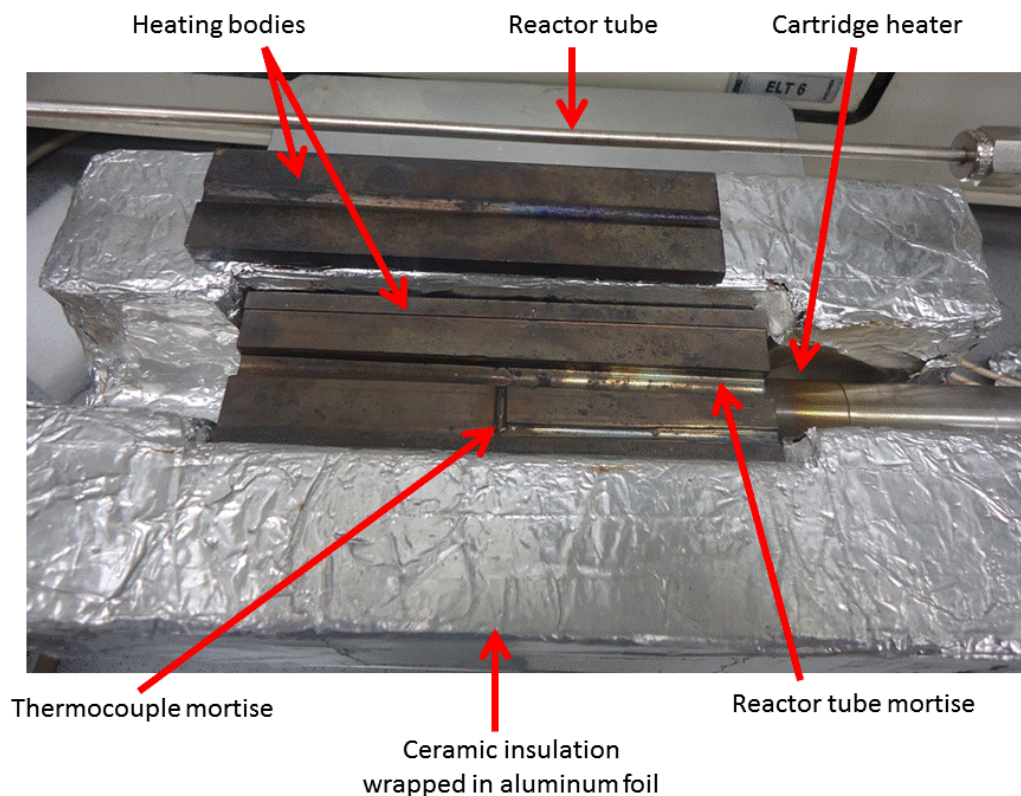


Figure 2.2 Reactor tube with heating system and insulation

As shown in Figure 2.1, at the inlet of the reactor tube a rupture disc RD-1(HiP) was connected for quick response pressure relief in case of overpressure. The pressure drop across the catalyst bed placed inside the reactor was measured with two pressure transmitters PI-4 and PI-5 (STW, Germany) connected to a digital pressure readout system (HaoYing, China). The pressure in the reactor system was controlled with a high pressure back pressure regulator (Jasco, BP-2080) specialised for supercritical operations having low internal dead volume. An inline 2 μ m filter frit F-4 was placed in the 1/8" fittings after the reactor tube in order to prevent the catalyst particles entering into back pressure regulator. The product stream from the outlet of back pressure regulator was fed to the analytical system (GC) through a transfer line heated at 150 °C to keep the carbon containing products in vapour phase. A volumetric flow meter (Agilent ADM 2000, not shown) was used to measure the flow at the outlet of GC.

2.2.4 Analytical System and Reactor Automation

2.2.4.1 Analytical System

The reactor system is equipped with a gas chromatograph (Bruker, GC 450) instrument having manual as well as online sample injection functionality. The GC was configured on the basis of all possible product components formed in CO₂ hydrogenation reaction as well as keeping in mind Fischer-Tropsch reaction products. Different valve combinations are integrated with the GC and a schematic representation of the valve configuration is shown in Figure 2.3. The GC has been configured with three 6 port Valco valves. Two independent parallel detection channels equipped with TCD (Thermal Conductivity Detector) and FID (Flame Ionization Detector) detectors are provided for the fast analysis. The valve compartment was heated by internal heating controller from the instrument. Helium was used as carrier gas on both the channels. The TCD channel was equipped with Hayesep-Q (0.5 m x 1/8" x 2 mm) and CP-Molsieve-13X (1.5 m x 1/8" x 2 mm) packed columns connected in series. Two independent 6-port valves were used for the injection of sample from a 10 µl and 250 µl sample loop on TCD and FID channels respectively. The first column on TCD channel pre-splits the product mixture into permanent gases (O₂, H₂, N₂, CO, CH₄) and other components like CO₂, methanol, dimethyl ether and hydrocarbons. Then the permanent gases were passed via a 6-port valve to the second column where they get separated. To the FID channel a CP-WAX 52CB (25 m x 0.53 mm, d_f = 2µm) capillary column was connected to separate compounds such as alcohols, aldehydes, acetates. The injector of FID channel was operated in split mode with split ratio of 1:10. The column oven was kept at constant temperature at 45 °C for 3.50 min to allow better separation of permanent gases. Followed by increasing the oven temperature to 150 °C at the rate of 15 °C/min and was held for 0.50 min. The total analysis time was 12 min

including the 0.50 min for the stabilisation of oven. A 4-port valve (not shown) was used as stream shut off valve during the online injection of sample.

For the data acquisition and analysis, Varian Galaxie software was used. The calibration of detected components was carried out by using external standard method. Gas mixtures of known composition were injected to generate a calibration curve in the acquisition software. For liquid samples such as methanol and methyl formate a 2 L Tedlar bag was used to make liquid components mixture in certain ratio. The bag was filled with nitrogen gas of specific volume (using a MFC) to take the liquid in vapor form. Appropriate syringes were used to draw the liquid components from reliable source and carefully inserted through the septum on valve quickly into the Tedler bag and closed the inert top valve. Vacuum pump was connected at the GC outlet and bag containing the liquid calibration components was connected to the GC inlet. The liquid components were allowed to flow into the GC sample loops by opening the valve of the Tedler bag when the vacuum pump fitted to the outlet of GC is switched on for one minute. After turning off the pump, the liquid components from the Tedlar bags were allowed to equilibrate in the sample loop for about 20 sec. Following this, the components were analyzed by GC in the usual manner.

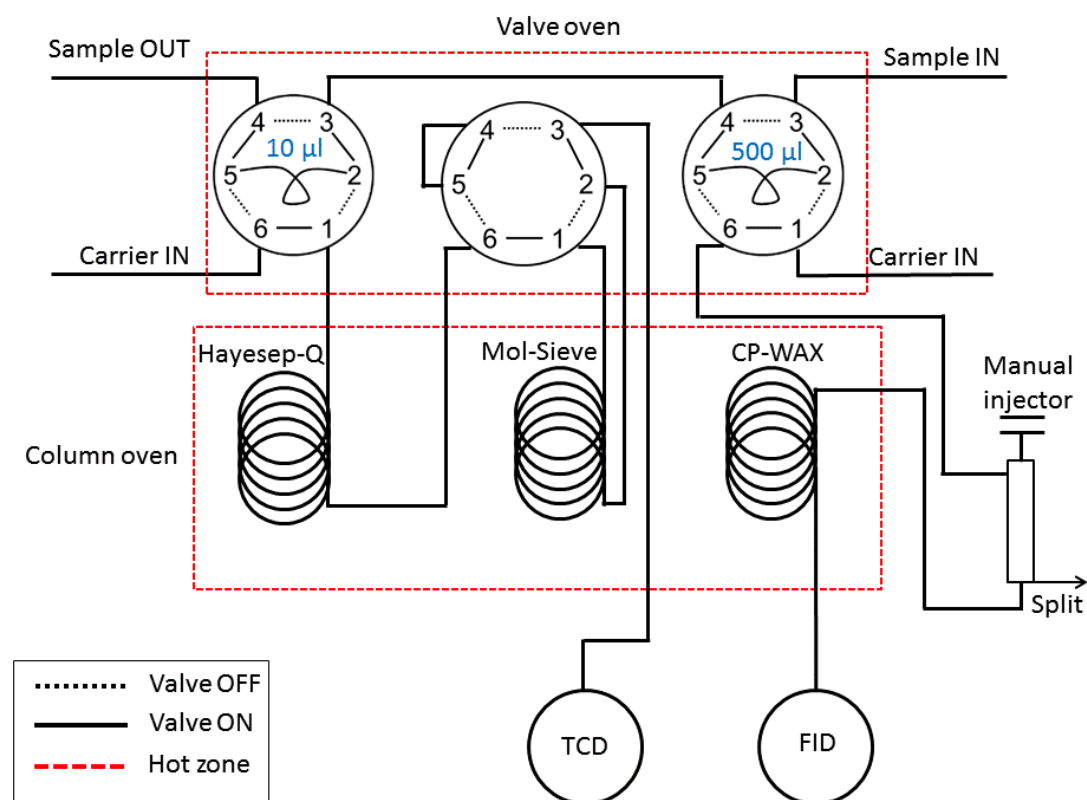


Figure 2.3 Schematic representation of GC configuration with sampling valves

2.2.4.2 Reactor Automation

The reactor automation was implemented using LabVIEW software (National Instruments). Figure 2.4 shows the screenshot of the LabVIEW program which was developed during the thesis time to monitor and control critical parameters of the high pressure plant remotely. The developed program is capable of communicating with CO₂ syringe pump, hydrogen mass flow controller, heating system of the reactor and the digital pressure readout system. The communication between various components and the computer was achieved using serial port communication. A 8-port RS232 communication hub (UPort 1610-8, MOXA) was connected to the computer via USB 2.0. To this hub, all the instruments were connected using DB9 RS-232 connector. In order to carry out the reactions in a highly safe manner, an internal software alarm

system was developed which keeps record of all the process values within the configured limit. Deviation of any process parameter from the desired value activates an emergency shutdown procedure. The shutdown procedure sets all the flow controllers to zero and turns off the heating system while displaying blinking alarms on the screen. As shown in Figure 2.4, the inlet and outlet pressure of reactor were monitored continuously and the corresponding pressure drop across the catalyst bed is displayed on the screen. If the value of pressure drop across the catalyst bed increases above the desired set value the emergency shutdown procedure gets activated. Any overshoot in temperature and in flow also activates the emergency shutdown procedure. Together with LabVIEW based safety system, all the devices have its own internal alarm facility which was configured carefully to ensure the safe operation of the reactor system.

To test the catalyst at different temperatures and flow conditions the temperature and flow program system was developed. As it can be seen in Figure. 2.4 the flow program system allows the different combinations of CO₂ and H₂ set points for the desired amount of time. As soon as the set time is elapsed, the next values were sent to the controllers making change in the setting of the flow controller. All the flow and temperature controllers can be operated in auto or manual mode. In auto mode the values from the temperature/flow program were sent to the instrument while in manual mode it was possible to enter the set points directly. The temperature control section also shows the heater power applied to the heating system together with the PID parameters. The amount of liquid CO₂ remaining in the pump along with the estimated run time was also displayed on screen. To have quick glance of process values, the XY plots of temperature and hydrogen flow against the real time were shown on the screen. The software also reads the data from volumetric flow meter (Agilent ADM 2000) connected to measure the flow of gaseous products at ambient conditions. All the

process values which are displayed and can be controlled from the software, were logged in a file along with the real time.

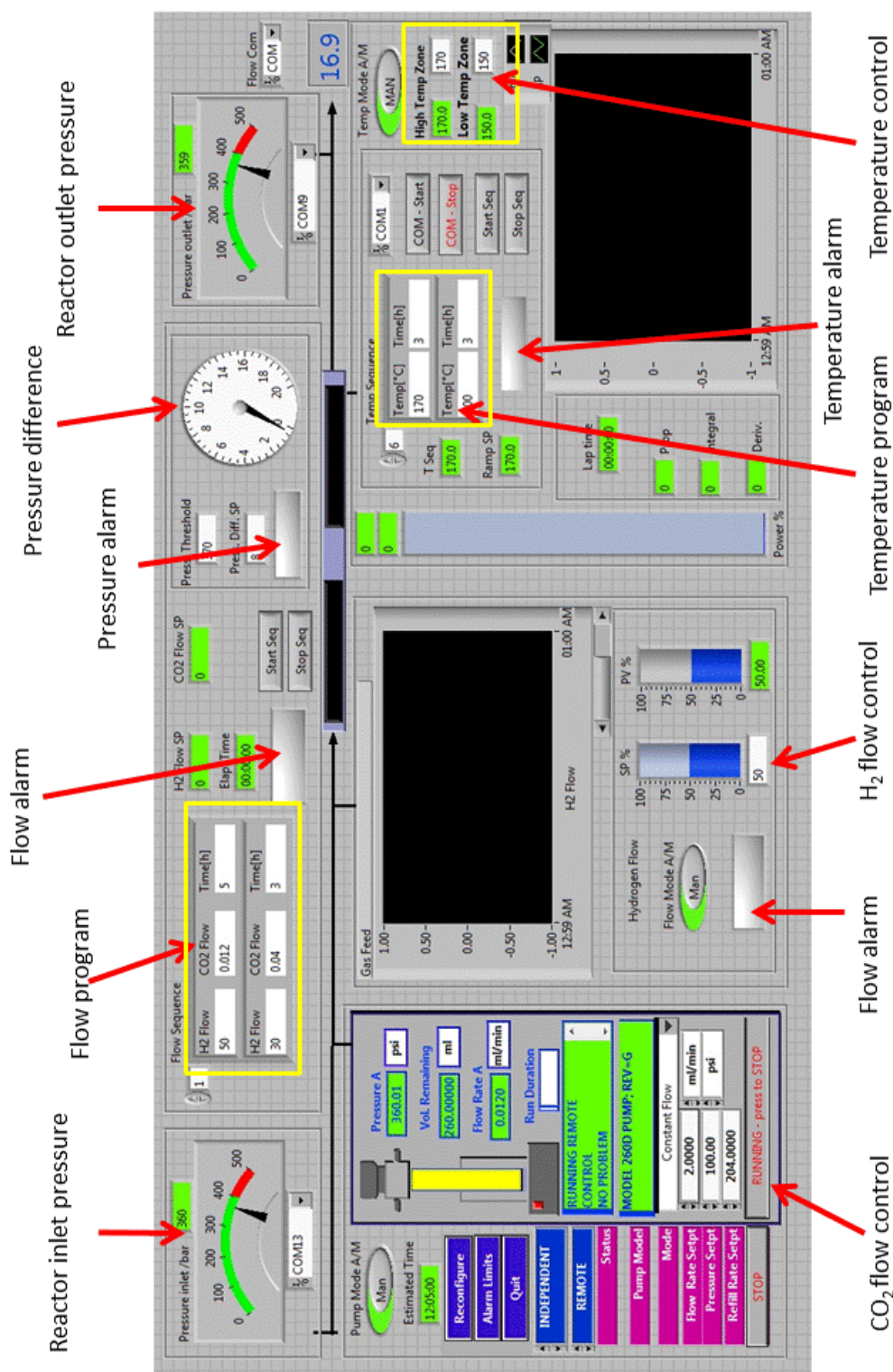


Figure 2.4 LabVIEW program control panel of high pressure plant

2. 3 Reactor Operation and Catalytic Activity Testing

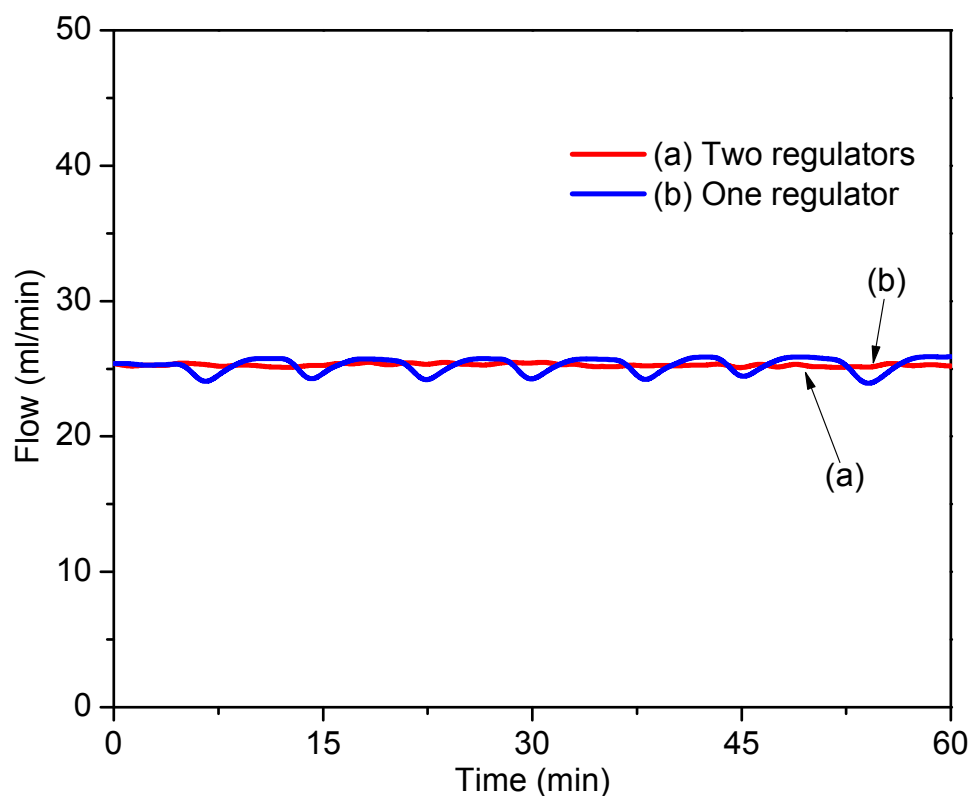


Figure 2.5 The hydrogen flow stability with one and two regulators

After the installation of reactor components, the commissioning and testing was of prime importance in order to ensure the stable and safe daily operation of the reactor. First, the hydrogen gas booster was tested to find out the optimum operating pressures of inlet gas and compressed air. The pressure and flow of the latter gas drives the mechanical compression in the gas booster. By keeping the inlet pressure of gas booster at 32 bar, the compressed air pressure was increased slowly to achieve the outlet pressure of 420 bar. It was found that with 6 bar of compressed air pressure the outlet pressure of 420 bar can be achieved. Due to the discontinuous flow arising from the gas booster, the pressure (PI-1) at booster outlet was found to be pulsating with the every boost cycle by ca. 1 bar. To avoid this, the high pressure needle valve (NV-1) was

adjusted to partially closed state, at the same time ensuring the flow through the needle valve. The high pressure mass flow controller is very sensitive to the inlet pressure/flow fluctuations which induced unsteady outlet flow. Hence, it was desirable to remove the pressure and flow pulses from the hydrogen line after compression. The pressure reducing regulator PR-1 was used to maintain the constant pressure of 400 bar at the inlet of mass flow controller. When operated, it was observed that the outlet flow at MFC was not stable. Figure. 2.5, curve (a) shows the behaviour of flow at MFC outlet with only one pressure regulator. This was due to the reason that, even at the lowest possible value, the flow coefficient of commercial pressure reducing regulator is much higher than the desired.

To solve this problem, a second pressure reducing regulator PR-2 was connected after the first regulator PR-1. A custom-made high pressure fittings with very small orifice was connected at the inlet of this pressure regulator to obtain the required flow coefficient. To maintain the stable operation, the outlet pressure of second regulator was kept at 380 bar while at 400 bar at the inlet. In Figure 2.5, curve (b), it can be seen that having two regulators connected in series greatly improved the flow stability. The default calibration of MFC was at 150 bar and for pure hydrogen. Since we were using 10 % argon gas premixed with hydrogen as an internal standard, it was necessary to perform the recalibration. The calibration of hydrogen mass flow controller was performed at 380 bar inlet pressure using BIOS, Drycal flow meter. The calibration curve for hydrogen/argon gas mixture (90/10 vol %) is shown in Figure. 2.6 .To ensure the stable operation of MFC, the pressure difference between inlet and outlet of MFC was kept at 20 bar, which allowed to perform the reactions up to pressure 360 bar.

The compression of liquid CO₂ was much more simple and straight forward due to the high pressure syringe pump. By running the syringe pump in refill mode the

liquid CO₂ from dip pipe cylinder was filled inside the cylinder of the pump. After filling, the inlet ball valve BV-2 was closed and pump was operated at constant pressure mode to achieve the desired CO₂ pressure.

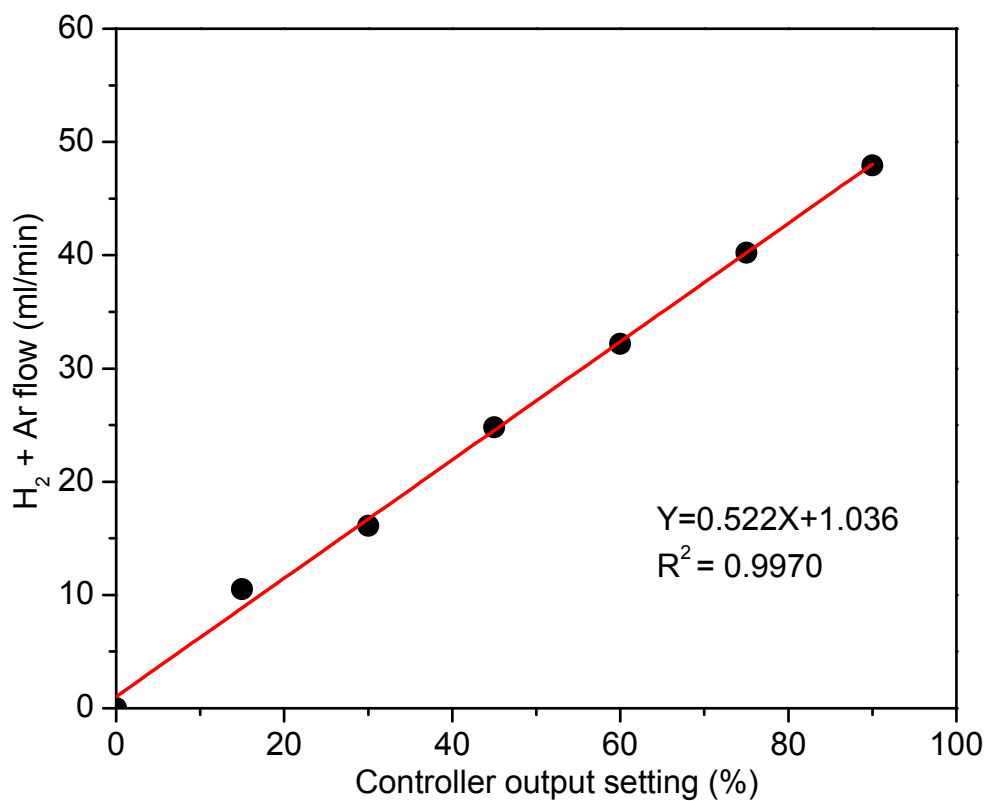


Figure 2.6 Hydrogen mass flow controller calibration curve. P_{Inlet}= 380 bar

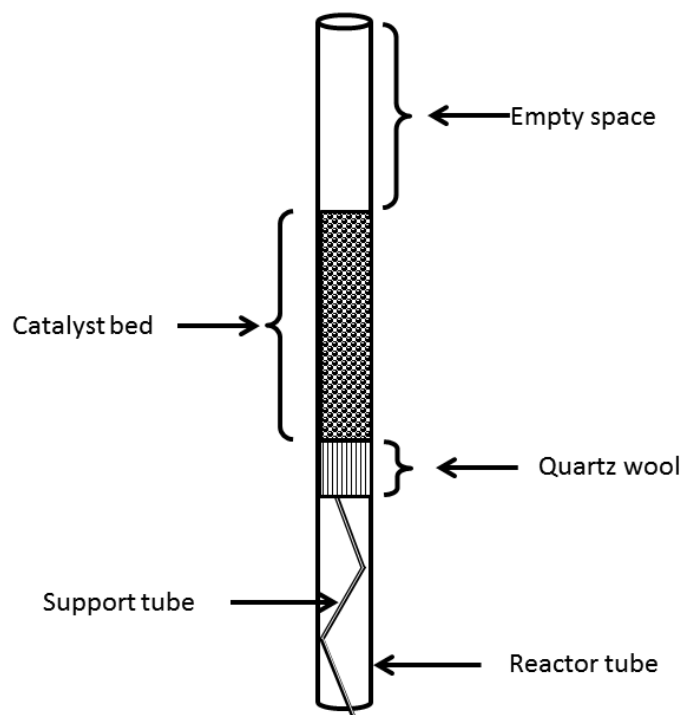


Figure 2.7 Placement of catalyst inside the reactor tube

For catalytic activity tests, the catalyst was charged inside a 1/8" tube having inner diameter of 1.75 mm. First, the catalyst powder was pressed in a pellet die with 5 ton of pressure to form a pellet of 2.5 mm thickness and of 1.6 cm in diameter. The pellet was then broken using mortar and pastel in to smaller particles and sieved to particle size of 100-300 μm . Depending upon the catalyst density, the required amount of catalyst was weighed carefully. Before loading the catalyst into the reactor tube, a small piece of hollow tube having length of ca. 3-4 cm was inserted from the bottom of reactor tube. This tube acts as a support for catalyst inside the reactor tube and prevents the moving of catalyst bed by pressure/flow. As shown in Figure 2.7, this hollow tube was bent at different positions, so that it was held inside the reactor under pressurised condition. A small portion of this tube was left outside of the reactor in order to allow

the easy withdrawal. Over this support tube, quartz wool was inserted carefully to form a packed bed of length ca. 4 mm. The catalyst particles were then poured inside the tube while tapping the reactor tube to ensure uniform distribution of particles inside the tube. The catalyst bed length could be anywhere between 2-10 cm depending on the studied GHSV. To recover the catalyst after the reaction, the reactor tube above the catalyst bed was kept empty.

The reactor tube was placed inside the furnace and was connected to the system using 1/8" compression fittings. The furnace was horizontally kept on a moving stage which allows up and down movement of the furnace. Before starting the reaction, the catalyst was reduced in the stream of H₂/Ar at 330 °C for 2 h at atmospheric pressure. The heating ramp rate was kept at 10 °C/min. After the reduction of catalyst, the heating was turned off to cool down the reactor tube. To improve the cooling efficiency the furnace was lowered so that the reactor tube was exposed to atmospheric temperature under the steady flow of H₂/Ar. Then the gas flow was turned off and the reactor was pressurised with liquid CO₂ up to the reaction pressure by running syringe pump in constant pressure mode. For the reactions below the critical pressure of CO₂, a thermal mass flow controller was used to feed gaseous CO₂. In this case the syringe pump was isolated from the system by closing the ball valve BV-3. After attaining the desired pressure, the pump was switched to constant flow mode in order to establish a steady liquid CO₂ flow (normally few µl/min) through the reactor. This was followed by tuning on the H₂/Ar mixture gas flow. The outlet stream from the BPR was fed to the online GC analysis system to determine the molar concentration of reactants and products. The BPR outlet flow was measured with volumetric flow meter to estimate the corresponding GHSV. The reactor was kept at ambient temperature until the steady state of molar fraction was reached. As shown in Figure. 2.8, approximately 3 hours are

required to achieve the steady molar concentration, measured by GC analysis . The long time span to reach the steady state was attributed to the very low reactant flow rate at high pressure.

The reactor tube was then positioned inside the furnace and covered with insulating material. The reaction was carried out at different temperatures ranging from 170 to 300 °C. The LabVIEW temperature program was used to scan the various temperatures. CO₂ conversion was determined directly from the CO₂ molar concentration measured by the TCD detector. The maximum standard deviation of CO₂ in the reaction feed was ± 0.5 % of the measured value. This was critical when CO₂ conversion was below 1 %. In those cases, CO₂ conversion was calculated from the carbon balance; based on the product concentrations for which the sensitivity, thus the accuracy, is higher. The detection limits for methanol and CO were 10 and 200 ppm, respectively, based on the signal to noise (S/N) of the chromatograms. This ensures accuracy of CO₂ conversion, better than 0.1 %. The conversion and selectivity values were calculated by averaging over several injections after product concentrations were stabilized. The tendency and accuracy of the catalytic performance were ensured by minimum two runs carried out on different days. The standard deviations for CO₂ conversion and product selectivities were < 2.2 %.

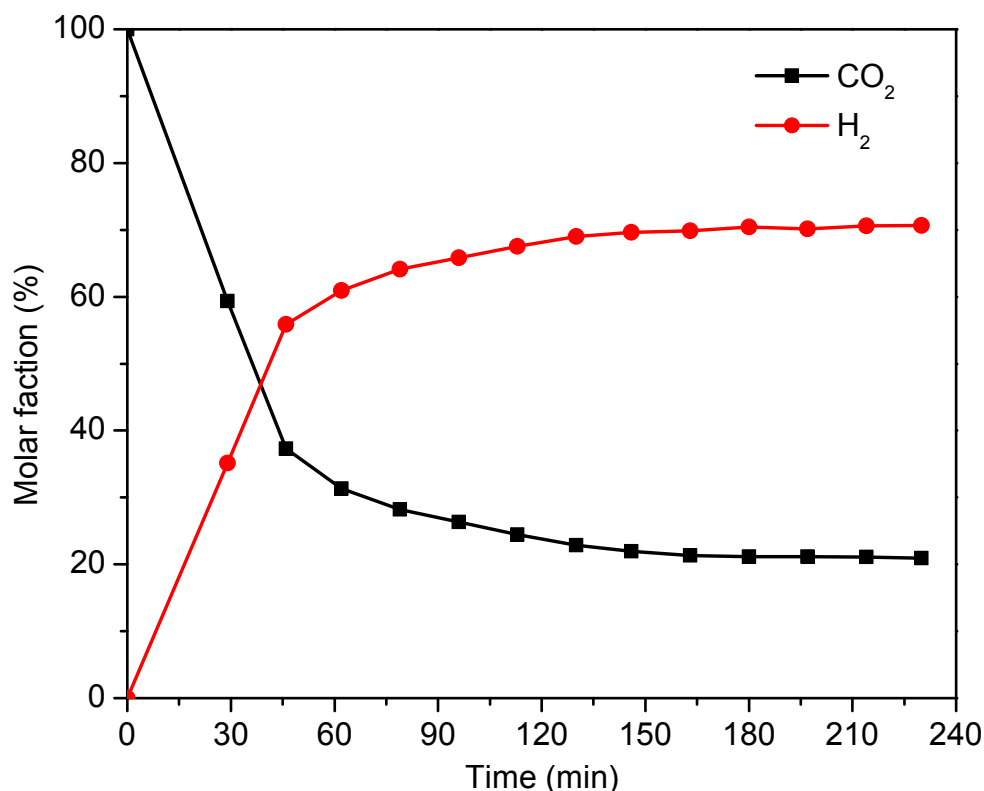


Figure 2.8 Time required to reach steady molar fractions of CO₂ and H₂ measured by GC

2. 4 Conclusions

A high pressure lab scale micro-reactor setup for the continuous catalytic hydrogenation of CO₂ at pressures up to 400 bar was successfully designed and constructed. Instability in the hydrogen flow was removed by placing two pressure reducing regulators in series. The product analysis was carried out by using online GC system equipped with two parallel detection channels. The GC method for product separation was successfully developed. The long stabilization time of reactant concentration was mainly due the high reaction pressure and low flow conditions. The in-house designed LabVIEW program facilitated the automation of reactor to monitor and control the critical parameters of the system remotely. The temperature and flow program feature in LabVIEW program allowed to scan various temperatures and flows

automatically for the given catalyst. Furthermore, the emergency shutdown function enabled unmanned and safe operation of reactor during the nights and over the weekend

References

1. E. R. Murphy, J. R. Martinelli, N. Zaborenko, S. L. Buchwald, K. F. Jensen, *Angew. Chem. Int. Edit.* **46**, 1734 (2007).
2. D. Gobby, et al., *J. Micromech. Microeng.* **11**, 126 (2001).
3. S. Hardt, F. Schönfeld, *AIChE J.* **49**, 578 (2003).
4. P. D. I. Fletcher *et al.*, *Tetrahedron* **58**, 4735 (2002).
5. M. W. Losey, R. J. Jackman, S. L. Firebaugh, M. A. Schmidt, K. F. Jensen, *J. Microelectromech. S.* **11**, 709 (2002).

3

Impact of K And Ba Promoters on CO₂ Hydrogenation Over Cu/Al₂O₃ Catalysts at High Pressure

3.1 Introduction

Cu-based catalysts have been extensively investigated for CO₂ hydrogenation to methanol. This chapter presents CO₂ hydrogenation over impregnated Cu/Al₂O₃ catalysts promoted with K and Ba at pressures up to 360 bar. The choice of the promoters is due to its high affinity with CO₂, forming carbonates which can be decomposed under mild conditions (1-3). The high affinity to CO₂ and the low stability of resulting carbonates under reducing atmosphere may offer great advantages to enhance the reaction rate and alter selectivity. The K promotion has been reported to enhance the CO formation in CO₂ hydrogenation reaction (4). However, the performance of K promoted catalyst under high pressures (up to 360 bar) is not well documented. In case of Ba promoter, a study on Cu/ZnO/Al₂O₃ catalysts promoted with some metal components including Ba has been reported for CO/CO₂ hydrogenation (5, 6). However, to the best of our knowledge, the promoter effects given solely by Ba and also for Cu/Al₂O₃ catalysts in CO₂ hydrogenation have not been reported.

This chapter presents the effects of high pressure and the promoters on the catalytic performance in CO₂ hydrogenation. The catalysts were prepared by impregnation method and characterized by XRD, H₂ temperature programmed reduction (H₂-TPR), BET surface area, N₂O pulse chemisorption, CO₂ temperature programmed

desorption (CO₂-TPD), and *in situ* diffuse reflectance infrared Fourier transform spectroscopy (DRIFTS) to explain possible origins of the differences in the catalytic performance.

3.2 Experimental

3.2.1 Catalyst Preparation

Cu/Al₂O₃ (18/82 wt %) catalyst was prepared by the incipient wetness impregnation method using copper nitrate hexahydrate (>98 %, Alfa Aesar) and γ -Al₂O₃ (Bimodal, Alfa Aesar). It was dried overnight in an oven at 100 °C and subsequently calcined in air at 400 °C for 4 h. Further, it was divided into three parts. The two parts were impregnated with barium acetate (>99 %, Sigma Aldrich) or potassium carbonate (>99 %, Acros) to obtain Cu-Ba/Al₂O₃ (5 wt % Ba / 95 wt % Cu/Al₂O₃) or Cu-K/Al₂O₃ (5 wt % K / 95 wt % Cu/Al₂O₃), respectively. The K and Ba promoted catalysts were dried overnight at 100 °C and calcined in air at 400 °C for 4 h. 170 mg of the prepared catalyst was used for catalytic testing.

3.2.2 Catalyst Characterization Methods

X-ray diffraction (XRD) patterns were recorded on Bruker AXS D8 Advance diffractometer equipped with a Cu tube, a Ge (1 1 1) incident beam monochromator ($\lambda = 0.1541$ nm), and a Vantec-1 PSD operated in transmission mode. Data were recorded in the range of 5-70° 2 θ with a step size of 0.02° and a counting time of 4 s per step. The crystallite sizes of CuO, Cu, and BaCO₃ mentioned in Table 3.1 were estimated from the full width at half maximum (FWHM) of corresponding peaks using Scherrer equation with the shape factor of 0.9 assuming the spherical particles (7). (2 0 -2)

Impact of promoters and high pressure on impregnated Cu/Al₂O₃ catalysts

reflection for CuO, (111) reflection for Cu, and (111) reflection for BaCO₃ were used to determine the crystallite size.

N₂ isotherms at -196 °C were measured on a Quantachrome Autosorb 1-MP analyzer. Prior to analysis, the samples were degassed in vacuum at 300 °C for 12 h.

H₂-TPR (Temperature Programmed Reduction) of the as-prepared catalysts (20 mg) was carried out on Thermo TPDRO 1100 equipped with a TCD detector. The samples were previously treated at 100 °C for 1 h under N₂ stream, and subsequently heated from 50 to 630 °C at the rate of 10 °C/min under a stream of 5 % H₂ in N₂ at 20 ml/min. Soda lime (CaO+Na₂O) trap was used to adsorb mainly H₂O and CO₂.

For CO₂-TPD (Temperature Programmed Desorption), the catalyst samples (20 mg) were firstly reduced in 5% H₂ in N₂ at 20 ml/min for 2 h at 330 °C, followed by exposure to CO₂ at 50 °C for 1 h at 20 ml/min. TPD was performed under H₂ flow at 20 ml/min to study the stability of adsorbed CO₂ under reducing environment as in CO₂ hydrogenation. The temperature was raised from 50 to 630 °C at the rate of 10 °C/min and maintained at 630 °C. The effluent gases were analysed on MS (mass spectrometer), Pfeiffer Omnistar GSD 301 C, without any trap.

The copper surface area and dispersion were measured using nitrous oxide pulse chemisorption method reported by Evans et al. (8) Prior to analysis, samples were reduced in 5% H₂ in He stream at 330 °C, followed by cooling to 90 °C under He flow. A known volume of N₂O was then injected as pulse by using a six port valve. The N₂O at the exit was trapped in liquid N₂ and evolved N₂ was measured on the calibrated mass spectrometer, Pfeiffer Omnistar GSD 301 C. Copper metal surface areas were calculated assuming 1.46×10^{19} copper atoms/m² (8). Though Ba and K components are known to promote N₂O decomposition, they are active only above 100 °C hence no

interference was assumed in this analysis from Ba and K on the N₂O decomposition and thus on the derived Cu surface area (9-11).

In situ DRIFTS measurements were performed using a reaction chamber (HVC-DRP, Harrick) mounted in a Praying Mantis (Harrick) DRIFTS (Diffuse Reflectance Infrared Fourier Transform Spectroscopy) optical system. The spectra were collected with a Bruker Vertex 70v FT-IR spectrometer equipped with a liquid-nitrogen-cooled MCT detector at 4 cm⁻¹ resolution. About 50 mg of a sample was loaded in the cell for each measurement. The flow of gases was controlled by means of mass flow controllers (Bronkhorst). The gases pass through the sample (catalyst) packed-bed, mimicking the plug-flow condition of the reaction. Prior to the measurements, sample powders were reduced *in situ* at 300 °C in H₂ stream (9 ml/min H₂ and 3 ml/min He) for 1.5 h. Subsequently, the system was cooled to 170 °C in the H₂ stream and then to the reactant mixture (CO₂:H₂ = 1:3, total flow 12 ml/min) until the signal in DRIFTS was stabilized. The spectra were recorded every 30 seconds to follow the reaction and stabilization process of the catalysts and the evolution of surface species. *In situ* DRIFTS study was carried out at the lowest examined temperature of the catalytic testing (170 °C) where the level of product formation was low and in some cases it was close to the detection limit of gas chromatography (GC) instrument used in catalytic testing. However, this temperature was chosen because the differences in the product selectivity were more prominent at lower temperatures and thus the surface species which are not stable at high temperatures can be more clearly observed.

3.3 Results and Discussion

3.3.1 XRD

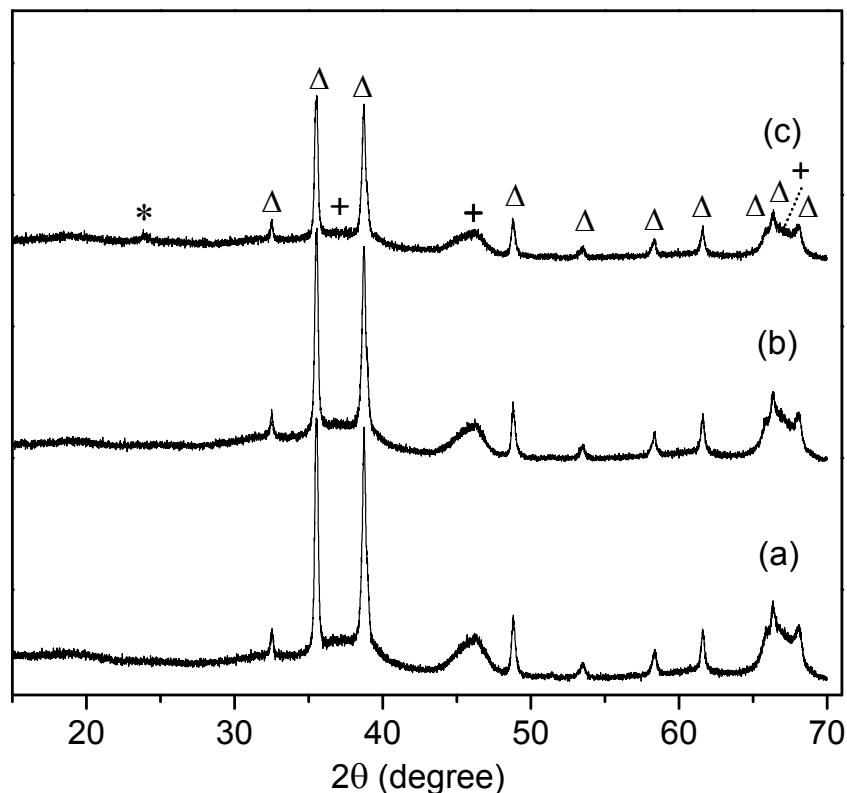


Figure 3.1 XRD patterns of the three as-prepared catalysts: (a) Cu/Al₂O₃, (b) Cu-K/Al₂O₃, (c) Cu-Ba/Al₂O₃. (Δ) copper oxide, (*) barium carbonate, and (+) γ-Al₂O₃.

Figure 3.1 shows the XRD patterns of the three catalysts before the reaction. Most of the peaks were assigned to copper oxide (CuO), confirmed by the reference JCPDS data 5-0661. Besides minor reflections due to γ-Al₂O₃ support, a very minor peak due to BaCO₃ was observed for Cu-Ba/Al₂O₃. In contrast, no reflections due to K₂CO₃ were observed for Cu-K/Al₂O₃. Both barium and potassium are expected to exist as respective carbonates based on the used precursor and calcination in air. The absence or minor presence of reflections in XRD indicates that K and Ba carbonates exist in a highly dispersed form such as nano-crystallites or thin layers. There was no change in the crystallite size of CuO in the three catalysts (Table 3.1).

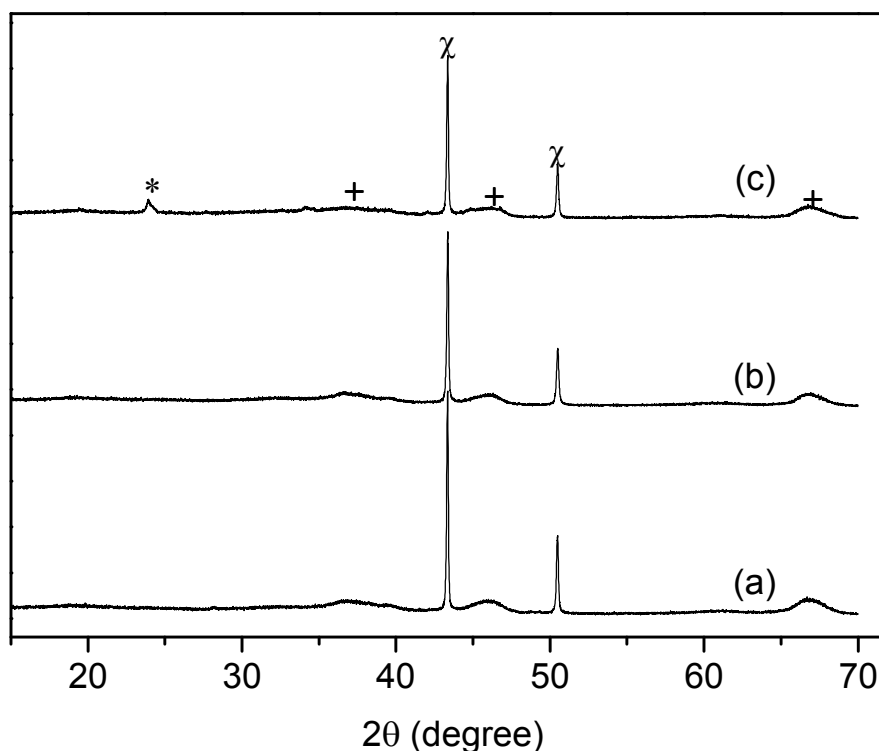


Figure 3.2 XRD patterns of the three catalysts after the reaction: (a) Cu/Al₂O₃, (b) Cu-K/Al₂O₃, (c) Cu-Ba/Al₂O₃. (χ)metallic copper, (*) barium carbonate, and (+) γ-Al₂O₃

Figure 3.2 shows the XRD patterns of the three catalysts after CO₂ hydrogenation at 360 bar (the catalysts tested under different pressure conditions show similar XRD patterns). Clearly, copper in the three catalysts exists in a metallic form as confirmed by JCPDS data 4-0836. Even after prolonged exposure to air (10 days), the patterns remained unaltered and copper stayed metallic, indicating full reduction of CuO to metallic Cu and possible sintering during the activation and reaction. The main difference between the three patterns was the presence of BaCO₃ in Cu-Ba/Al₂O₃, more pronounced than in the as-prepared catalyst (Figure 3.1). The crystallite size of BaCO₃ in as-prepared and used Cu-Ba/Al₂O₃ catalyst was estimated to be 7.7 and 12.3 nm, respectively. This implies that the barium particles agglomerated and/or sintered during the reaction, although the crystallite size remained very small. Interestingly, the

Impact of promoters and high pressure on impregnated Cu/Al₂O₃ catalysts

reflections due to K₂CO₃ were not observed even after the reaction, indicating that the K component remained in a highly dispersed state during the reaction.

3.3.2 Textural Properties

Table 3.1 BET surface area, pore volume, Cu surface area after reduction pretreatment, and average crystallite size of CuO for as-prepared catalyst and Cu for spent catalysts after the reaction.

	BET surface area (m ² /g)	Pore volume (cm ³ /g)	S _{Cu} (m ² /g _{cat})	Cryst. size of CuO (nm)	Cryst. size of Cu (nm)
Al ₂ O ₃	247	1.08	-	-	-
Cu/Al ₂ O ₃	184	0.65	2.25	50.5	270.2
Cu-K/Al ₂ O ₃	181	0.60	0.74	50.5	217.9
Cu-Ba/Al ₂ O ₃	166	0.59	3.36	50.5	243.3

Table 3.1 summarizes the results obtained by the physisorption analysis along with the specific copper surface area (S_{Cu}) of the three catalysts. After the loading of copper on alumina the BET surface area was reduced from 247 to 184 m²/g. There was significant reduction in the average pore volume of Cu/Al₂O₃ compared to that of Al₂O₃, indicating the pore filling by the copper component. After the potassium promotion to Cu/Al₂O₃, no remarkable change in the BET surface area was observed. In the report by Levy and Bauer, the rise in surface area of potassium doped alumina was observed up to 0.03 ion ratio of K/Al, and above 0.03 until 0.07 of K/Al the surface area decreased close to that of alumina (12). The K/Al ion ratio of our study was 0.064 and negligible change in the BET surface area may have the same origin. Further to this observation, Kantschewa et al. reported a strong interaction of potassium with alumina by forming AlOK groups and that some potassium even penetrates into subsurface layers, reducing the surface concentration of potassium (13).

In contrast to the BET surface area, a strong decrease in copper surface area, i.e. from 2.25 to 0.74 m²/g, was observed upon K promotion. As reported by Chen et al (4), it can be due to the homogeneous coverage of copper particles by the potassium component, explaining the similar BET surface area of Cu-K/Al₂O₃ to that of Cu/Al₂O₃. This highly dispersed form of the K component also explains the low crystallinity of K₂CO₃ in Cu-K/Al₂O₃ XRD pattern reported above. On the other hand, the addition of the barium component resulted in further decrease in BET surface area of Cu/Al₂O₃. It is interesting that a higher copper metal area was observed upon Ba promotion compared to that of Cu/Al₂O₃. The decrease in BET surface area indicates partial coverage of the barium component on the alumina surface and preventing the agglomeration of copper particles, thus possibly enhancing the specific copper surface area. Furthermore, negligible influence on the pore volume was found by K and Ba promotion.

3.3.3 H₂-TPR

The reducibility of Cu in the three catalysts was studied by H₂-TPR and the profiles are presented in Figure 3.3. Two clear peaks were observed for Cu/Al₂O₃ (profile (a)). They were ascribed to the reduction of the highly dispersed CuO species, occurring at a lower temperature, and of the bulk-like CuO phases, occurring at a higher temperature, (14) denoted as β and γ peaks, respectively. K promotion did not alter the general profile thus the reducibility of the Cu component (profile (b)). It slightly increased the stability of CuO by 21 and 20 °C for β and γ peaks, respectively.

Interestingly, Ba promotion resulted in a completely different H₂-TPR profile. Deconvolution obtained by Gaussian functions clarifies that the profile is comprised of three peaks (profile (c)). There was no change in reduction temperature of highly

Impact of promoters and high pressure on impregnated Cu/Al₂O₃ catalysts

dispersed CuO (β peak), but the amount of hydrogen uptake to reduce this copper species decreased significantly in comparison to Cu/Al₂O₃. On the other hand, the position of γ peak shifted to much lower temperature, indicating that Ba promotion facilitates the reduction of bulk copper species. Also, an additional reduction peak, denoted as γ_1 , was observed and the reduction temperature was very close to that of the β peak.

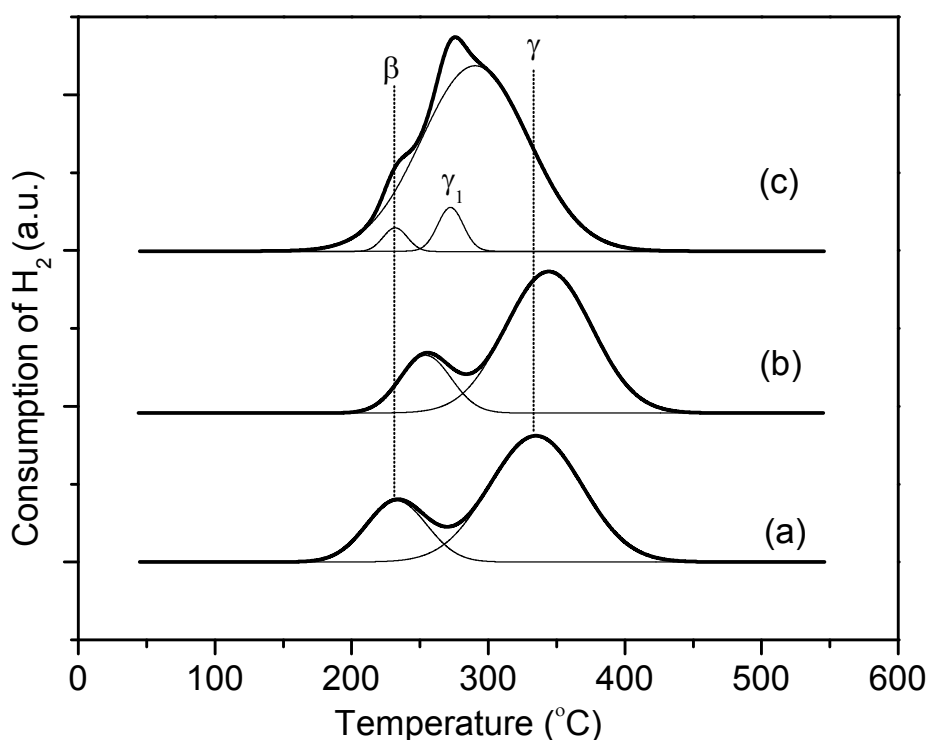


Figure 3.3 H₂-TPR profiles of (a) Cu/Al₂O₃, (b) Cu-K/Al₂O₃, and (c) Cu-Ba/Al₂O₃.

Summarizing, barium promotion facilitates CuO reduction and all the copper species are reduced at the similar temperature within a narrow temperature window. The origin of the drastic change in the H₂-TPR profile of Cu-Ba/Al₂O₃ remains unclear, but it may be related to the melting of Ba species under this reduction condition where water is also formed (2). This wetted barium hydroxide like species may promote Cu reduction.

3.3.4 CO₂-TPD

In addition to modifying the surface sites of the Cu and Al₂O₃ surfaces, K and Ba may function as a CO₂-capturing component during the reaction because of the high activity of their oxides and hydroxides with CO₂ to form respective carbonates. On the other hand, inorganic carbonates are typically stable and high temperature is required for decomposition (decomposition temperature of K₂CO₃ and BaCO₃ are ca. 887 and 1347 °C, respectively (15, 16)), although nano-crystallites of these carbonates show significantly lower decomposition temperatures (2, 17). In this study, we adapted the impregnation method and precursors so that low decomposition temperature could be obtained. (2) Also, it has been reported that formate species dominate over Cu/Al₂O₃ catalyst surface in the reaction gas mixture of CO₂ and H₂ at elevated temperatures (18) and formate species may be formed during the CO₂-TPD of this study. In order to understand the stability of CO₂ adsorbed and stored as carbonates and/or formates, CO₂-TPD study was performed after pre-reduction of the catalysts to render K and Ba components in their oxide form before CO₂ adsorption (their decomposition was confirmed by MS). CO₂ desorption was studied under H₂ atmosphere in order to study the stabilities of such adsorbed and carbonate/formate species under a reductive environment as in the target reaction. Figure 3.4 shows the CO₂-TPD profiles in the presence of hydrogen. CO₂ desorption on Cu/Al₂O₃ shows a single peak at 102 °C denoted as peak (I). Bönicke et al. studied CO₂-TPD on a stepped copper (332) surface and showed a desorption peak of CO₂ at 103 °C (19). Further, Chen et al. reported that the CO₂ desorbed at 102 °C could originate from the decomposition of formate species formed in presence of H₂ on the surface of copper (4).

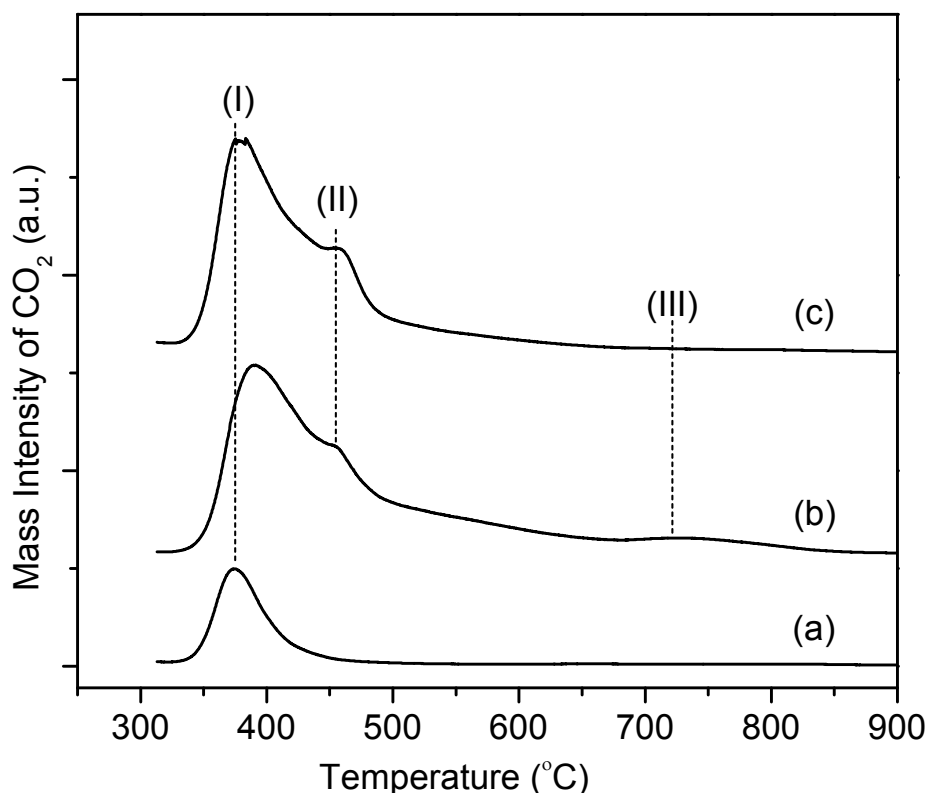


Figure 3.4 CO₂-TPD profiles of (a) Cu/Al₂O₃, (b) Cu-K/Al₂O₃, and (c) Cu-Ba/Al₂O₃ in the presence of H₂

The amount of CO₂ desorbed was significantly higher for the K and Ba promoted copper catalyst, revealing that K and Ba promotion provides additional active site to enhance the concentration of the surface formate and/or carbonate species. The amount of CO₂ desorption peak (I) was significantly increased after the addition of K and Ba promoters, indicating the number of CO₂ adsorption sites were increased as compared to the unpromoted catalyst. In case of the K promoted catalyst, peak (I) at 103 °C shifted to 115 °C, and two additional peaks at 185 (II) and 450 °C (III) were observed. Jørgensen et al. also observed peaks (II) and (III) on K/Cu(110) at a high coverage of potassium on copper (17). The density of the adsorption site for peak (III) was correlated to the coverage of K adatoms (17). These peaks were ascribed to two different surface carbonate species desorbing above 177 °C. Here, as evident from the

BET surface area and copper metal surface area, potassium components cover the copper particles and likely creates adsorption sites similar to those on the K-Cu interface, in addition to the sites available on the alumina surface. On the other hand, the Ba promoted catalyst showed the identical position of peak (I), while a prominent peak (II) was observed at 180 °C and no peak (III) was detected. Assuming that peak (I) originates from the decomposition of surface formates and peak (II) and (III) from that of surface carbonates, the profile indicates the presence of only one type of carbonate species on Cu-Ba/Al₂O₃. The peak (II) can be attributed to the carbonate on a specific surface site formed by Cu and Ba interactions, similar to the case of Cu-K/Al₂O₃. Based on the high accessibility of the Cu surface in Cu-Ba/Al₂O₃ (Table 3.1), the barium components predominantly cover the alumina surface and not the copper surface. Importantly, the major desorption peaks (I) and (II) fall well within the temperature range at which reaction was carried out, suggesting the high reactivity of CO₂ captured as surface carbonate and formate species and that the adsorption site corresponding to these peaks may play crucial roles in determining the catalytic performance.

3.3.5 CO₂ Hydrogenation

3.3.5.1 Unpromoted Cu/Al₂O₃

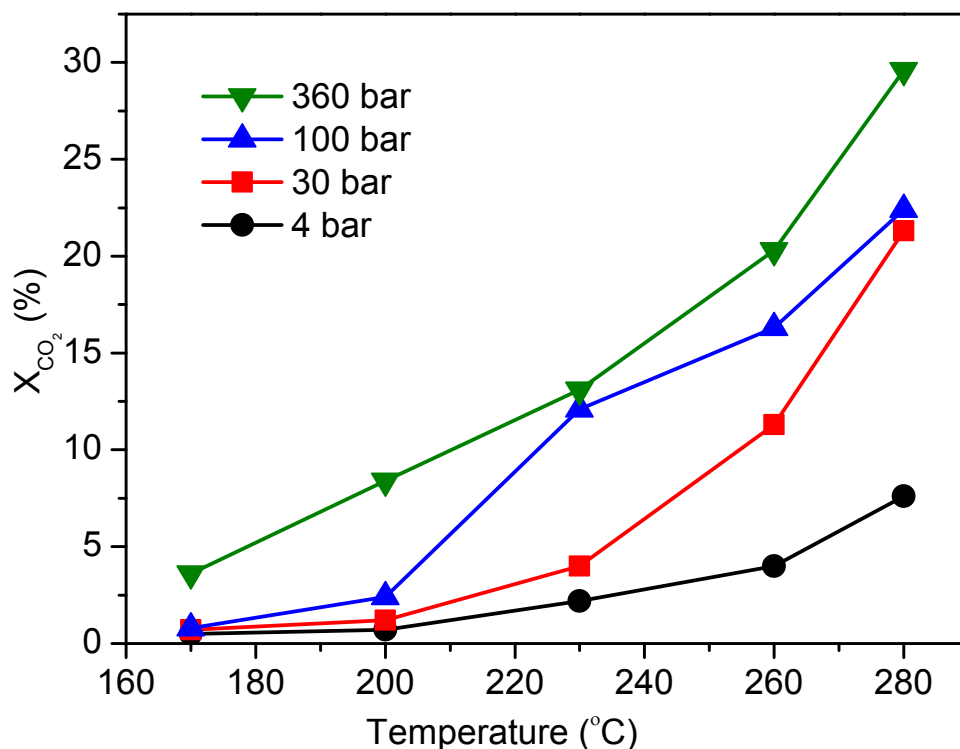


Figure 3.5 CO₂ conversion for the Cu/Al₂O₃ catalyst against temperature at different pressure conditions at GHSV = 4000 h⁻¹ and CO₂:H₂ = 1:3.8.

First, catalytic performance of the unpromoted Cu/Al₂O₃ catalyst in CO₂ hydrogenation was evaluated. Figure 3.5 shows the CO₂ conversion obtained under different temperature (170-280 °C) and pressure (4-360 bar) conditions. Large impacts of reaction pressure and temperature on the catalytic performance were evidenced. High CO₂ conversion was observed at higher pressures and particularly at higher temperatures. The maximum CO₂ conversion attained was 29.6 % at 360 bar at 280 °C. Carbon monoxide, methanol, methyl formate, and dimethyl ether were the products detected.

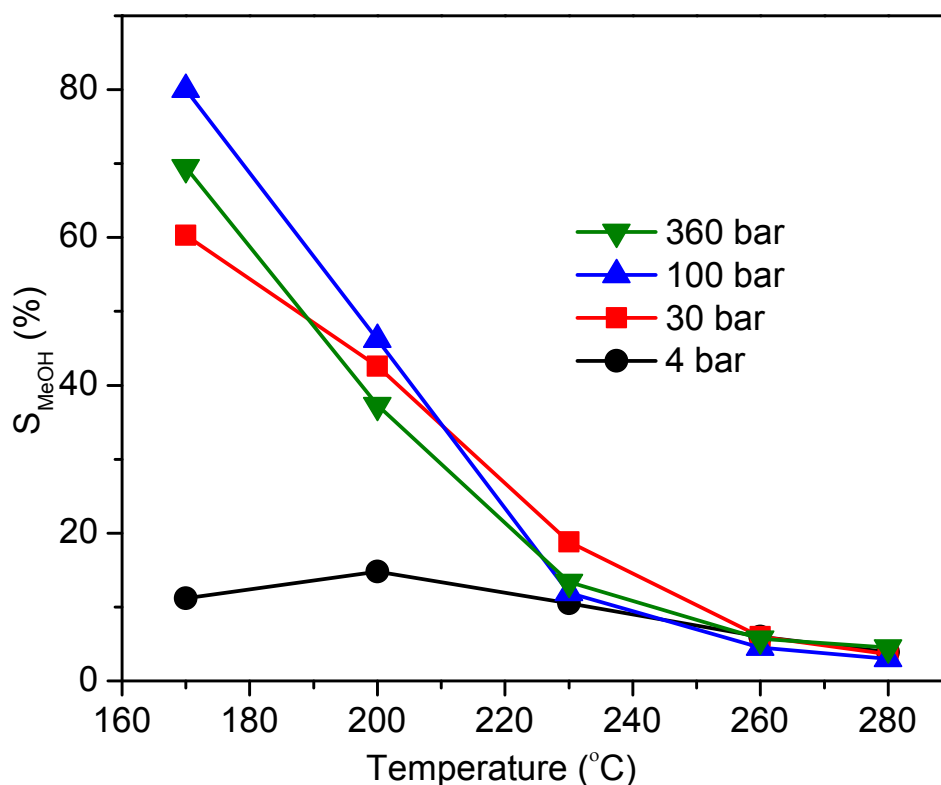


Figure 3.6 Methanol selectivity for the $\text{Cu}/\text{Al}_2\text{O}_3$ catalyst against temperature at different pressure conditions at $\text{GHSV} = 4000 \text{ h}^{-1}$ and $\text{CO}_2:\text{H}_2 = 1:3.8$.

Figure 3.6 shows the influences of pressure and temperature on methanol selectivity. At high pressures ($>30 \text{ bar}$), methanol selectivity was higher at lower temperatures. The rise in pressure resulted in increase in CO_2 conversion, as clear from Figure 5, while retaining the similar level of methanol selectivity, thus enhancing methanol productivity at low temperatures. Interestingly, with the increase in reaction temperature methanol yield increased and reached plateau at 4 and 30 bar (Appendix A, Table A.1). In contrast, it decreased at 100 and 360 bar because of enhanced catalytic activity towards RWGS above $230 \text{ }^{\circ}\text{C}$. The comparison at $200 \text{ }^{\circ}\text{C}$ showed over 7-fold increase in methanol yield when the reaction pressure was raised from 30 to 360 bar. The highest methanol yield of $103.4 \text{ mg}\cdot\text{g}_{\text{cat}}^{-1}\cdot\text{h}^{-1}$ was achieved at $200 \text{ }^{\circ}\text{C}$ and 360 bar. Among the data above the confident accuracy for CO_2 quantification and the detection

Impact of promoters and high pressure on impregnated Cu/Al₂O₃ catalysts

limit of the products (the cases where CO₂ conversions were > 1 %), the highest methanol selectivity was 69.5 % at 360 bar with good methanol yield of 75.0 mg·g_{cat}⁻¹·h⁻¹ at the lowest examined temperature of 170 °C.

The CO selectivity was greatly increased at higher temperatures as expected from thermodynamics because of the endothermic nature of RWGS reaction. As the reaction temperature was raised from 170 to 280 °C, roughly 15-, 71-, 146-, and 28-fold increases in CO productivity were observed at 4, 30, 100 and 360 bar, respectively (Appendix A, Table A.1) Pressure had an impact on the RWGS reaction activity, but its influence was minor compared to that of temperature as expected from the thermodynamic calculation (20). The highest CO yield of 718.2 mg·g_{cat}⁻¹·h⁻¹ was observed at 280 °C, 360 bar with a high CO selectivity of 91.7%.

The formation of dimethyl ether was significant, in some cases with its selectivity and yield exceeding those of methanol (at 260, 280 °C at 30, 100 bar). The formation of dimethyl ether was more significant above 200 °C. The highest yield of 130.9 mg·g_{cat}⁻¹·h⁻¹ was observed at 280 °C, 100 bar (Appendix A, Table A.1).

Trace amount of methyl formate was also observed at 30 bar which was completely absent at 4 bar. Further rise in pressure increased methyl formate selectivity, with maximum of 3.1 % at 360 bar and at 170 °C. Above 260 °C the formation of methyl formate was found suppressed.

3.3.5.2 Potassium and Barium Promoted Cu/Al₂O₃

CO₂ hydrogenation over the K and Ba promoted Cu/Al₂O₃ catalysts was tested under the identical conditions as above. Figure 3.7 depicts CO selectivity observed for the Cu-K/Al₂O₃ catalyst under various conditions of pressure and temperature. In agreement with the literature, (18) addition of K effectively suppressed the formation of

methanol and promoted CO formation. RWGS reaction was very selective; the selectivity to CO was always higher than 95.0 % above 230 °C at all investigated pressures (Figure 3.7).

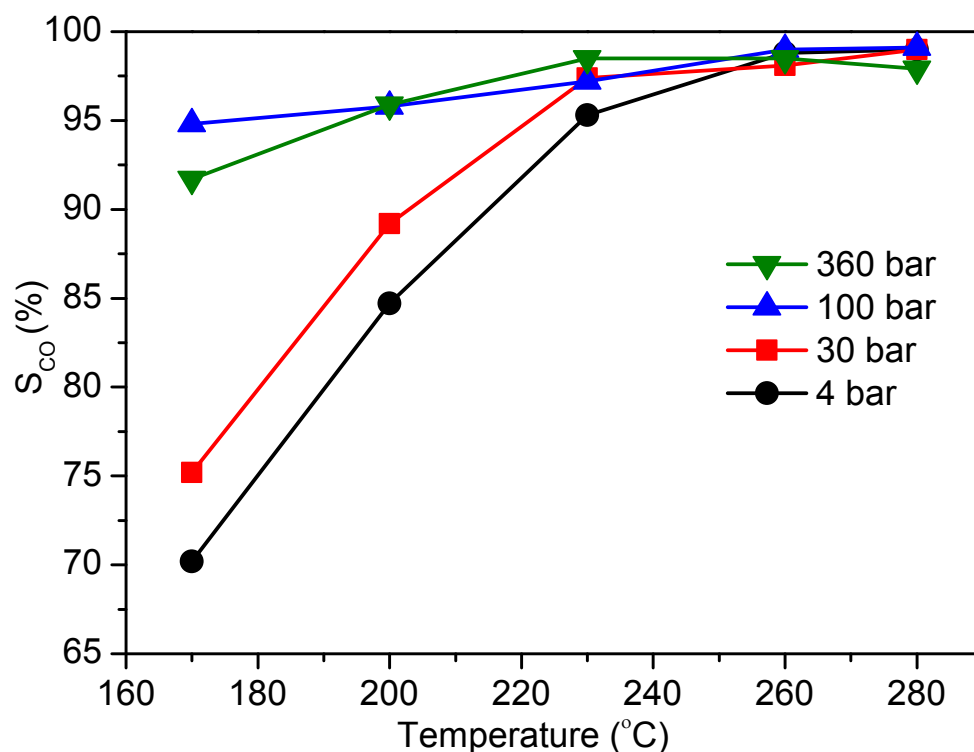


Figure 3.7 CO selectivity for the Cu-K/Al₂O₃ catalyst against temperature at different pressure conditions at GHSV = 4000 h⁻¹ and CO₂:H₂ = 1:3.8.

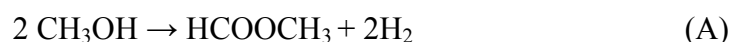
Although the level of CO₂ conversion was very close to that observed for Cu/Al₂O₃ (Appendix A, Table A.2), it is remarkable to observe 94.8 % CO selectivity under the condition (170 °C, 100 bar) where the highest methanol selectivity 80.0 % was achieved for Cu/Al₂O₃ (Figure 3.6), inverting the selectivity between the two main reactions. The selectivity to methanol for Cu-K/Al₂O₃ was always lower than that of Cu/Al₂O₃ except one condition at the lowest temperature and pressure (170 °C, 4 bar) where the methanol selectivity was 29.8 % and the value is less accurate due to the very low CO₂ conversion (Appendix A, Table A.2). K promotion fully suppressed the

Impact of promoters and high pressure on impregnated Cu/Al₂O₃ catalysts

formation of dimethyl ether (Figure 3.9) and methyl formate (Appendix A, Table A.2), whose formations were detected for Cu/Al₂O₃, and CO and methanol were the only products detected under the investigated conditions.

In contrast, Ba promotion positively affected methanol selectivity particularly at low temperatures (Appendix A, Table A.3). Figure 3.8 compares the methanol selectivities for the unpromoted and the K and Ba promoted Cu/Al₂O₃ catalysts at 200 °C at different pressures, highlighting the promoter effects of Ba in methanol synthesis and those of K in RWGS. Similar to K, the promotional effect of Ba was valid (ca. 20 % increase in methanol selectivity compared to the unpromoted catalyst) at all examined pressures and more notable at lower temperatures (Figure 3.8, Appendix A, Table A.3). The increased methanol selectivity of the Ba promoted catalyst was accompanied by slight reduction in CO₂ conversion as compared to the unpromoted and K promoted catalysts. The slight decrease in methanol selectivity above 100 bar can be explained by the formation of methyl formate, whose formation was appreciable for the unpromoted and Ba promoted catalysts (Appendix A, Table A.3). Methyl formate with selectivity of 10.3 % was observed at 360 bar and at 170 °C.

Yu et al. reported that methanol can react with formate species adsorbed on catalyst surfaces to produce methyl formate by transesterification reaction (21). Alternatively, dehydrogenation of methanol can lead to the formation of methyl formate as in reaction (A)



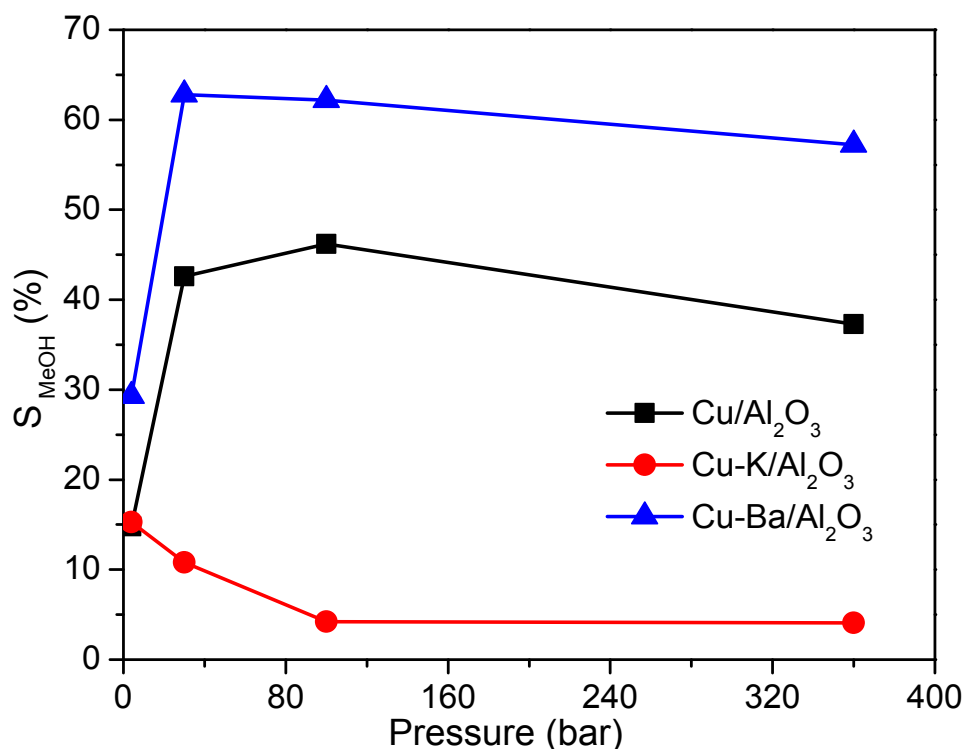


Figure 3.8 Methanol selectivity for the three catalysts at different pressures, $T = 200\text{ }^{\circ}\text{C}$, $\text{GHSV} = 4000\text{ h}^{-1}$, and $\text{CO}_2:\text{H}_2 = 1:3.8$.

A study by Tonner et al. showed that Raney copper, consisting of porous copper with small amount of residual high surface area alumina, was active for dehydrogenation of methanol to methyl formate (22). In our reaction condition, both pathways are possible to form methyl formate, although our high pressure condition of 360 bar likely promoted the formation of surface formate intermediates to promote the former reaction. Also the absence of methyl formate at the lowest examined pressure supports that this would be the most probable pathway. Moreover, the dehydrogenation reaction mentioned in equation A may not be favoured due to the high concentration of H_2 in the reaction.

Moreover, both promoters efficiently suppressed the formation of dimethyl ether which was produced for the unpromoted catalyst (Figure 3.9) in some cases in a greater yield than methanol. Dimethyl ether formation is assumed to occur via dehydration of

methanol. An increase in residence time at higher pressures due to the constant GHSV of this work may have promoted the conversion of methanol to dimethyl ether for the unpromoted catalyst. This was evidenced by the results at 4, 30, and 100 bar (Appendix A, Table A.1). Interestingly, at 360 bar the formation of dimethyl ether was found to be reduced at all examined temperatures.

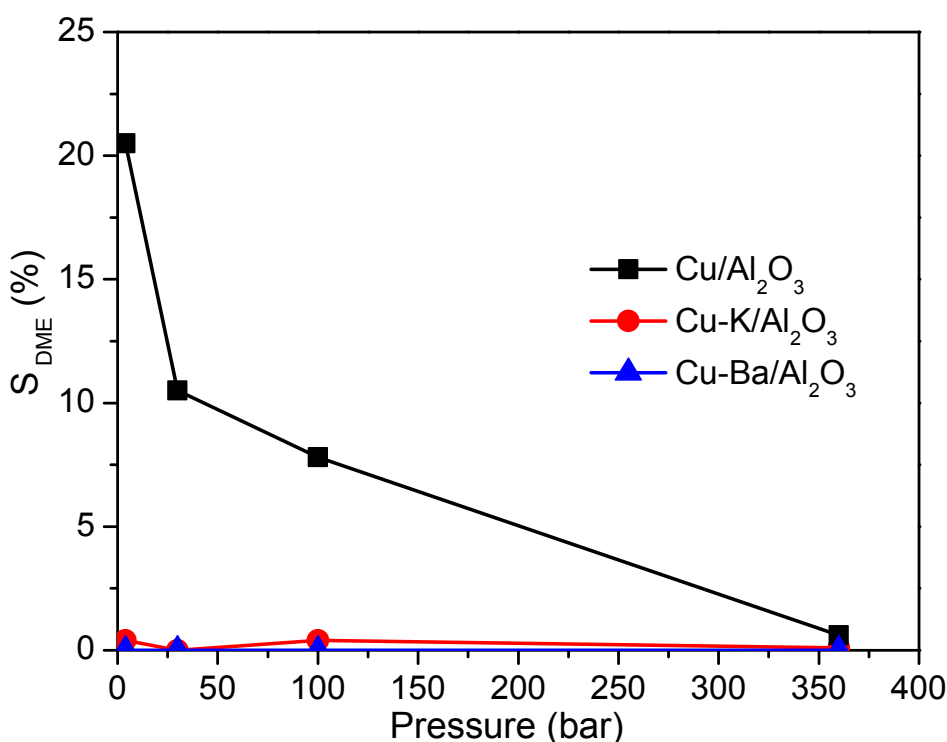


Figure 3.9 Dimethyl ether selectivity for the three catalysts at different pressures, T = 200 °C, GHSV = 4000 h⁻¹, and CO₂:H₂ = 1:3.8.

3.3.6 *In Situ* DRIFTS Study

Surface species present during the reaction on the unpromoted and promoted Cu catalysts were investigated by *in situ* DRIFTS to clarify the influences of the promoters on the formation of specific surface species and thus the catalytic performance. Figure 3.10 compares the DRIFT spectra of the surface species formed on the bare support (γ -Al₂O₃) and on Cu/Al₂O₃ catalyst in the reaction mixture (CO₂:H₂ = 1:3) at the lowest temperature examined in this study (170 °C). This temperature condition was chosen

because the promoter effects were most prominently observed. Although the examined pressure was atmospheric, similar promoter effects as at high pressure conditions of this study were assumed.

Figure 3.10 (a) shows the DRIFT spectra obtained for the γ -Al₂O₃ support. There was no change with the spectral features and only the absorbance of the bands increased with time. The prominent bands formed at 1653, 1435 and 1228 cm⁻¹ are assigned to surface bicarbonates (23-25). The bicarbonate species dominates the surface of the alumina under the reaction condition in the absence of metal components. The minor bands at 1472 and 1389 cm⁻¹ can be assigned to the asymmetric and symmetric OCO stretching frequencies of a monodentate carbonate (26-28). As reported by Bando et al., the formation of carboxylate species was indicated by the broad bands at 1560 and 1360 cm⁻¹ (23). Absence of bands in the CH stretching region rules out the formation of surface formate species on γ -Al₂O₃.

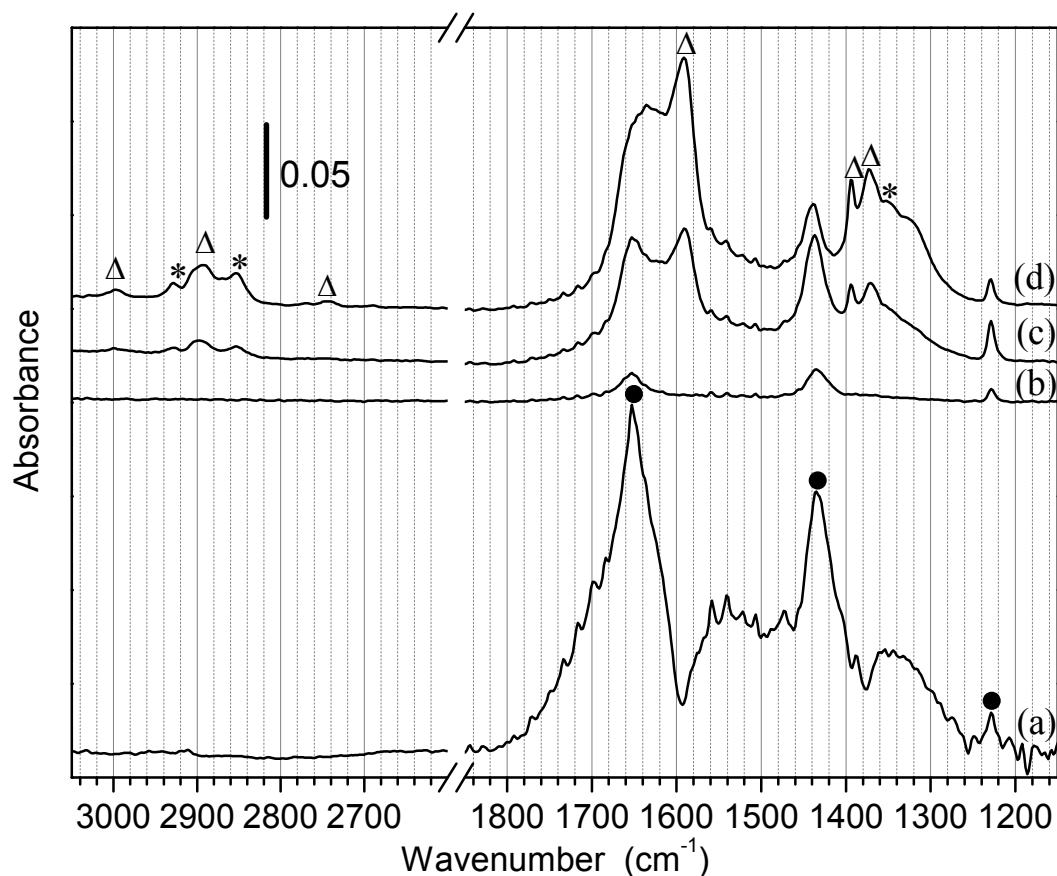


Figure 3.10 *In situ* DRIFT spectra of catalysts when exposed to CO₂:H₂ = 1:3 at 170 °C for (a) Al₂O₃ after 10 min and for Cu/Al₂O₃ after (b) 1, (c) 3, and (d) 10 min.

Characteristic bands of the following surface species are shown with symbols: (●) bicarbonate, (Δ) formate on alumina, (*) formate on copper.

Surface species drastically changed when Cu was present on the surface of γ -Al₂O₃. Figure 3.10 (b-d) shows the evolution of surface species during the reaction over Cu/Al₂O₃. Initially, rapid formation of bicarbonate species was observed (Figure 3.10 (b)), most likely formed on the alumina surface. As the bicarbonate bands gained intensity further, the formation of bidentate formates on Cu was evidenced by the bands at 2930, 2850, and 1350 cm⁻¹(29). For the bidentate formates on Cu, an additional band at ca. 1580 cm⁻¹ is expected, but this was not firmly confirmed due to the broader nature of the band with less intensity compared to the band at 1350 cm⁻¹(29). The sharp bands at 1597, 1394, and 1377 cm⁻¹ can be assigned to formates on alumina (30). Also, the

positions of the bands in the C-H stretching region (2999, 2890, and 2743 cm^{-1}) are identical to those observed when formic acid is adsorbed and evacuated at 200 °C on alumina (23). Therefore, we assign these bands to formate species on the alumina surface. At the steady state (Figure 3.10 (d)) the bicarbonate bands became less intense, while the formate bands became more prominent. This contrast in the surface species given by the presence or absence of Cu clearly indicates that the formate species formed on the Cu surface migrate to the alumina surface and gradually covers the latter surface during the reaction. The gradual decrease of bicarbonate species indicates the replacement of bicarbonate species by formate species on the alumina surface.

Furthermore, the effects of K and Ba promoters on the formation of surface species were investigated by the identical experiments with Cu-K/ Al_2O_3 and Cu-Ba/ Al_2O_3 (Figure 3.11). Similar to the case of Cu/ Al_2O_3 , initially the formation of bicarbonate species was confirmed but to a lesser extent for Cu-Ba/ Al_2O_3 (Figure 3.11 (a-c)) with a similar temporal profile as observed for Cu/ Al_2O_3 ; an initial increase and later decrease of the bicarbonate bands with time. This is likely due to the modification of the alumina surface by the Ba promoter as evidenced from less formation of bicarbonate species and less distinct formate species on alumina. Importantly, bidentate formate species on the Cu surface was confirmed by the bands at 2930, 2850, and 1350 cm^{-1} , even more clearly identifiable than the case of the unpromoted Cu catalyst. The results prove a good accessibility of the Cu surface under the reaction condition when promoted with Ba.

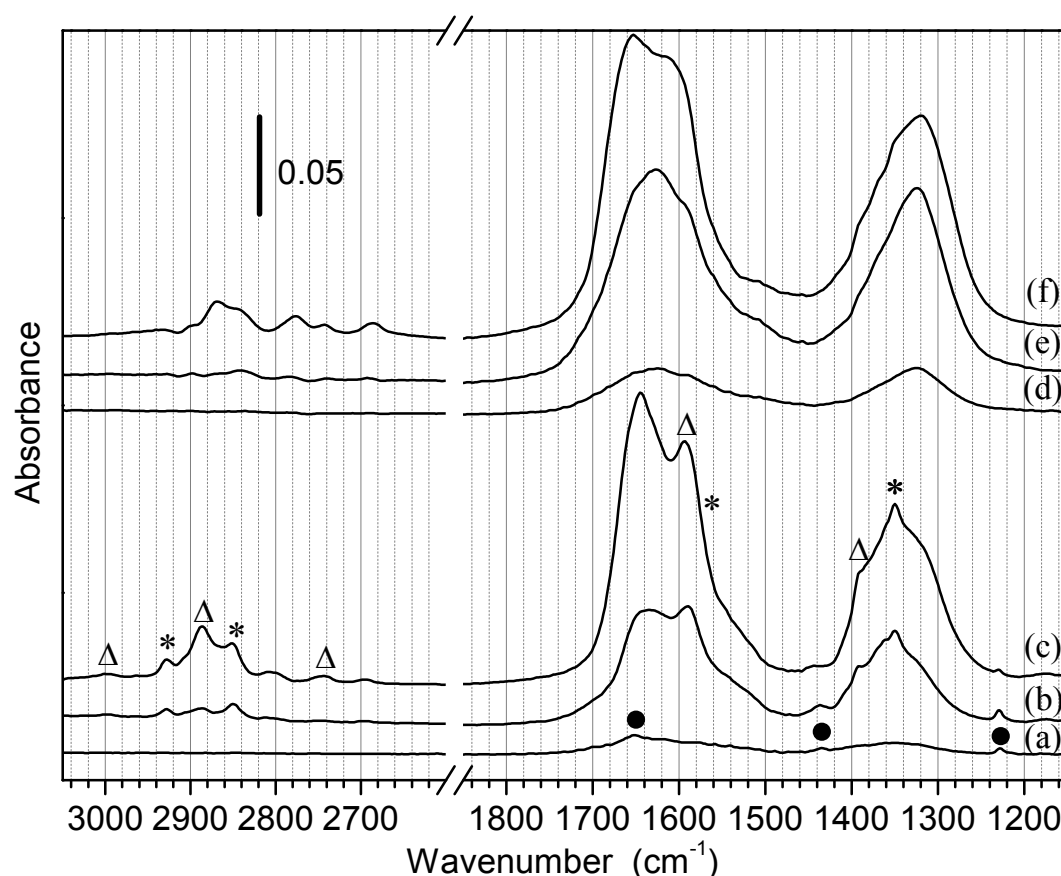


Figure 3.11 *In situ* DRIFT spectra of catalysts when exposed to CO₂:H₂ = 1:3 at 170 °C for Cu-Ba/Al₂O₃ after (a) 1, (b) 3, and (c) 10 min and for Cu-K/Al₂O₃ after (d) 1, (e) 3, and (f) 10 min. Characteristic bands of the following surface species are shown with symbols: (●) bicarbonate, (Δ) formate on alumina, (*) formate on copper

More prominent promoter effects on the type of formed surface species were evidenced for Cu-K/Al₂O₃ (Figure 3.11 (d-f)). Notably, no formation of bicarbonate species was observed from the initial period of the reaction, and the absence of formate species on Cu was suggested both in the C-H and C-O stretching regions. This is clear evidence that the K promoter is well dispersed and strongly modified the surface properties of both Cu and alumina. The bands at 2775, 2685, 1590, 1350-1330 cm⁻¹ are assigned to the bidentate formate due to the specific interactions with K (13, 31, 32). Different spectral features in the C-H stretching region compared to those of Cu/Al₂O₃

and Cu-Ba/Al₂O₃ as well as the very broad feature of the two bands between 1700 - 1200 cm⁻¹ imply that various configurations of formate species exist on the surface. Figure 3.12 shows the pictorial representation of possible intermediates and the arrangements of promoters on the surfaces of the three catalysts indicated from *ex situ/in situ* characterization results.

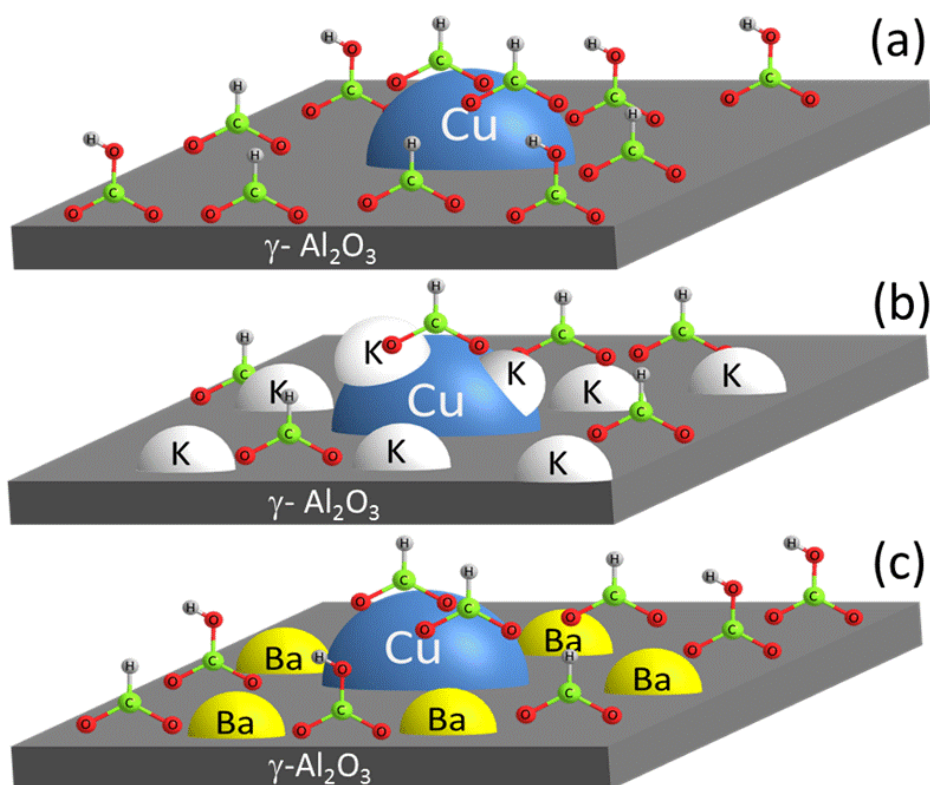


Figure 3.12 Pictorial representation of possible intermediates and arrangement of promoters on the catalyst surface derived from characterization techniques and *in situ* IR study. (a) Cu/Al₂O₃, (b) Cu-K/Al₂O₃, and (c) Cu-Ba/Al₂O₃

3.3.7 Impact of K and Ba Promoters and Possible Reaction Mechanisms

The catalytic tests clearly showed the prominent effects of K/Ba promoters to the Cu/Al₂O₃ catalyst and on the product selectivity in methanol synthesis at low and elevated pressures. For Cu/Al₂O₃ and Cu-Ba/Al₂O₃, the productivity of methanol was

found always higher than those reported in literature under similar GHSV conditions, (33-35) benefited from our high-pressure approach. All three catalysts greatly enhanced the RWGS activity at higher temperatures. At 4 bar, the obtained conversions for Cu/Al₂O₃ and Cu-K/Al₂O₃ catalysts were comparable to those reported for Cu/SiO₂ and K promoted Cu/SiO₂ (4).

The addition of K and Ba promoters played significant roles in selecting the path over the two major competitive reactions, i.e. methanol synthesis and RWGS, occurring in CO₂ hydrogenation reaction. Although controversies exist on the reaction mechanisms, it has been widely reported in literature that formate dissociation, forming CO, is the major reaction path for RWGS reaction, (36-41) while hydrogenation of formate species is the major one for the methanol formation (36, 42-46). Correlating the results obtained in the present investigation to those in the literature, we propose that the addition of K promoter enhances the formate dissociation capability; whereas the addition of Ba promoter inhibits the dissociation process or promotes the formate hydrogenation process.

As evident from characterization results, the K promotion to the Cu/Al₂O₃ catalyst strongly reduced the Cu metal surface area and slightly altered the BET surface area, indicating that the K promoter covers most of the Cu surface with very high dispersion, possibly as a thin layer, as suggested by XRD. The shifting to higher temperatures of the two peaks for the reduction of CuO in H₂-TPR (Figure 3.3) and also of the peak (I) in CO₂-TPD (Figure 3.4) of the Cu-K/Al₂O₃ catalyst compared to those of the unpromoted one indicates hindering the reduction process and thus low hydrogenation activity of the Cu, possibly due the coverage of the K promoter over Cu surface. The absence of formates directly associated with Cu and bicarbonate species on the alumina surface clarified by *in situ* DRIFTS study also confirms the full coverage of

Cu surface and a strong modification of surface acidity by the K promoter. It identified the presence of unique types of surface formates interacting with K by the creation of active sites at the interface between Cu and K (4, 18, 47). The dominant presence of formates interacting with K-Cu and over the alumina surface without exposed Cu surface promoted dissociation of formates over the formate hydrogenation, resulting in the high RWGS selectivity of Cu-K/Al₂O₃

In case of the Ba promotion, a significant reduction in BET surface area was observed with unexpected increase in copper metal surface area. The XRD pattern of the as-prepared and spent catalyst revealed that the barium component exists as barium carbonate but in highly dispersed state as indicated by the very broad and weak diffraction peaks. The Ba promoter obviously interacts with Cu components during the activation (reduction in H₂ process, Figure 3.3), facilitates the reduction of CuO, and prevents the sintering as observed by the smaller Cu crystallite size in Cu-Ba/Al₂O₃ than that in Cu/Al₂O₃, while keeping the Cu surface exposed and not covering it as evidenced from *in situ* DRIFTS study. The CO₂-TPD study (Figure 3.4) showed the increased amount of released CO₂ from the surface species while retaining the same desorption temperature of peak (I) of Cu/Al₂O₃. This result indicates higher concentration of surface species, formates according to the *in situ* DRIFTS study, when the catalyst is promoted with Ba and the easiness of their decomposition as in Cu/Al₂O₃. According to the higher temperature of the peak (I) observed for Cu-K/Al₂O₃, this decomposition of surface formates is assisted by exposed Cu surface. It is generally accepted that higher Cu metal surface area is beneficial for methanol synthesis by CO₂ hydrogenation (48). The exposed high metallic Cu surface as well as the low stability of the surface formate species in the Ba promoted catalyst likely promoted its

hydrogenation to methanol rather than formate dissociation leading to the formation of CO.

During the reaction, the Ba promoter might not exist as barium carbonate as observed in XRD of the as prepared and spent Cu-Ba/Al₂O₃ catalysts. It is possible that carbonates were formed after the exposure of catalyst to air. The absence of barium carbonates after the reduction was also reported by Weigel et al. by *in situ* IR spectroscopy (49). It is most likely that barium exists as hydroxide or oxide, forming transient carbonate species. Millar et al. have reported that alkali ions form hydroxylic species in the presence of water (50). According to reactions (1) and (2), water is the side product and always present during CO₂ hydrogenation. Therefore, it is unlikely that barium can exist in an oxide state under the reducing reaction conditions and in presence of water. The XRD pattern obtained after the reaction shows increased crystallite size of barium carbonate. The proneness of barium hydroxides to form large particles by agglomeration was reported in the study of Vedage et al. (6). From these observations, we speculate that the barium component remains in a hydroxide state, temporarily forming its carbonates, during the reaction.

Moreover, the formation of dimethyl ether was observed mainly for Cu/Al₂O₃. It has been proven that the selective dehydration of methanol is conditioned by the acidic function of the solid-acid catalysts such as γ -alumina, (51, 52) which was used in this study as the support material. Although γ -alumina catalyses the methanol dehydration reaction to form dimethyl ether, Xu et al. reported that water blocks the active sites through competitive adsorption with methanol on the catalyst surface (53). Also, the study by Jun et al. showed that an addition of water rapidly (in ca. 20 min) deactivates the alumina catalyst activity towards dimethyl ether synthesis (54). The formation of methanol or CO involves the formation of equal amount of water. In this study, the

highest amount of methanol and CO was observed at 360 bar, which in return implies the highest amount of water formation under these conditions. Thus, a significant amount of water formed during the reaction might have modified the surface sites of γ -alumina, inhibiting the formation of dimethyl ether as evidenced by the strong suppression of the reaction at 360 bar for Cu/Al₂O₃. Also, this reaction was fully suppressed in case of K promotion and efficiently suppressed in case of Ba promotion. It is possible that acidic sites on the alumina were neutralised by the addition of alkali and alkaline earth metal components. In case of K promotion, no dimethyl ether formation was observed likely due to the high level of suppression of methanol synthesis activity as well as homogeneous coverage of the catalyst surface by the K component. In case of Ba promoter, higher productivity of methanol as well as its major coverage over the alumina support, as indicated by significantly less amount of bicarbonate species over Cu-Ba/Al₂O₃ compared to that observed over Cu/Al₂O₃, resulted in a good level of inhibition of the dehydration activity of alumina, thus the efficient suppression for dimethyl ether formation, and enhancement of methanol selectivity.

Furthermore, Ai studied the impact of alkali and alkaline earth metal on dehydrogenation activity of methanol to methyl formate (48). Both types of promoters showed increase in the activity but the effect was more prominent in the latter case. The findings were explained by the modification of acid-base properties of the support and metal catalyst. Although both K and Ba promoters were reported to enhance the activity in methanol dehydrogenation, we observed the formation of methyl formate with increase in pressure and at low temperatures with Cu-Ba/Al₂O₃. It is speculated that under these reaction conditions the concentration of methanol became sufficiently high to produce methyl formate by the enhanced methanol productivity from the positive

impacts of high-pressure and Ba promotion. On the other hand, no methyl formate could be detected because of the low activity of Cu-K/Al₂O₃ in methanol synthesis.

3.4 Conclusions

The positive impacts of high pressure conditions to achieve high conversion and selectivity towards methanol in CO₂ hydrogenation reaction have been shown. As expected, reaction temperature had a drastic influence on catalytic performance. It has been clearly demonstrated that low temperatures and high pressures are favourable conditions for methanol synthesis using the Cu/Al₂O₃ catalyst prepared by the impregnation route of this work. The formation of dimethyl ether over Cu/Al₂O₃ due to dehydration of methanol, mediated by the surface acidity of alumina, was greatly suppressed at 360 bar. This shows that increase in pressure strongly enhances the catalyst activity and it is likely that amount of water formed as co-product is sufficiently high to inhibit the side dehydration reaction to dimethyl ether.

Potassium and barium promotion had great influence on selection of the CO₂ hydrogenation pathways. K and Ba promotion enhanced CO and methanol selectivity, respectively, the tendency being particularly prominent at lower temperatures. Effect of the promoters on product distribution profile was found to be consistent with increase in pressure; where effect of K promoter was more prominent than the Ba. Both promoters efficiently hindered the formation of dimethyl ether, which can be correlated with the neutralisation of alumina acidity by the promoters. Further increase in pressure to 360 bar resulted in the observation of good amount of methyl formate along with methanol for Cu-Ba/Al₂O₃, which was explained by the unique combination of the high methanol production and the modified surface acid-base property given by the Ba promotion. The

promoter effects on the surface species under reaction conditions have been clearly identified by *in situ* DRIFTS study.

Both promoters were highly dispersed over the catalyst; the Ba component exists as small crystallites mainly on the alumina support but interacts strongly with Cu and promotes the reducibility of Cu, while the K component exists as nano-crystallites or thin layers covering the surfaces of both the alumina and copper. The high accessibility and enhanced reducibility of the Cu surface of the Ba promoted catalyst was beneficial for the formation of surface formates and further hydrogenation to methanol. On the other hand, for Cu-K/Al₂O₃ the Cu surface was covered by K promoter and the hydrogenation ability of Cu was hindered by the promotion. This effect and enhanced formation of surface formates on the alumina surface by the K promotion likely led to enhanced probability of surface formate decomposition, as the major path for RWGS reaction.

References

1. M. Piacentini, M. Maciejewski, A. Baiker, *Appl. Catal. B-Environ.* **59**, 187 (2005).
2. N. Maeda, A. Urakawa, R. Sharma, A. Baiker, *Appl. Catal. B-Environ.* **103**, 154 (2011).
3. Y. Liu, M. Meng, X.-G. Li, L.-H. Guo, Y.-Q. Zha, *Chem. Eng. Res. Des.* **86**, 932 (2008).
4. C.-S. Chen, W.-H. Cheng, S.-S. Lin, *Appl. Catal. A-Gen.* **238**, 55 (2003).
5. F. Meshkini, M. Taghizadeh, M. Bahmani, *Fuel* **89**, 170 (2010).
6. A. Vedage G, B. Himelfarb P, W. Simmons G, K. Klier, in *Solid State Chemistry in Catalysis*. (American Chemical Society, 1985), 279, pp. 295-312.
7. A. S. Nowick, *AIChE J.* **2**, 140 (1956).
8. J. W. Evans, M. S. Wainwright, A. J. Bridgewater, D. J. Young, *Appl. Catal.* **7**, 75 (1983).
9. B. Abu-Zied, S. Soliman, *Catal. Lett.* **132**, 299 (2009).

10. S. Xie, J. H. Lunsford, *Appl. Catal. A-Gen.* **188**, 137 (1999).
11. M.-Y. Kim *et al.*, *Korean J. Chem. Eng.* **27**, 76 (2010).
12. R. M. Levy, D. J. Bauer, *J. Catal.* **9**, 76 (1967).
13. M. Kantschewa, E. V. Albano, G. Ertl, H. Knözinger, *Appl. Catal.* **8**, 71 (1983).
14. W.-P. Dow, Y.-P. Wang, T.-J. Huang, *J. Catal.* **160**, 155 (1996).
15. I. Arvanitidis, D. Siche, S. Seetharaman, *Metall. Mater. Trans. B* **27**, 409 (1996).
16. R. L. Lehman, J. S. Gentry, N. G. Glumac, *Thermochim. Acta* **316**, 1 (1998).
17. M. E. Jørgensen, P. J. Godowski, J. Onsgaard, *Vacuum* **48**, 299 (1997).
18. D. B. Clarke, A. T. Bell, *J. Catal.* **154**, 314 (1995).
19. I. A. Bönicke, W. Kirstein, F. Thieme, *Surf. Sci.* **307-309, Part A**, 177 (1994).
20. L. Hui, L. Zanchun, Z. Bingchen, *Fuel Sci. Technol. Int.* **12**, 815 (1994).
21. K. M. K. Yu, C. M. Y. Yeung, S. C. Tsang, *J. Am. Chem. Soc.* **129**, 6360 (2007).
22. S. P. Tonner, D. L. Trimm, M. S. Wainwright, N. W. Cant, *Ind. Eng. Chem. Prod. Rd.* **23**, 384 (1984).
23. K. K. Bando, K. Sayama, H. Kusama, K. Okabe, H. Arakawa, *Appl. Catal. A-Gen.* **165**, 391 (1997).
24. J. Baltrusaitis, J. H. Jensen, V. H. Grassian, *J. Phys. Chem. B* **110**, 12005 (2006).
25. A. M. Turek, I. E. Wachs, E. DeCanio, *J. Phys. Chem.* **96**, 5000 (1992).
26. J. F. Edwards, G. L. Schrader, *J. Phys. Chem.* **88**, 5620 (1984).
27. J. F. Edwards, G. L. Schrader, *J. Phys. Chem.* **89**, 782 (1985).
28. J. F. Edwards, G. L. Schrader, *J. Catal.* **94**, 175 (1985).
29. Y. Yang *et al.*, *Catal. Lett.* **125**, 201 (2008).
30. R. G. Greenler, *J. Chem. Phys.* **37**, 2094 (1962).
31. G. J. Millar, C. H. Rochester, K. C. Waugh, *J. Catal.* **155**, 52 (1995).
32. J. D. Donaldson, J. F. Knifton, S. D. Ross, *Spectrochim. Acta* **20**, 847 (1964).
33. H. Sakurai, M. Haruta, *Catal. Today.* **29**, 361 (1996).
34. H. Sakurai, M. Haruta, *Appl. Catal. A-Gen.* **127**, 93 (1995).
35. J.-L. Dubois, K. Sayama, H. Arakawa, *Chem. Lett.* **21**, 5 (1992).
36. J. Yoshihara, C. T. Campbell, *J. Catal.* **161**, 776 (1996).
37. C.-S. Chen, W.-H. Cheng, S.-S. Lin, *Catal. Lett.* **68**, 45 (2000).
38. T. Shido, Y. Iwasawa, *J. Catal.* **140**, 575 (1993).
39. H. Arakawa, J. L. Dubois, K. Sayama, *Energ. Convers. Manage.* **33**, 521 (1992).
40. T. van Herwijnen, W. A. de Jong, *J. Catal.* **63**, 83 (1980).

41. T. van Herwijnen, R. T. Guzalski, W. A. de Jong, *J. Catal.* **63**, 94 (1980).
42. I. Chorkendorff, P. A. Taylor, P. B. Rasmussen, *J. Vac. Sci. Technol., A* **10**, 2277 (1992).
43. P. A. Taylor, P. B. Rasmussen, I. Chorkendorff, *J. Chem. Soc. Faraday. T.* **91**, 1267 (1995).
44. P. B. Rasmussen, M. Kazuta, I. Chorkendorff, *Surf. Sci.* **318**, 267 (1994).
45. T. Fujitani, I. Nakamura, T. Uchijima, J. Nakamura, *Surf. Sci.* **383**, 285 (1997).
46. P. B. Rasmussen *et al.*, *Catal. Lett.* **26**, 373 (1994).
47. G. J. Millar, C. H. Rochester, K. C. Waugh, *J. Chem. Soc. Faraday. T.* **88**, 1477 (1992).
48. M. Ai, *Appl. Catal.* **11**, 259 (1984).
49. J. Weigel, A. Wokaun, K. Horbaschek, A. Baiker, *Berich. Bunsen. Gesell.* **101**, 1097 (1997).
50. G. J. Millar, C. H. Rochester, K. C. Waugh, *J. Catal.* **142**, 263 (1993).
51. F. Yaripour, M. Mollavali, S. M. Jam, H. Atashi, *Energy Fuels* **23**, 1896 (2009).
52. R. S. Schiffino, R. P. Merrill, *J. Phys. Chem.* **97**, 6425 (1993).
53. M. Xu, J. H. Lunsford, D. W. Goodman, A. Bhattacharyya, *Appl. Catal. A-Gen.* **149**, 289 (1997).
54. K.-W. Jun, H.-S. Lee, H.-S. Roh, S.-E. Park, *Bull. Korean Chem. Soc* **24**, 106 (2004).

4

High Pressure CO₂ Hydrogenation Over Co-precipitated Cu/ZnO/Al₂O₃ Catalysts

4.1 Introduction

The catalyst synthesis method plays important role in determining the catalytic activity in a specific reaction. It is widely known that catalysts prepared by co-precipitation technique could yield better catalytic performance if the synthesis conditions are controlled carefully. Together with a best performing catalyst, the reaction parameters also needs to be carefully optimized to improve the process efficiency. CO₂ hydrogenation to methanol usually suffers low CO₂ conversion and low space time methanol yields, and often requires the recycling of the feed gas to enhance the overall productivity of the process. According to thermodynamics, decrease in temperature and increase in reaction pressure should favour the methanol formation (1). Ipatieff and Monroe reported high pressure CO₂ hydrogenation up to 412 bar over Cu/Al₂O₃ catalysts in a fixed bed reactor, which showed remarkable selectivity to methanol and high conversion of CO₂ (2). However, in their study the gas hourly space velocity (GHSV), indicative of the productivity of the reaction, was very low (ca. 1,000 h⁻¹) to make the process practically viable.

This chapter presents a high pressure (up to 360 bar) CO₂ hydrogenation process using coprecipitated Cu/ZnO/Al₂O₃ catalysts. The reaction parameters such as CO₂:H₂ feed ratio, temperature, pressure and GHSV were optimized to achieve full one-pass

conversion of CO₂ while retaining high productivity of methanol. The catalytic performance of high pressure methanol synthesis reaction is compared with theoretical chemical equilibria to gain mechanistic and energetic insights. Further, the performance of commercial methanol synthesis catalyst was evaluated to show the general applicability of the developed process and methanol space time yields obtained at different GHSVs are presented.

4.2 Methods

4.1 Catalyst Synthesis

For the synthesis of Cu/ZnO/Al₂O₃, aqueous solutions of 0.2 M copper nitrate hexahydrate (98-102 %, Alfa Aesar), 0.2 M zinc nitrate hexahydrate (98%, Sigma-Aldrich), and 0.2 M aluminium nitrate nonahydrate (≥98 %, Fluka) with 0.5 M potassium hydroxide (≥85 %, Sigma-Aldrich) were slowly added together, in a round bottom flask to precipitate the corresponding hydroxides. Deionized water was used for catalyst synthesis. During the precipitation, the round bottom flask was heated at 80 °C under constant stirring, and the pH of the solution with precipitate was maintained between 9.5-10.5. The precipitate was aged for two days, filtered, and washed with water until the pH of the washed solution reached the value of 7.5. Then, the sample was dried at 100 °C overnight, crushed, and calcined in air at 400 °C for 4 h to yield Cu/ZnO/Al₂O₃. Using similar method coprecipitated Cu/Al₂O₃ catalyst was prepared. Another Cu/Al₂O₃ (18/82 wt %) catalyst was prepared by the incipient wetness impregnation method. The preparation method and catalyst properties are described elsewhere (3). A commercial methanol synthesis catalyst was purchased from Alfa Aesar (Product ID: 45776). Prior to charging the catalysts into reactor, they were pelletized, crushed, and sieved a size of 100–300 μm. Elemental composition, Cu

surface area, CuO crystallite size and BET surface area of the synthesized and commercial catalysts are listed in Table 4.1. For methanol synthesis, 170 mg of Cu/ZnO/Al₂O₃ (I) was used. In the study of very low to high GHSVs using the commercial catalyst, 1000, 85 or 42.5 mg of the catalyst was used for the catalytic tests in the range of 425, 10,000–40,000 or 81,000–182,000 h⁻¹, respectively.

4.2 Catalyst Characterization

XRD patterns were recorded on Bruker AXS D8 Advance diffractometer equipped with a Cu tube, a Ge (1 1 1) incident beam monochromator ($\lambda = 0.1541$ nm), and a Vantec-1 PSD operated in transmission mode. Data were recorded in the range of 5-70° 2 θ with a step size of 0.02° and a counting time of 4 s per step. The crystallite sizes of CuO, Cu, and BaCO₃ mentioned in Table 3.1 were estimated from the full width at half maximum (FWHM) of corresponding peaks using Scherrer equation with the shape factor of 0.9 assuming the spherical particles (4). (2 0 -2) reflection for CuO, (111) reflection for Cu, and (111) reflection for BaCO₃ were used to determine the crystallite size.

N₂ isotherms at -196 °C were measured on a Quantachrome Autosorb 1-MP analyzer. Prior to analysis, the samples were degassed in vacuum at 300 °C for 12 h.

The copper surface area and dispersion were measured using nitrous oxide pulse chemisorption method reported by Evans et al. (5). Prior to analysis, samples were reduced in 5% H₂ in He stream at 330 °C, followed by cooling to 90 °C under He flow. A known volume of N₂O was then injected as pulse by using a six port valve. The N₂O at the exit was trapped in liquid N₂ and evolved N₂ was measured on the calibrated mass spectrometer, Pfeiffer Omnistar GSD 301 C. Copper metal surface areas were calculated assuming 1.46×10^{19} copper atoms/m² (5).

The elemental composition was determined by ICP analysis. The amount of K in the prepared catalysts was <0.05 wt % according to ICP analysis, ensuring virtually complete removal of the precipitating agent.

4.3 Thermodynamic Calculation

Thermodynamic equilibrium calculations were performed using the Soave-Redlich-Kwong (SRK) equation of state (EOS). The SRK-EOS binary interaction parameters for CO, CO₂, H₂, methanol, and water were taken from the optimized values recently reported by van Bennekom and coworkers for methanol synthesis processes (6). A single phase (vapor) was assumed and the calculations were performed by minimization of Gibbs free energy using the Gibbs reactor implemented in the DWSIM package.

The total pressure of 330 and 182 bar was investigated to mimic our experimental condition of 360 and 200 bar because of the presence of 10 % Ar in H₂ for GC analysis in our reaction mixture (e.g. we have CO₂:H₂:Ar = 1:10:1.11 in case CO₂:H₂ = 1:10 is shown). For the sake of comparison, the same calculation was performed at 30 bar.

For the most proper calculation, one should take into account the phase separation as described in van Bennekom et al.(6, 7), which likely takes place below 200 °C above 200 bar at CO₂:H₂ = 1:3. Our optimal reaction conditions are at considerably higher temperatures with much higher H₂ partial pressure. Therefore, we expect that we have one phase system under most of the reported conditions, although detailed investigation by experiments and theory is necessary.

4.3 Results and Discussion

4.3.1 Physicochemical Characterization

Table 4.1 BET surface area, Cu surface area after reduction pretreatment, and average crystallite size of CuO for as-prepared and commercial catalysts.

Catalyst	BET surface area (m ² /g)	Elemental analysis (wt %)			S _{Cu} (m ² /g _{cat})	Cryst. size of CuO (nm)
		CuO	ZnO	Al ₂ O ₃		
Cu/Al ₂ O ₃ (Impr.)	184	-	-	-	2.2	50.5
Cu/Al ₂ O ₃	168	43.3	0	56.7	6.4	9.7
Cu/ZnO/Al ₂ O ₃ (I)	125	27.8	26.5	45.7	1.7	6.9
Cu/ZnO/Al ₂ O ₃ (II)	22	46.7	43.9	9.3	4.2	16.0
Commercial catalyst*	-	63.5	24.7	10.1	17.5	3.9

* The commercial catalyst contains 1.3 % MgO.

Table 4.1 shows physicochemical characterization data of all the catalysts investigated in this study. As expected the co-precipitated catalyst shows smaller crystallite size when compared with the impregnated catalyst. The effect of copper and zinc loading can be recognized by the reduction in copper metal surface area. The catalysts containing ZnO show reduction in copper metal surface area compared to the co-precipitated Cu/Al₂O₃. The BET surface area was found to be decreasing at lower Al₂O₃ content in the catalysts. Among all, the commercial catalyst showed the smallest crystallite size with the highest copper metal surface area.

4.3.2 CO₂ Hydrogenation

4.3.2.1 Feed Ratio Study

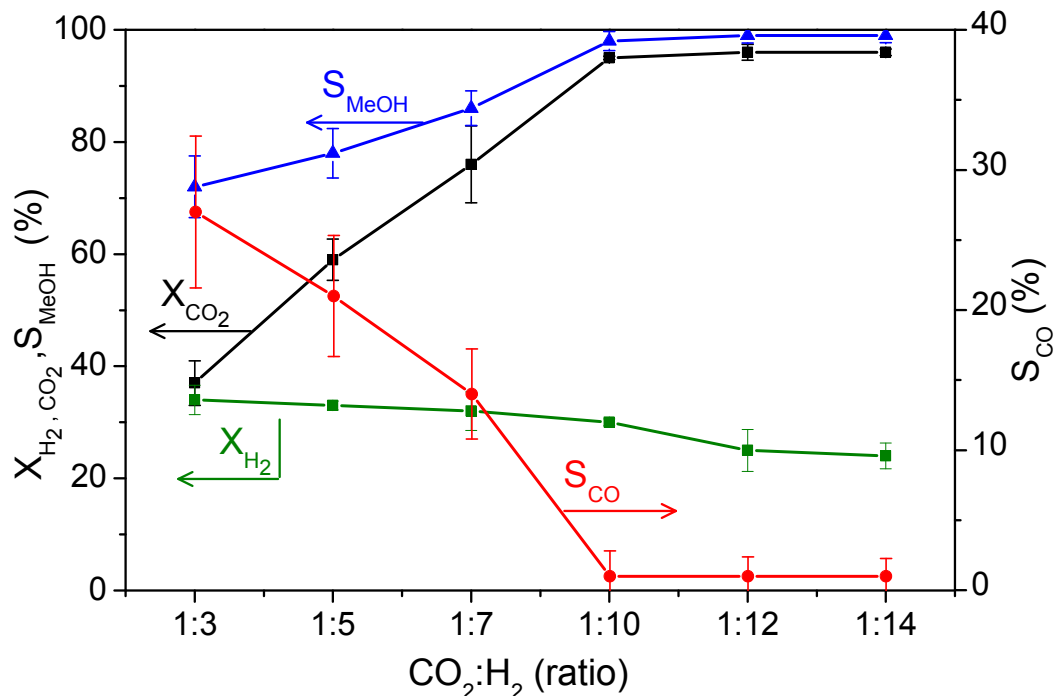


Figure 4.1 Effects of the CO₂:H₂ feed ratio on CO₂ conversion (X_{CO_2}), H₂ conversion (X_{H_2}) and selectivity to CO (S_{CO}), and methanol (S_{MeOH}) in CO₂ hydrogenation over the Cu/ZnO/Al₂O₃ catalyst. Reaction conditions: T = 260 °C, P = 360 bar, GHSV = 10,471 h⁻¹.

Figure 4.1 summarises the effects of feed composition on CO₂ conversion and product selectivity over the Cu/ZnO/Al₂O₃ (I) catalyst at 260 °C, 360 bar, and GHSV of 10,471 h⁻¹. At the conventional CO₂:H₂ molar ratio of 1:3 defined by the stoichiometry of CO₂ hydrogenation to methanol, CO₂ conversion was 37 % with 72 % methanol selectivity. Drastic rise in both values was observed when H₂ partial pressure was further increased to CO₂:H₂ = 1:10. At this ratio CO₂ conversion was outstanding (95 %) with high methanol selectivity (98 %), suppressing CO formation to a negligible extent. Under this condition the methanol weight time yield (WTY) was found to be 1.2

$g_{\text{MeOH}} \cdot g_{\text{cat}}^{-1} \cdot h^{-1}$. The WTYs were smaller at the high H₂ partial pressures due to lower CO₂ mass flow at the constant GHSV (Appendix B, Table B.1).

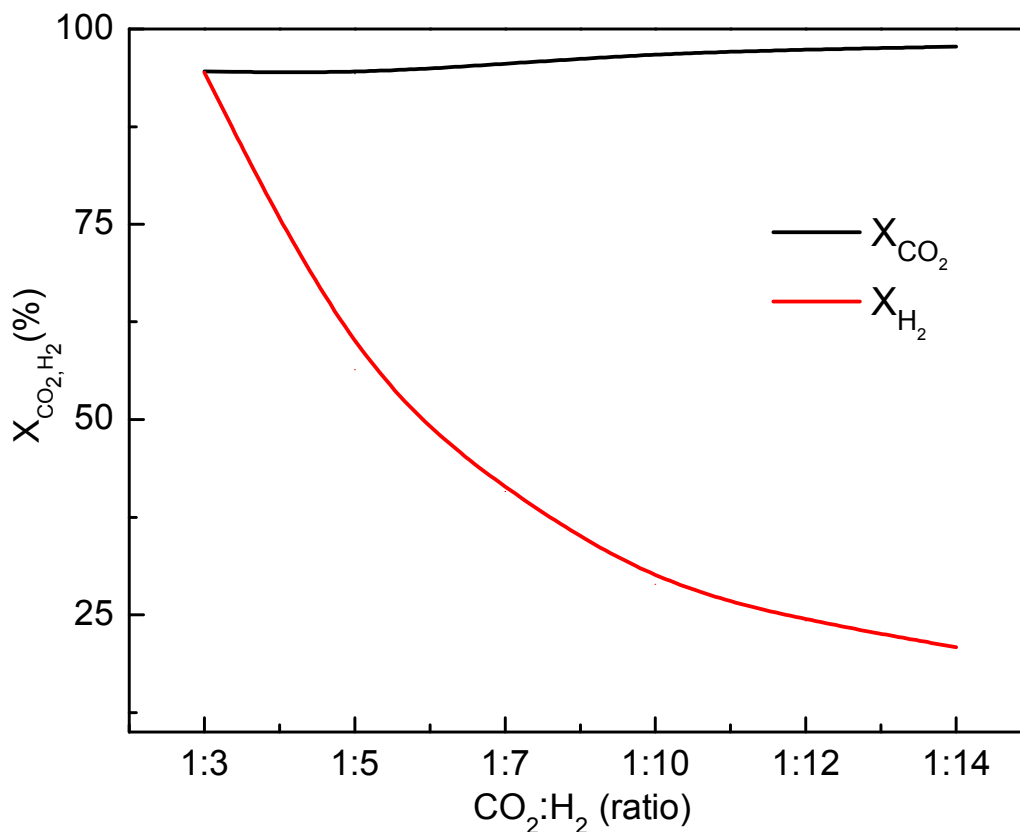


Figure 4.2 Equilibrium conversion of CO₂ (X_{CO₂}) and H₂ (X_{H₂}) at different feed ratios at P = 330 bar, T = 260 °C.

Figure 4.2 depicts the equilibrium conversion for CO₂ and H₂ at various feed ratios at 260 °C and 330 bar. These values for CO₂ and H₂ at various CO₂:H₂ ratios under this reaction condition show interesting insights of the catalytic performance. It is worth highlighting that the equilibrium conversion is very high (>94 %) even when the mixture is at the stoichiometric ratio (CO₂:H₂ = 1:3) under the high pressure condition. Starting from 1:3 ratio, the CO₂ conversion was found to be gradually increasing at higher H₂:CO₂ ratio. Experimentally at CO₂:H₂ = 1:<10, the conversion values are far from the equilibrium values, while at 1:≥10 the values are in a very good agreement

with the calculated equilibrium conversion values. The results indicate that at the feed ratio of $1:\geq 10$ the process operates in the thermodynamic regime reaching the equilibrium CO_2 conversion and methanol selectivity under the investigated condition, whereas at the feed ratio of $1:< 10$ the reaction falls into the kinetic regime. Judging from the similar theoretical equilibrium conversion at the different $\text{CO}_2:\text{H}_2$ ratios, the experimentally observed outstanding CO_2 conversion and methanol selectivity at high H_2 partial pressure (i.e., $\text{CO}_2:\text{H}_2 = 1:\geq 10$) are most likely due to the rate acceleration for methanol formation by the high H_2 partial pressure. Besides, the H_2 conversion was observed to be decreasing with the increase in H_2 partial pressure, as expected from the excess of H_2 relative to CO_2 . However, it should be noted that the energy efficiency towards methanol formation was greatly enhanced at $\text{CO}_2:\text{H}_2 = 1:\geq 10$ because of the suppressed, competitive RWGS ($\text{CO}_2 + \text{H}_2 \rightarrow \text{CO} + \text{H}_2\text{O}$) reaction. The H_2 consumption rate at conventional feed ratio of 1:3 was found to be $88 \text{ mmol}\cdot\text{g}_{\text{cat}}^{-1}\cdot\text{h}^{-1}$ towards methanol and $11 \text{ mmol}\cdot\text{g}_{\text{cat}}^{-1}\cdot\text{h}^{-1}$ towards CO formation, whereas at 1:10, it was $110 \text{ mmol}\cdot\text{g}_{\text{cat}}^{-1}\cdot\text{h}^{-1}$ and almost exclusively used for the production of methanol. This is an important fact in practice because at high H_2 partial pressure the energy (incl. hydrogen molecules as chemical energy) and time (thus for better yield) required for methanol production are minimized and solely used for methanol synthesis. Also, this demonstrated the documented analogies of high pressure advantages between methanol synthesis and classic Haber-Bosch ammonia synthesis processes by achieving the equilibrium yield. (8)

4.3.2.2 Temperature Study

Figure 4.3 shows the effects of temperature on the catalytic performance at 360 bar, $\text{CO}_2:\text{H}_2 = 1:10$, and GHSV of $10,471 \text{ h}^{-1}$. A rise in temperature greatly enhanced

High pressure CO₂ hydrogenation over co-precipitated Cu/ZnO/Al₂O₃ catalysts

CO₂ conversion, reaching the maximum at 260 °C with the aforementioned outstanding methanol productivity. Further rise in temperature resulted in methanol selectivity decrease and in apparent compensating increase in CO formation.

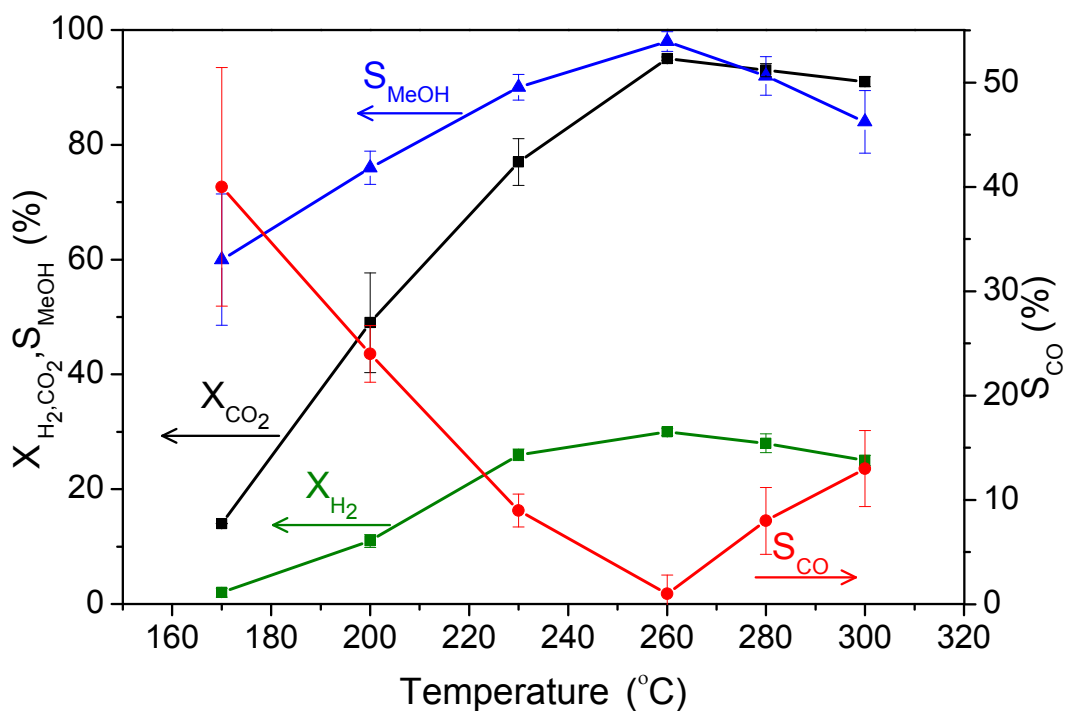


Figure 4.3 Effect of temperature on CO₂ conversion (X_{CO_2}), H₂ conversion (X_{H_2}) and selectivity to CO (S_{CO}) and methanol (S_{MeOH}) over the Cu/ZnO/Al₂O₃ (I) catalyst.

Reaction conditions: P = 360 bar, GHSV = 10,471 h⁻¹, CO₂:H₂ = 1:10.

At a lower pressure of 200 bar, a similar trend with a maximum in the catalytic performance at 280 °C was observed ($X_{CO_2} = 79\%$, $S_{MeOH} = 88\%$) (Appendix B, Figure B.1). This great enhancement in methanol selectivity upon temperature increase is surprising at first glance because the competitive RWGS reaction is an endothermic reaction and higher temperature should facilitate the reaction with respect to methanol synthesis that is an exothermic reaction and preferable at lower temperature (1, 9).

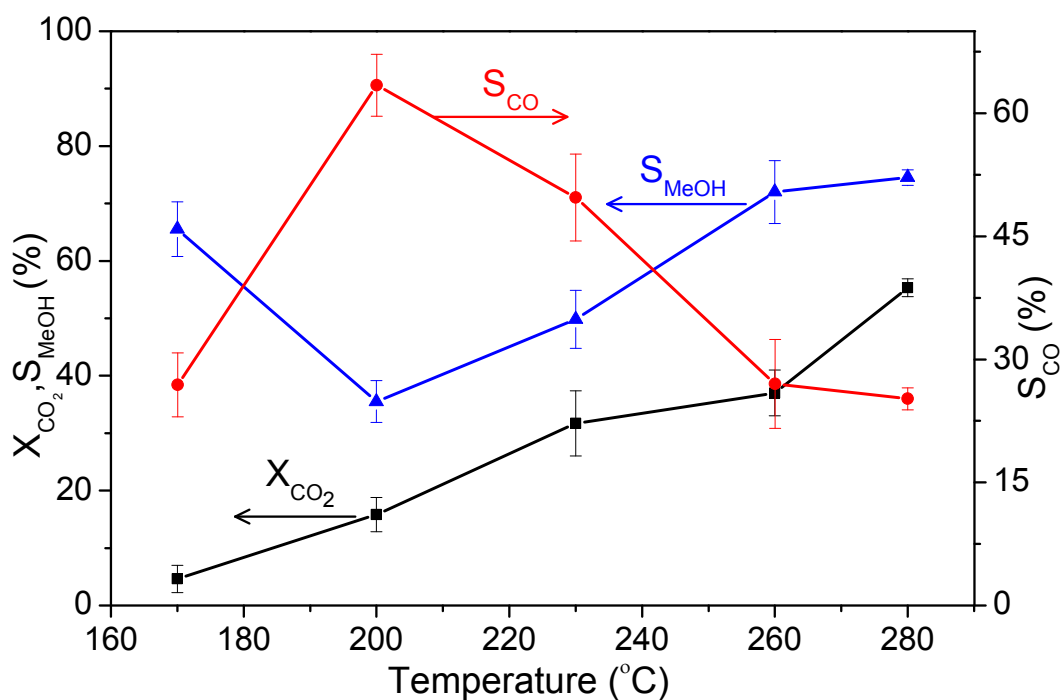


Figure 4.4 Effect of temperature on CO_2 conversion (X_{CO_2}) and product selectivity in CO_2 hydrogenation reaction over the Cu/ZnO/Al₂O₃ (I) catalyst. Reaction conditions: $P = 360$ bar, $GHSV = 10,471$ h⁻¹, $CO_2:H_2 = 1:3$.

Figure 4.4 summarizes the effect of temperature on the catalytic performance at the conventional feed $CO_2:H_2$ ratio of 1:3, at 360 bar and $GHSV$ of 10,471 h⁻¹ over the co-precipitated Cu/ZnO/Al₂O₃ (I) catalyst. Unlike the 1:10 feed ratio, the CO selectivity was found to be increasing from 170 to 200 °C. Above 200 °C the reaction follows the similar pattern of product distribution profiles (increase in methanol selectivity and CO_2 conversion at higher temperatures) as it was observed for the 1:10 feed ratio. A maximum of the CO_2 conversion and methanol selectivity was not observed in the temperature range investigated. The highest CO_2 conversion of 55 % was obtained at the highest measured temperature of 280 °C with good methanol selectivity of 75 %. The corresponding weight time yield was also observed to be 1.4 g_{MeOH}·g_{cat}⁻¹·h⁻¹, which was slightly higher than that of 1:10 ratio under the identical pressure and $GHSV$ conditions. This can be correlated to the increased mass flow rate of CO_2 due to the

High pressure CO₂ hydrogenation over co-precipitated Cu/ZnO/Al₂O₃ catalysts

increased CO₂ partial pressure. However, the outlet stream contains 25 % CO and unconverted CO₂, rendering the 1:10 feed ratio to be attractive in practice where little amounts of CO and CO₂ were observed

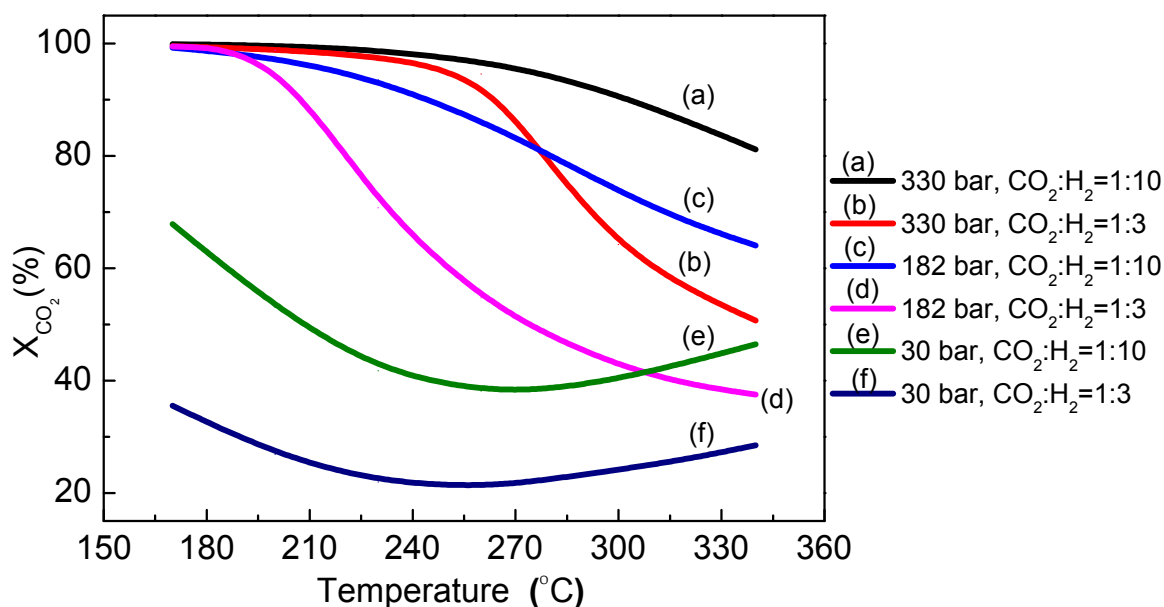


Figure 4.5 Equilibrium conversion of CO₂ at different conditions of feed CO₂:H₂ ratio and pressure as a function of temperature.

Equilibrium conversion of CO₂ at different conditions of feed CO₂:H₂ ratio and pressure as a function of temperature is shown in Figure 4.5. At 330 bar and at the feed ratio of CO₂:H₂ = 1:10, the decrease in CO₂ conversion was observed with increase in temperature, more prominently above 250-270 °C. It should be noted that at the same pressure and at the feed ratio of 1:3 the decrease in CO₂ conversion is significantly more pronounced (with a drastic decrease above 250 °C) compared to that of 1:10 ratio. Similar trend was observed at 182 bar. Interestingly at 182 bar, the decrease in CO₂ conversion was commenced at much lower temperature than at 330 bar and much more easily recognized in the case of the 1:3 feed ratio. We also calculated the low pressure (30 bar) equilibrium conversion values at 1:3 and 1:10 feed ratio. Unlike the high

pressure conditions, at 30 bar the equilibrium conversion passes through a minimum in the temperature range of 260 °C and increases onwards. This rise in CO₂ conversion can be correlated with the increased RWGS activity since as it can be seen in Figure 4.5 the methanol selectivity was found to be significantly decreased with increase in temperature at 30 bar.

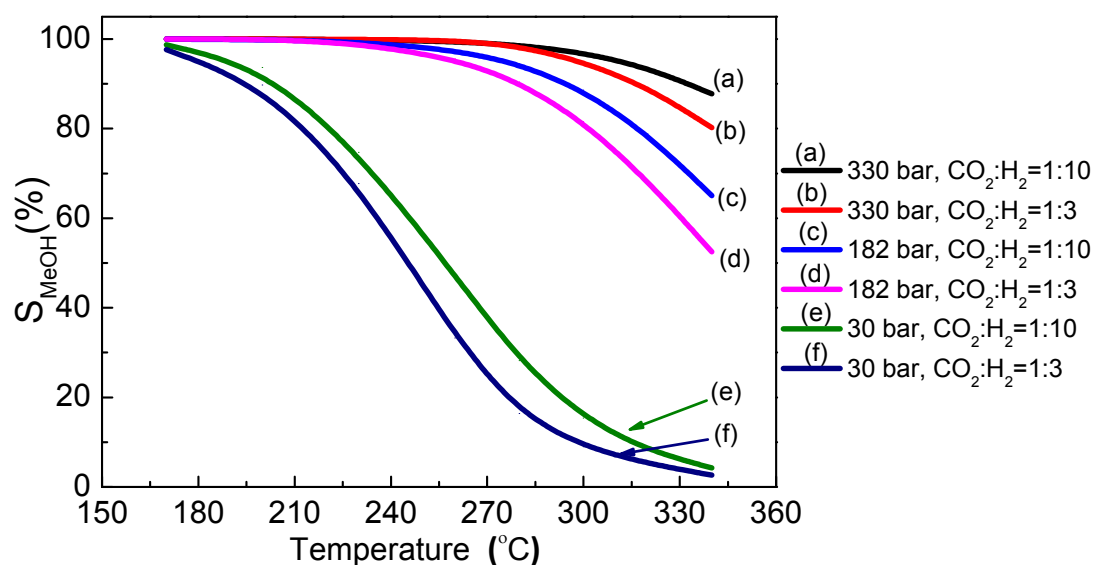


Figure 4.6 Methanol selectivity (S_{MeOH}) at equilibrium under different conditions of the feed CO₂:H₂ ratio and pressure as a function of temperature.

Figure 4.6 shows the methanol selectivity at equilibrium conversions at various temperature, pressure and feed CO₂:H₂ ratio. With increase in temperature up to 260 °C, no significant change in methanol selectivity was observed for high pressure conditions of 330 and 182 bar, as well as for different feed ratios of CO₂:H₂. Further rise in temperature resulted in lowered methanol selectivity. At 30 bar methanol selectivity was found to be drastically decreased with increase in temperature. It appears that at lower pressure, CO formation is preferred over methanol synthesis when temperature was increased, whereas thermodynamically at high pressure methanol is formed more favourably. In reality, the formed CO may be converted to methanol efficiently at high

High pressure CO₂ hydrogenation over co-precipitated Cu/ZnO/Al₂O₃ catalysts

pressure due to more facile volume contraction of CO compared to CO₂. This may also explain the carbon source for methanol synthesis at high pressures. Detailed thermodynamic analysis and further experiments are necessary to confirm this interpretation.

4.3.2.4 GHSV Study

Table 4.2. Catalytic activity test for Cu/ZnO/Al₂O₃ (I) at two different GHSVs at T= 260 °C, P = 360 bar and CO₂:H₂ = 1:10.

GHSV (h ⁻¹)	CO ₂ conv. (%)	Selectivity (%)			
		CO	CH ₄	CH ₃ OH	CH ₃ OCH ₃
20,000	86.5	6.3	0.0	92.2	1.5
10,471	95.3	1.4	0.3	98.2	0.0
5,000	96.6	3.5	0.0	93.2	3.2

Table 4.2 shows the effect of GHSV on the CO₂ conversion and product selectivity. Increase in GHSV to 20,000 h⁻¹ resulted into lowering the CO₂ conversion to 86 % along with slight reduction in selectivity towards methanol. The weight time yield at this increased GHSV condition was observed to be 1.99 g_{MeOH}·g_{cat}⁻¹·h⁻¹, the highest among all the studies reported here using the self-made Cu/ZnO/Al₂O₃ catalyst. Whereas reducing GHSV to 5000 h⁻¹ showed very similar observation for methanol synthesis while CO₂ conversion (97 %) was found to be highest among all investigations of this work. The results at 5,000 h⁻¹ may be due to a side reaction started to be operative at the very long contact time of the product (methanol) with the catalyst, as evidenced by the higher production of DME. The optimum GHSV was found to be 10,471 h⁻¹ where higher conversion and high methanol selectivity was observed.

Table 4.3 Catalytic activity test for the commercial methanol synthesis catalyst at various GHSVs, at T= 260 °C, P = 360 bar and CO₂:H₂ = 1:10.

GHSV (h ⁻¹)	CO ₂ Conv. (%)	Selectivity (%)				Yield (mg·g _{cat} ⁻¹ ·h ⁻¹)			
		CO	CH ₄	CH ₃ OH	CH ₃ CH ₂ OH	CO	CH ₄	CH ₃ OH	CH ₃ CH ₂ OH
425	94.8	1.4	5.9	92.5	0.2	4.9	11.8	370.4	1.18
10,000	95.8	1.4	0.0	98.6	-	10.1	0.0	797.7	-
20,000	95.7	1.8	0.0	98.2	-	24.7	0.0	1582.0	-
40,000	89.9	4.9	0.0	95.1	-	128.0	0.0	2890.1	-
80,000	78.8	10.3	0.0	89.7	-	474.0	0.0	4778.3	-
131,000	71.8	19.9	0.0	80.1	-	1359.5	0.0	6314.3	-
182,000	65.8	22.7	0.0	77.3	-	1972.4	0.0	7729.1	-

Moreover, the commercial methanol synthesis catalyst was also tested under similar reaction conditions. Excellent catalytic performance similar to that shown in Figures 4.1 and 4.2 was confirmed. Table 4.3 shows the effect of GHSV on the catalytic performance of the commercial methanol synthesis catalyst. Increase in GHSV up to an extremely high level (182,000 h⁻¹) resulted in lowering CO₂ conversion from 95.8 to 65.8 % along with decrease in selectivity towards methanol. Nevertheless high CO₂ conversion and high methanol selectivity were maintained and thus WTY of methanol drastically increased at higher GHSV's. The highest methanol WTY of 7.7 g_{MeOH}·g_{cat}⁻¹·h⁻¹ was obtained at 182,000 h⁻¹. This value is by far superior to any of values reported to date. It is also important to note that CO selectivity increased at higher GHSV's whereas methanol selectivity was lowered, indicating more CO production at shorter contact time and assisting the suggested reaction path of methanol synthesis via CO. With decrease in space velocity to extremely low level (425 h⁻¹) the CO₂ conversion was found to be slightly reduced. However, there was an interesting change in the product

distribution was observed. As it can be seen, methanol selectivity was lowered to 92.5 % with the appearance of methane and ethanol at selectivity of 5.9 % and 0.2 % respectively. If it is assumed that methanol formation pathway goes through CO formation then it is likely that the formed CO goes to the methane formation considering the highly increased contact time. From this observation it is clear that deviations from the optimum conditions proposed in this report can result in the transition of reaction from thermodynamic controlled to kinetically controlled regime.

4.3.2.5 Effect of Zinc Addition and Synthesis Method

Figure 4.7 shows the effect of temperature on the catalytic performance of a co-precipitated Cu/Al₂O₃ catalyst under the optimal conditions of CO₂:H₂ ratio, pressure, and space velocity found for the Cu/ZnO/Al₂O₃ catalyst. Similar to the co-precipitated Cu/ZnO/Al₂O₃ (I) catalyst, the Cu/Al₂O₃ catalyst showed a great increase in methanol selectivity and CO₂ conversion at higher temperatures except the case where the temperature was increased from 170 to 200 °C. No maximum in methanol productivity was found in the range of temperature examined. Good level of CO₂ conversion (82 %) with high methanol selectivity (92 %) was obtained at 280 °C. Based on this result using the catalyst without a Zn component, it can be concluded that the outstanding catalyst performance is related mainly to pressure, the feed composition and to the catalyst synthesis method, thus to the specific state of Cu in the catalyst (10).

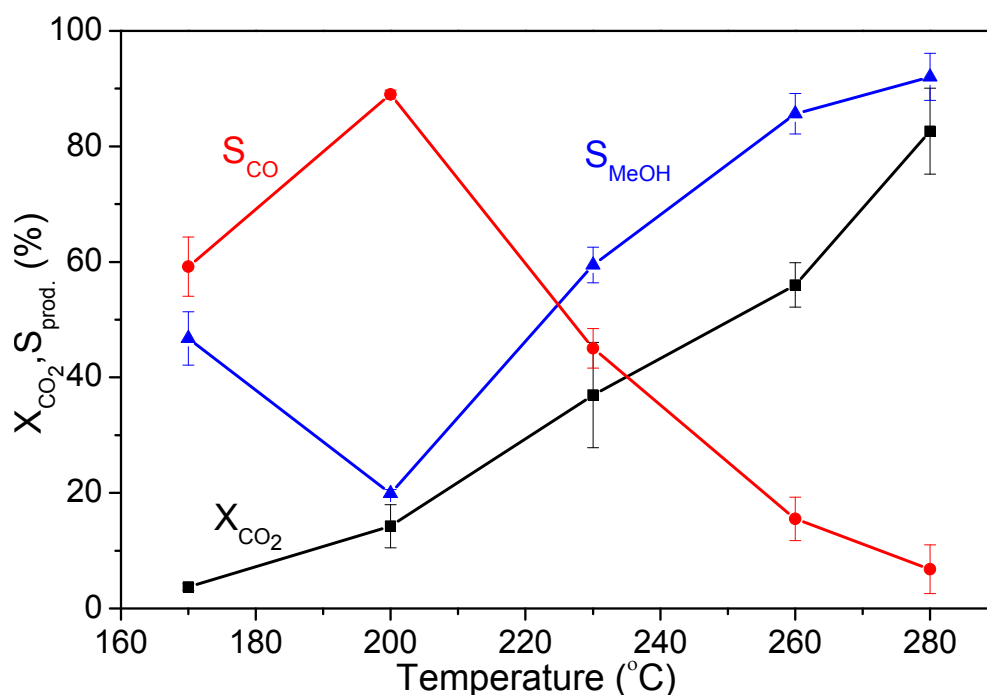


Figure 4.7 Effect of temperature on CO_2 conversion (X_{CO_2}) and selectivity to CO (S_{CO}) and methanol (S_{MeOH}) over co-precipitated Cu/Al_2O_3 catalyst. Reaction conditions: $P = 360$ bar, $GHSV = 10,471\ h^{-1}$, $CO_2:H_2 = 1:10$.

The results obtained with the Cu/Al_2O_3 catalyst prepared by the impregnation route, under the feed ratio of 1:3 and 1:10 at 360 bar and $GHSV$ of $10,471\ h^{-1}$, are shown in Table 4.4. As expected from thermodynamics but contrary to the findings for the co-precipitated catalysts, the CO selectivity monotonously increased with temperature and reaching a maximum of 89.0 % at 260 °C at the feed ratio of 1:3. The highest methanol selectivity of 66.8 % was obtained at the lowest examined reaction temperature and it decreased at higher temperatures. When the reaction was performed at 1:10 feed ratio, a similar tendency was observed. The major product was CO at all the measured temperatures. In the light of methanol selectivity, the lower CO_2/H_2 ratio of 1:10 was not beneficial, but the CO selectivity decreased compared to that obtained at 1:3 ratio at higher temperatures. The methanol production seems enhanced at 1:10 ratio, but under this condition the secondary reaction of methanol to DME occurred as

High pressure CO₂ hydrogenation over co-precipitated Cu/ZnO/Al₂O₃ catalysts

evidenced from the appreciable selectivity of 25.3 % at 280 °C at 1:10 ratio. This study clearly shows a great difference in the catalytic performance between the catalysts prepared by co-precipitated and impregnation routes.

Table 4.4 Effect of temperature and feed ratio on CO₂ conversion and product selectivity over impregnated Cu/Al₂O₃ catalyst. Reaction conditions: P = 360 bar, GHSV = 10,471 h⁻¹

Temp. (°C)	Feed Ratio CO ₂ :H ₂	CO ₂ Conv. (%)	Selectivity (%)			
			CO	HCOOCH ₃	CH ₃ OH	CH ₃ OCH ₃
170	1:3	2.7	33.0	0.0	66.8	0.1
200	1:3	7.5	47.1	0.5	51.8	0.4
230	1:3	13.2	75.1	0.0	23.9	0.9
260	1:3	22.1	89.0	0.0	8.9	2.0
280	1:3	29.6	89.0	0.0	7.4	3.7
170	1:10	4.0	75.4	0.0	24.2	0.4
200	1:10	12.4	68.0	0.1	30.3	1.6
230	1:10	21.0	76.6	0.1	19.0	4.3
260	1:10	34.6	75.2	0.0	10.9	13.8
280	1:10	39.9	68.2	0.0	6.5	25.3

4.3.2.5 Catalyst Stability Test

The Cu/ZnO/Al₂O₃ (I) catalyst was subjected to a life time test at different feed ratios. Table 4.5 shows the stability test carried out up to 128 hours of continuous operation. The data presented demonstrates the excellent stability of catalyst over the measured time period of operation. The catalyst retained its activity even if the feed ratio changed from 1:10 to 1:1 and then back to the 1:10 condition

Table 4.5 Catalyst stability test for Cu/ZnO/Al₂O₃ (I) under varying conditions of feed ratio with GHSV= 10,471 h⁻¹ and P = 360 bar

Time (h)	CO ₂ :H ₂ feed ratio	Temp. (°C)	CO ₂ Conv. (%)	Selectivity (%)		
				CO	CH ₄	CH ₃ OH
20	1:3.6	280	70	14	1	85
43	1:3.6	280	71	15	1	85
60	1:10	280	94	3	1	96
84	1:5.8	280	87	10	1	89
96	1:7.8	280	91	6	1	93
100	1:1	280	27	39	0	61
113	1:10	280	94	3	1	95
120	1:10	280	94	4	1	95
128	1:10	260	95	2	0	97

4.3.2.6 Comparing Thermodynamic Calculations and Experimental Results

Ipatieff and Monroe reported that under high pressure conditions, CO₂ is first reduced to CO via the RWGS reaction accompanying the formation of water, and subsequently to formaldehyde as a secondary reaction. The formed formaldehyde was suggested to be further reduced to methanol via two pathways; one via direct hydrogenation and the other via Cannizzaro reaction (2). It is widely accepted that methanol is directly formed from CO₂ rather than CO (11-13), however this may be applicable to reactions at low or moderate pressures. In context with such high pressure and with obtained high conversions, the pathway for methanol formation via CO, suggested by Ipatieff and Monroe, is indeed in accordance with our observation. The high selectivity to CO at lower temperatures can be explained by the slow secondary reaction of CO towards the formation of methanol. Likely, this secondary reaction is accelerated by increasing temperature, particularly at high pressure, and also the amount

of methanol is greatly enhanced due to the increased amount of CO produced by the endothermic RWGS reaction.

In addition, the formed water may promote CO hydrogenation as reported in literature (14). As mentioned previously without mechanistic studies or *operando* observation of active sites and species, which is out of scope of the current investigation, this study points that CO₂ hydrogenation to methanol proceeds via CO formation under high pressure conditions. Recent investigation by Bennekom et al. on methanol synthesis from CO-rich or CO₂-rich syngas showed that >90 % CO₂ conversion and high selectivity to methanol could be achieved at specific conditions (e.g. 200 bar and 210 °C) due to phase separation of products (methanol and water) by condensation, thus unlimiting the one-phase equilibrium conversion (7). One possible explanation of the high catalytic performance of this work may also be due to a similar phase separation; however, the study by Bennekom et al. showed marked lowering of CO₂ conversion in the temperature range reported to be optimal from this work and thus only phase behaviour cannot explain the high catalytic performance and rather thermodynamics and rate enhancement at high H₂ pressure more likely play decisive roles under the conditions of this work.

Comparing the obtained results to the thermodynamic calculations (Figures 4.5 and 4.6), above 260 °C the reaction reaches close to the equilibrium conversion; hence falling into thermodynamic regime. This thermodynamic control can be clearly confirmed by reproduction of the trend for the unexpected decrease in CO₂ conversion above 260 °C, accompanying decrease in methanol selectivity (Figures 4.3 vs. 4.5 and 4.6). On the other hand, below 260 °C the CO₂ conversion was far from equilibrium and the enhanced methanol selectivity towards higher temperature up to 260 °C can be

regarded due to the kinetic control. When the reaction is kinetically controlled, the high selectivity to CO is more pronounced (Figure 4.3) as observed for the aforementioned kinetically controlled regime (Figure 4.1) at $\text{CO}_2:\text{H}_2 = 1:<10$. This observation suggests that the CO_2 hydrogenation to methanol proceeds via CO.

It is intriguing to notice that with the $\text{Cu}/\text{Al}_2\text{O}_3$ catalyst prepared by the impregnation route the formation of products was observed to be in accordance with the thermodynamic principles, i.e. better methanol selectivity at lower temperatures and higher CO selectivity and higher CO_2 conversion at higher temperatures, but with overall poor catalytic performance very far from the equilibrium (Table 4.4). There may be some differences in the nature of active sites of the catalysts prepared by the impregnation and co-precipitation routes. Also, the boosting in catalytic performance with a maximum at a specific temperature was not observed with the $\text{Cu}/\text{ZnO}/\text{Al}_2\text{O}_3$ catalyst at the conventional $\text{CO}_2:\text{H}_2$ ratio of 1:3 (Figure 4.4). The absence of the maximum is likely due to the kinetic control by the poorer catalytic performance at the lower H_2 partial pressure as evidenced by the higher CO selectivity (Figure 4.4).

4.4 Conclusions

The catalytic system described in this work provides an efficient and highly productive processing strategy for CO_2 conversion at a single step. The high-pressure approach using a conventional $\text{Cu}/\text{ZnO}/\text{Al}_2\text{O}_3$ methanol synthesis catalyst under specific reaction conditions for CO_2 hydrogenation remarkably boosted methanol selectivity and productivity by (i) the high H_2 partial pressure to enhance the reaction rate and (ii) thermodynamically favoured high CO_2 conversion and methanol selectivity at high pressure. The preliminary experiments with the commercial catalyst showed extraordinary high methanol productivity at very high GHSVs, possibly justifying the

capital and manufacturing costs of high-pressure processes. Negligible pressure drops under the examined GHSVs are the advantage of compressive reactants at high pressure. The consumed hydrogen was exclusively utilized for methanol formation at increased hydrogen partial pressure, thereby increasing the efficiency of the process towards methanol synthesis by suppressing chemical and thermal energy consumption for RWGS reaction. Moreover, the excess of hydrogen remaining in stream present under the optimal reaction condition reported in this work can be fed directly to another identical or multiples of high-pressure reactors with possible reduction in their sizes, so that compression of hydrogen may only require at initial stage whereas methanol productivity would be multiples of connected reactors. In such configurations, the recycling of H₂ can be minimized or potentially omitted.

References

1. W. Wang, S. Wang, X. Ma, J. Gong, *Chem. Soc. Rev* **40**, 3703 (2011).
2. V. N. Ipatieff, G. S. Monroe, *J. Am. Chem. Soc.* **67**, 2168 (1945).
3. A. Bansode, B. Tidona, P. R. von Rohr, A. Urakawa, *Catal. Sci. Technol.* **3**, 767 (2013).
4. A. S. Nowick, *AIChE J.* **2**, 140 (1956).
5. J. W. Evans, M. S. Wainwright, A. J. Bridgewater, D. J. Young, *Appl. Catal.* **7**, 75 (1983).
6. J. G. v. Bennekom, J. G. M. Winkelman, R. H. Venderbosch, S. D. G. B. Nieland, H. J. Heeres, *Ind. Eng. Chem. Res.* **51**, 12233 (2012).
7. J. G. van Bennekom *et al.*, *Chem. Eng. Sci.* **87**, 204 (2013).
8. G. Natta, in *Catalysis*, P. H. Emmet, Ed. (Reinhold, New York, 1995), pp. 349-411.
9. C. Yang *et al.*, *Catal. Today.* **115**, 222 (2006).
10. M. Behrens *et al.*, *Science* **336**, 893 (2012).
11. G. C. Chinchin, P. J. Denny, D. G. Parker, M. S. Spencer, D. A. Whan, *Appl. Catal.* **30**, 333 (1987).

12. K. C. Waugh, *Catal. Today*. **15**, 51 (1992).
13. J. B. Hansen, in *Handbook of Heterogenous Catalysis*, H. K. a. J. W. G. Ertl, Ed. (Wiley-VCH GmbH, Weinheim, 1997), pp. 1856.
14. J. Saussey, J. C. Lavalley, *J. Mol. Catal.* **50**, 343 (1989).

5

Synthesis of Dimethyl Ether and Hydrocarbons via High Pressure CO₂ Hydrogenation

5.1 Introduction

Together with methanol, the products derived from methanol have vital roles in chemical industry. Among others, dimethyl ether (DME) and hydrocarbons are commercially important chemicals which can be produced from the methanol. DME is the simplest of the ethers. Although it is a gas at ambient conditions (normal boiling point of $-25.1\text{ }^{\circ}\text{C}$) it can be easily liquefied at low pressures (6.06 bar at $30\text{ }^{\circ}\text{C}$) and can thus be handled as a liquid in many applications. DME is a potential substitute for diesel oil owing to its better combustion performances particularly given its high cetane number, which is greater than 55, when compared with 40–55 of common diesel fuel. Due to this and other attractive properties such as biodegradability as well as economic benefits of producing such fuel, DME synthesis has recently gained significant industrial attention. Dehydration of methanol over solid acid catalysts such as $\gamma\text{-Al}_2\text{O}_3$ or H-ZSM-5 yields DME. Synthesis of DME from CO₂ hydrogenation composed of two routes; a two-step process where methanol is synthesized on a metallic catalyst and subsequently dehydrated on an acid catalyst and a single-step process using a bifunctional catalyst to perform the two steps simultaneously (1, 2).

Generally, synthesis of hydrocarbons from CO₂ can be also divided into two categories; methanol mediated and non-methanol-mediated reactions (3, 4). In the

methanol-mediated approach, CO₂ and H₂ react over e.g. Cu–Zn-based catalysts to produce methanol, which is subsequently transformed into other hydrocarbons such as gasoline. In the case of non-methanol-mediated process, CO₂ hydrogenation proceeds via two steps; RWGS reaction and FT synthesis (5), however the methanol-mediated approach has advantages in product selectivity and energy requirements of the plant operation.

This chapter presents one step conversion of CO₂ to DME, and methanol mediated synthesis of hydrocarbons based on the high-performance methanol synthesis process. As described in Chapter 4, under optimised conditions, almost full one-pass conversion of CO₂ to methanol was obtained. The results for one step conversion of CO₂ into DME via *in situ* conversion of methanol using physically mixed, pre-pelletized Cu/ZnO/Al₂O₃ (II) and H-ZSM-5 catalysts and its various combinations are shown in this chapter. Furthermore, it is shown that the effluent stream of methanol, rich in H₂ and water, from the methanol synthesis reactor can be directly fed to a reactor containing the H-ZSM-5 catalyst for selective production of alkane or alkene, depending on the operating pressure of the secondary reactor.

5.2 Methods

5.2.1 Catalyst Synthesis

Methanol synthesis catalyst Cu/ZnO/Al₂O₃ (II) was prepared by coprecipitation technique mentioned in Chapter 4. The physicochemical characterization for this catalyst is described in Section 4.3.1. The H-ZSM-5 catalyst was prepared by calcination of NH₄-ZSM-5 (Alfa Aesar, SiO₂ : Al₂O₃ = 50:1) in air at 400 °C for 4 hours.

5.2.2 Catalytic Testing

For the synthesis of DME, H-ZSM-5 (150 mg) was physically mixed with Cu/ZnO/Al₂O₃ (II) (170 mg) and charged into one reactor, or the two catalysts were charged separately into two reactors connected in series. In case of physical mixing the catalysts were palletised, crushed and sieved independently and mixed.

For hydrocarbon synthesis, H-ZSM-5 (170 mg) was charged into a reactor connected in series after the reactor containing Cu/ZnO/Al₂O₃ (II) for methanol synthesis. The temperature of the secondary reactor containing H-ZSM-5 was controlled independently from the first one. For alkane synthesis, the reactor with H-ZSM-5 was placed before the back pressure regulator, thus kept at the same pressure as the first one (Figure 5.3). While in alkene synthesis the secondary reactor was located after the back pressure regulator (Figure 5.4) and kept at the atmospheric pressure. It should be noted that GHSVs for the combined processes (DME and hydrocarbon synthesis) were calculated based on the amount of the methanol synthesis catalyst in the reactor.

5.3 Results and Discussion

5.3.1 DME Synthesis

Figure 5.1 shows the catalytic results obtained for one step DME synthesis by physically mixing the Cu/ZnO/Al₂O₃ (II) and H-ZSM-5 catalysts. Despite the presence of H-ZSM-5 catalyst in a physically mixed state, the catalytic system exhibited similar levels of CO₂ conversion as in methanol synthesis. The DME selectivity was found to be always above 80 % starting from the lowest examined temperature and was the highest (89 %) at 300 °C. The CO₂ conversion at those conditions was found to be ≥ 95 % or even higher (97 % at 280 °C). Above 280 °C the rest of products mainly contains methanol with traces of CO (< 0.3 %).

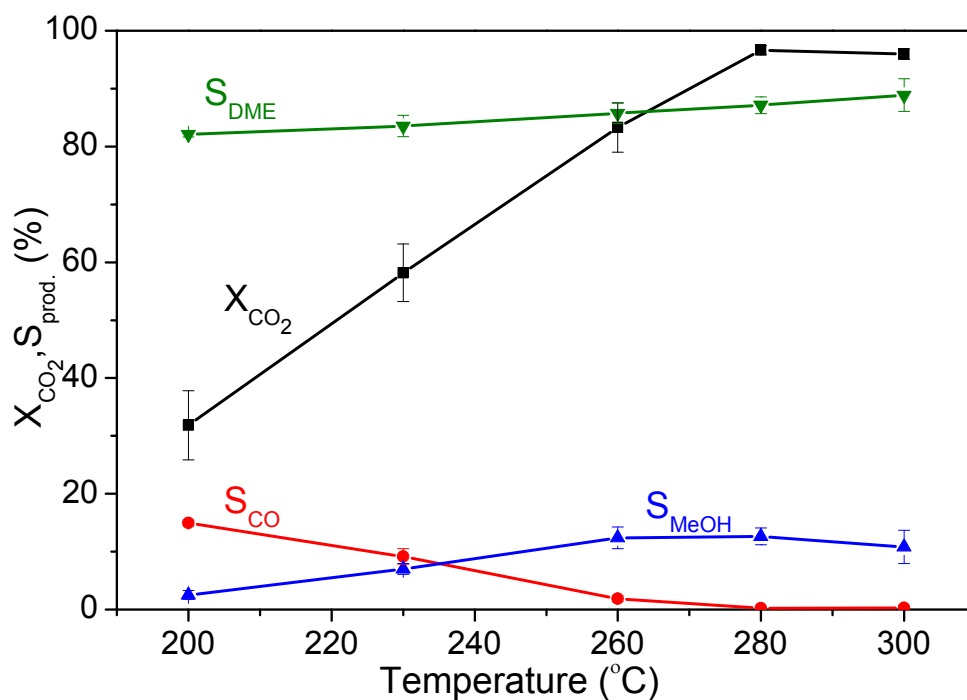


Figure 5.1 Effects of temperature on CO_2 conversion (X_{CO_2}) and selectivity to CO (S_{CO}), methanol (S_{MeOH}), and DME (S_{DME}) in one step CO_2 hydrogenation into DME over physically mixed $Cu/ZnO/Al_2O_3$ (II) and H-ZSM-5 catalysts. Reaction conditions: $P = 360$ bar, $GHSV = 10,471$ h^{-1} , $CO_2:H_2 = 1:10$.

This reaction was also performed by separating two catalysts into respective reactors connected in series. Figure 5.2 depicts the results obtained for one step conversion of CO_2 and H_2 into DME over sequentially placed $Cu/ZnO/Al_2O_3$ (II) and H-ZSM-5 catalytic reactors. The obtained results are closely comparable to that of physically mixed $Cu/ZnO/Al_2O_3$ (II) and H-ZSM-5 catalysts. The highest CO_2 conversion of 93 % was observed at 280 °C with DME selectivity of 87 %. The highest DME selectivity of 90 % was observed at 260 °C and the DME selectivity decrease at higher temperatures was compensated by increased methanol production. This result shows that one step conversion of CO_2 into DME can be achieved keeping similar performance by either physically mixing or keeping the catalysts in separate reactors connected in series.

Synthesis of dimethyl ether and hydrocarbons via high pressure CO₂ hydrogenation

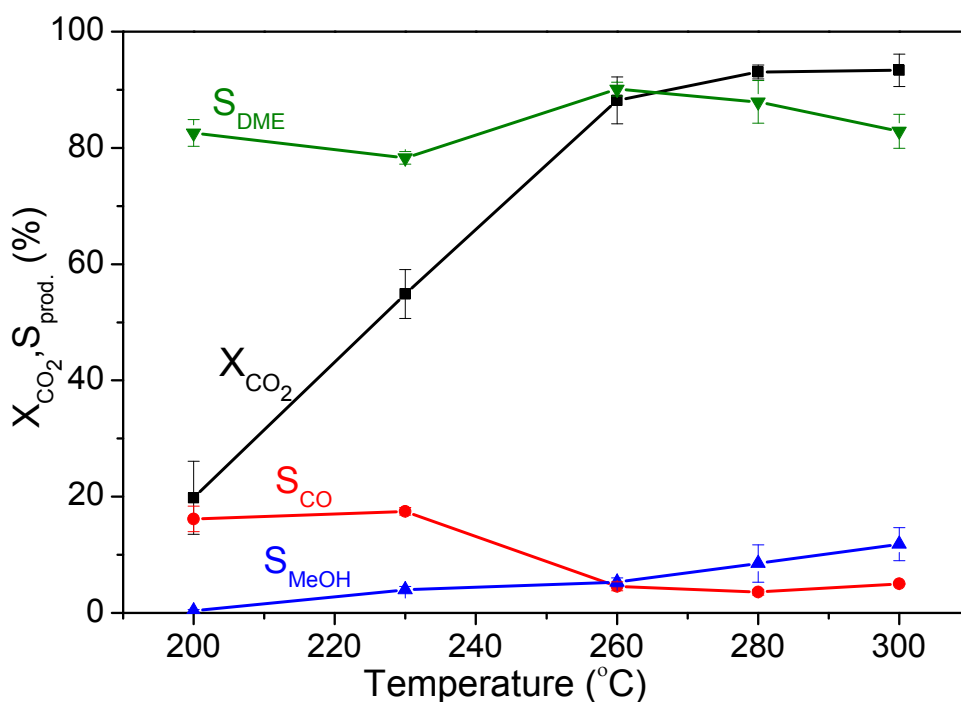


Figure 5.2 Effect of temperature on CO₂ conversion (X_{CO_2}) and selectivity to CO (S_{CO}), methanol (S_{MeOH}), and DME (S_{DME}) in one step CO₂ hydrogenation into DME over sequentially placed Cu/ZnO/Al₂O₃ (II) and H-ZSM-5 catalytic reactors. Reaction conditions: $P = 360$ bar, $GHSV = 10471$ h⁻¹, CO₂:H₂ = 1:10.

5.3.2 Hydrocarbon Synthesis

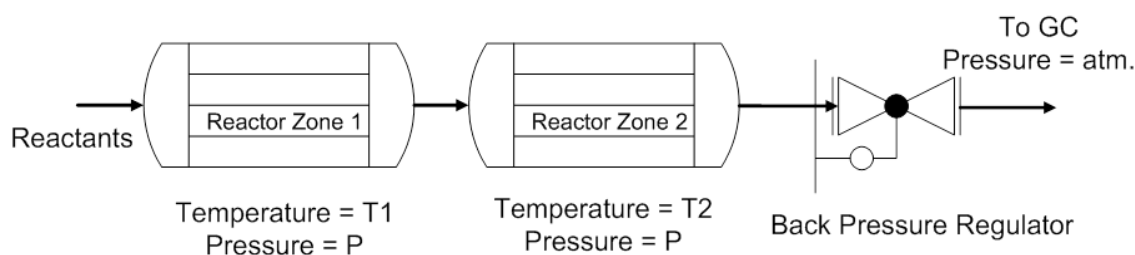


Figure 5.3. Reactor configuration to operate two reactors at the same pressure but at different temperatures.

The experiments towards the synthesis of alkanes and alkenes from the methanol obtained in CO₂ hydrogenation, were carried out using the same catalysts (Cu/ZnO/Al₂O₃ (II) and H-ZSM-5) without any purification step by changing reactor

configuration and operating conditions. First, we placed the Cu/ZnO/Al₂O₃ (II) and H-ZSM-5 catalysts in series, in the respective tubular reactors maintained at different temperatures at the same pressure (Figure 5.3).

Table 5.1. Alkane and alkene synthesis via CO₂ hydrogenation by a sequential process of methanol synthesis and subsequent methanol-to-alkane/alkene reaction. Reaction conditions: GHSV = 10,471 h⁻¹, CO₂:H₂ = 1:10, T(Cu/ZnO/Al₂O₃ (II) catalyst bed) = 260 °C, T(H-ZSM-5 catalyst bed) = 375 °C. The operation pressure of the first reactor was 360 bar and the pressure of the second reactor was varied and shown in the table

Exp. No.	P (bar)	CO ₂ conv. (%)	Selectivity (%)									
			DME	CO	MeOH	CH ₄	Eth-ane	Eth-ylene	Pro-pane	Pro-pylene	butane	Iso-butane
1	360	94	4	3	6	5	20	1	24	0	10	26
2	1	97	10	2	21	0	4	9	4	33	11	4

Table 5.1, experiment no. 1 illustrates the CO₂ conversion and product distribution when the reactor packed with Cu/ZnO/Al₂O₃ (II) was kept at 260 °C while that of H-ZSM-5 was kept at 375 °C, 360 bar. The dominant products were hydrocarbons ranging from C₁ to C₄, i.e. ethane (20 %), propane (24 %) and isobutane (26 %). The overall hydrocarbon selectivity was found to be 85 %. The hydrogenation activity towards alkanes was apparently enhanced under the pressurized conditions since the effluent of methanol synthesis reactor was H₂-rich. This approach is similar to Haldor Topsøe's TIGAS process (6) which converts synthesis gas to gasoline in single loop, however the carbon source in our reaction was CO₂ instead of CO.

Synthesis of dimethyl ether and hydrocarbons via high pressure CO₂ hydrogenation

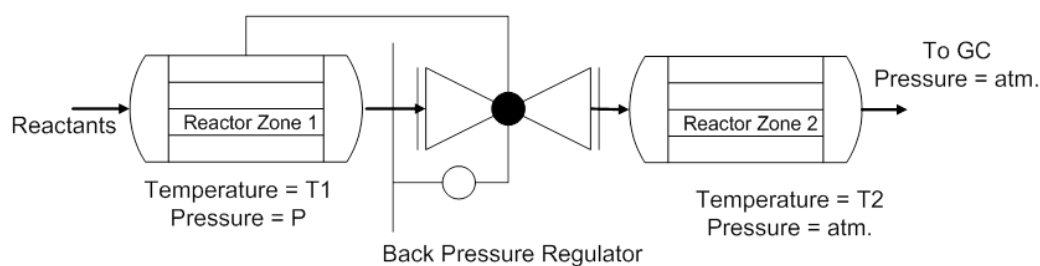


Figure 5.4. Reactor configuration to operate two reactors at different pressures and temperatures (the pressure of the second reactor is atmospheric).

Further encouraging results were obtained when the second reactor filled with the H-ZSM-5 catalyst was maintained at atmospheric pressure by simply changing the location of the back pressure regulator used for pressure regulation (Figure 5.4), while the rest of the conditions were kept identical. Experiment no. 2 in Table 1 shows contrasting product distribution compared to experiment no. 1. The major product was propylene with 33 % selectivity which was totally absent in experiment no. 1. Methanol (21 %), DME (10 %), ethylene (9 %) and butane (11 %) were among the rest of major products.

5.4 Conclusions

The results presented in this chapter show that one step transformation of CO₂ to DME by the co-presence of the H-ZSM-5 catalyst can be achieved without changing the optimised process conditions described in Chapter 4, retaining similar CO₂ conversion levels. It has been demonstrated that the placement of solid acid catalyst (H-ZSM-5), either in physically mixed state with Cu/ZnO/Al₂O₃ (II) or in the separate reactor connected in series, doesn't affect the catalytic results. Furthermore, the methanol-, water-, and H₂-rich, stream can be directly fed to the reactor containing the H-ZSM-5 catalyst and good selectivity to alkane or alkene were attained depending on the

operating pressure of the secondary reactor. This would instigate further development of CO₂ to olefins and/or gasoline processes via one step hydrogenation process.

References

1. G. A. Olah, A. Goepfert, G. K. S. Prakash, *J. Org. Chem.* **74**, 487 (2008).
2. D. Mao *et al.*, *J. Catal.* **230**, 140 (2005).
3. K. Fujimoto, T. Shikada, *Appl. Catal.* **31**, 13 (1987).
4. G. Kishan, M.-W. Lee, S.-S. Nam, M.-J. Choi, K.-W. Lee, *Catal. Lett.* **56**, 215 (1998).
5. S. Abelló, D. Montané, *ChemSusChem* **4**, 1538 (2011).
6. J. Topp-Jørgensen, in *Stud. Surf. Sci. Catal.*, D. M. Bibby, C. D. Chang, R. F. Howe, S. Yurchak, Eds. (Elsevier, 1988), Volume 36, pp. 293-305.

6

High Pressure Capillary Cell for *Operando* X-Ray Absorption Spectroscopy Studies of CO₂ Hydrogenation Reaction

6.1 Introduction

X-ray absorption fine structure (XAFS) is one of the major spectroscopic techniques employed to study heterogeneous catalysts. It can shed light on local atomic and geometric structures of catalyst together with electronic structures such as oxidation states (1, 2). XAFS studies on methanol synthesis catalysts exist at low to moderate pressures (up to 100 bar), being relevant for the current processes (3-5). The major obstacle in such measurements is the necessity of high pressure and temperature resistant reactor cell equipped with X-ray transparent windows and allowing the flow of reactants to mimic the action of plug flow reactor. Numerous *in situ* reactor cell designs have been reported in literature with their distinct advantages and disadvantages. A very good comprehensive review of such cells has been published (6). The use of capillary as an *operando* reactor cell has been reported for several X-ray absorption and diffraction studies (7-10). Clausen et al. reported a reaction cell consisting of a quartz capillary connected to stainless steel tube fittings, capable of reaching pressure of 50 bar for combined XRD study and catalytic tests (11). Wallen et al. reported a high pressure (up to 160 bar) capillary XAFS cell. In their study, a fused silica capillary with 360 μm outer diameter and 250 μm inner diameter was used (12). This capillary was fixed to a standard high pressure fitting using Vespel ferrule and was used to acquire XAFS

spectra of high pressure liquid and supercritical fluid solutions. A number of examples exist in the literature, where the use of capillary cells have been successfully employed to study the catalysts under realistic working conditions (4, 13, 14). There is a preceding example of a continuous-flow high pressure cell reported for heterogeneous catalytic reaction of alcohol oxidation at up to 150 bar by Grunwaldt et al. (15). However, to the best of our knowledge, continuous-flow high pressure capillary cell reaching 200 bar for XAFS investigation of methanol synthesis catalyst, with ease in its construction has not been reported to date.

This chapter describes a fused silica based capillary micro-reactor cell with unique coiled heating system, capable of withstanding pressures of several hundred bar at ambient temperature and of 320 bar at 280 °C and also acting as a fixed-bed plug flow reactor in CO₂ hydrogenation to methanol. Importantly all the critical components in construction of this cell are commercially available and do not require highly skilled machining. It makes the cell easy to construct, handle and operate at relatively low cost. We also show that the capillary cell functions as a conventional fixed-bed micro-reactor at high pressure to obtain reliable catalytic results and thus can be used as *operando* XAFS cell with additional functionality for combined Raman measurements.

6.2 Experimental

6.2.1 XAFS Measurements:

All the experiments were performed on BL22-CLÆSS beamline at ALBA synchrotron light facility (Barcelona, Spain) operating at 100 mA of stored current. The extended X-ray absorption fine structure (EXAFS) measurements were performed in transmission configuration at the Cu K-edge (8979 eV) using the Si(111) crystals of a fixed exit double crystal monochromator (DCM) working in continuous scan mode. A

monochromator feedback controller (MoCo), developed at the ESRF (Grenoble, France) and operating in position mode, was used in tandem with the DCM to compensate low frequency drifts. High order harmonics were rejected using the Rh stripe of the vertically collimating mirror before the DCM. The toroidal mirror after the DCM at the Rh stripe focalized vertically the beam at the sample position. 10^{13} photons/sec were achieved at the focal spot of $300 \times 150 \mu\text{m}^2$ (V \times H). The incident and transmitted X-ray beam were detected by ionization chambers filled with the required gases. The signals coming from the ionization chambers were filtered, converted and amplified by the in-house developed ALBA electrometers. Good quality XAFS spectra of 1.2 keV were acquired in 5 min.

6.2.2 Catalyst Synthesis

The catalysts used in this study were prepared by the co-precipitation method described in Chapter 4.

6.2.3 Capillary Cell Design and Setup

6.2.3.1 Coiled Heater System

Figure 6.1 shows the image of the fully assembled capillary micro-reactor cell. The cell consists of a polyimide coated fused silica capillary (Molex) as a micro-reactor with 662 μm outer diameter (OD), 247 μm ID and ca. 15 cm in length. The polyimide coating gives inherent strength and flexibility to the capillary and also prevents scratches on the walls of capillary which may act as a breaking point after pressurising. Typical catalyst loading inside this capillary was ca. 10 mg. The catalyst was pressed into a pellet, crushed and then sieved to the size of 40-100 μm . The loading of the catalyst particles inside the capillary was achieved by temporarily sealing one end of capillary with Parafilm sealing film while keeping the other end

open and holding the capillary vertically. The catalyst particles were poured from the open end with careful tapping of the capillary, allowing catalyst particles to move towards the sealed end.

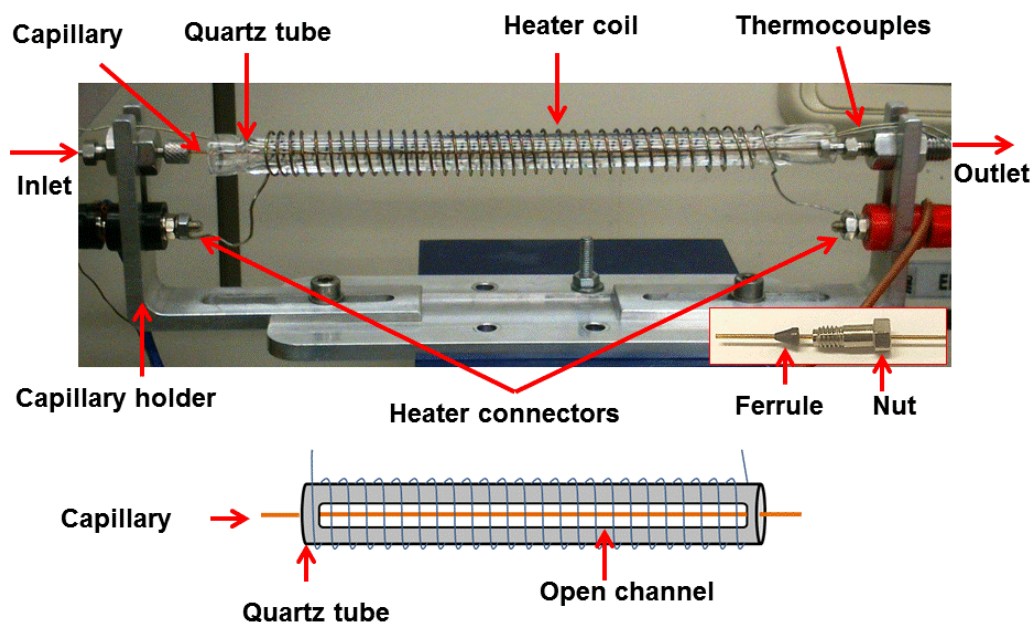


Figure 6.1 Fully assembled capillary micro-reactor cell with a coiled heating system (top) with schematic representation of open channel on quartz tube for light path (bottom)

After filling, the capillary was held horizontally and the temporary seal was removed. The capillary was placed in a rectangular holder with the use of two VICI (Valco) bulkhead compression fittings, reducing union of 1/32"-1/16" size. The capillary was fixed to the bulkhead union with the use of 1/32" ferrule and nut system as shown in the inset of Figure 6.1, similar to regular compression fittings. We used the VICI polyimide ferrule (Valcon) instead of Vespel ferrules, considering low thermal expansion coefficient, and it provided an extra grip on the capillary to give an excellent sealing without leak at high pressures and temperatures. This approach avoids the use of adhesive material which requires several hours of curing time to get

dry and may start leaking at higher temperature or pressure. Out of the two bulkhead unions, one union has an internal stainless steel frit having mesh size of 10 μm . The catalyst was held inside the capillary against this frit to avoid the wash out of catalyst particles due to flow and/or pressure. The bulkhead union with frit was outlet of this reactor system whereas the other one was inlet, both unions being further connected to 1/16" tubing.

The unique part of this micro-reactor cell is the heating system. The fused silica capillary was placed in a quartz tube having a small aperture channel on both sides (Figure 6.1). This quartz tube is heated by a resistive heating wire (Alloy Wire International, Nickel Chrome, 80/20) coiling around it. The temperature control of the heating wire and thus the capillary was achieved by means of a programmable PID controller (output current = 5 A, output voltage = 0.24 V AC or 15 V DC). To ensure the uniform temperature throughout the quartz tube, three thermocouples were inserted at different positions of the capillary in the axial direction. Satisfactory temperature gradient (± 4 °C) was confirmed during the operation of the cell.

6.3.2.2 Gas Blower Heating System

During our first measurement using the above mentioned heating coil system, we observed unusual noise in XAFS measurements. The noise was found to be increased when the capillary was pressurised and heated to the reaction temperature which made it impossible to record good quality spectra. Due to the limited beam time and to solve the problem quickly as well as to explore different heating options, we replaced the coiled heating system by a hot air blower and could acquire good quality spectra. To find out the origin of the noise using temperature controller with coiled heating system, a careful study with various heating system configurations was

performed during the following beam time. The origin of the problem and the solution has been identified and they are described in detail in Section 6.3.5.

Figure 6.2 shows the image of *in situ* XAFS transmission micro-reactor cell mounted at CLÆSS beamline of ALBA synchrotron facility. The catalyst bed was heated by a hot air blower having a nozzle of 10 mm OD with a built-in temperature controller pointing from top of capillary as shown in Figure 6.2. The nozzle of the hot air blower was kept at the minimal distance to the capillary so as to keep the catalyst bed under a constant temperature zone. Two thermocouples were placed exactly below the capillary in order to measure the temperatures around the capillary. Homogeneous temperature at the outlet of the hot air blower has been confirmed with a few degrees fluctuation along the 10 mm OD of the nozzle. Similar quality spectra could be obtained by the coiled heating system (Figure 6.1) after identifying the problem for lower signal to noise (S/N) (Section 6.2.5), but the XAFS spectra using the gas blower heater are reported here.

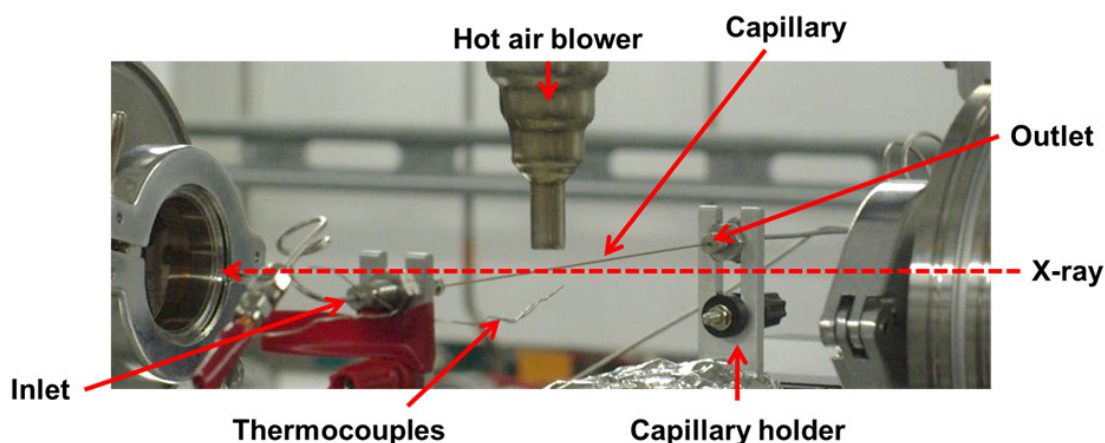


Figure 6.2 Image of fully assembled *in situ* XAFS transmission cell at CLÆSS beamline of ALBA synchrotron light facility.

6.2.4 CO₂ Hydrogenation Setup

Figure 6.3 shows the schematic diagram of the experimental setup for CO₂ hydrogenation used for *in situ* XAFS measurements. The experimental setup is simple and consists of a high pressure syringe pump (Teledyne Isco) which allows the compression of fluids up to 500 bar with pumping accuracy of 1 μL/min and was connected to the inlet of the capillary micro-reactor cell via 1/16" tubing. The outlet of the reactor was connected to an automatic back pressure regulator (BPR, Jasco BP-2080) which maintained constant pressure inside the cell. The outlet of BPR was connected to a mass spectrometer (Pfeiffer Vacuum, Omnistar) and to a vent system.

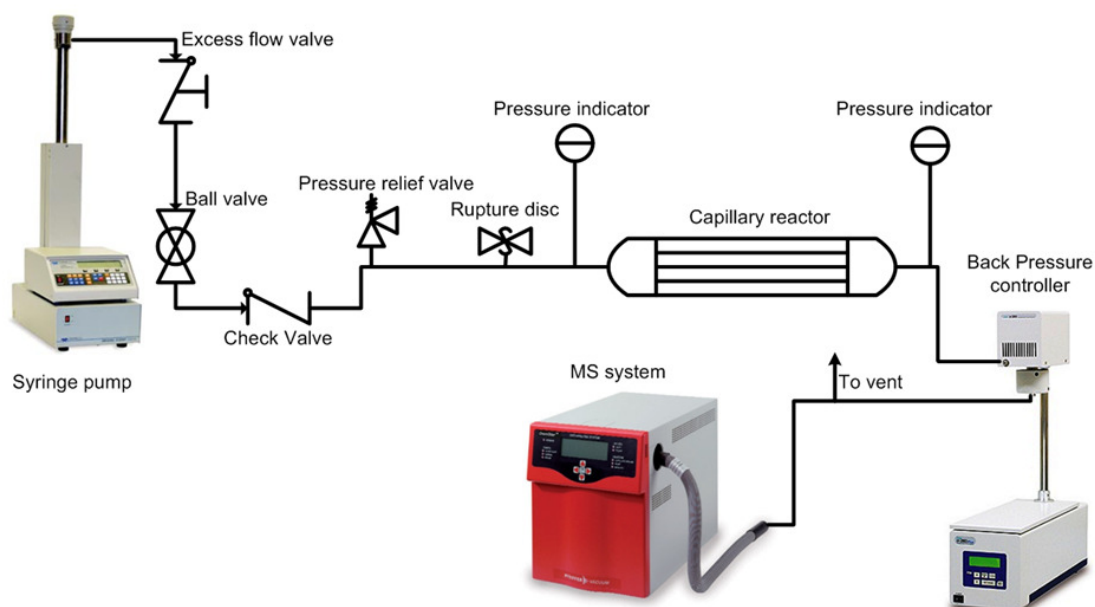


Figure 6.3 Schematic diagram of CO₂ hydrogenation reaction setup used at the synchrotron facility.

The syringe pump was filled with CO₂:H₂ = 1:3 gas mixture and was operated under a constant flow rate, while the desired pressure set point was defined by the BPR. The pressure difference between the catalyst bed was monitored by two pressure indicators connected at the inlet and outlet of the capillary as shown in Figure 6.3.

Digital pressure indicators were also built-in on syringe pump and on the BPR. Since the syringe pump was operated in the constant flow mode against the pressure held by BPR, an excess flow valve was installed between the syringe pump and cell. This excess flow valve prevents sudden release of gas from the pump caused by any major leakage in the downstream. Since safety is always of prime importance, the pressures were monitored and regulated remotely using a computer connected via wireless network and the fluid flow rate was set sufficiently low. Also, a pressure relief valve and a rupture disc were installed in the system, venting the gas properly to avoid any accumulated pressure exceeding our safety threshold.

6.2.4 Raman Spectroscopy

Raman spectra were recorded using B&W Tek dispersive i-Raman spectrometer equipped with a 532 nm excitation laser. The phase behaviour of CO₂ was studied by continuously passing CO₂ into the empty capillary at 0.2 mL/min at various pressure and temperature conditions so that the phase changes between the gas, liquid, and supercritical states took place. The Raman probe was fixed on a motorized x-y-z stage to facilitate the alignment of the laser focus inside the capillary with a submicron positioning accuracy. The heating was achieved by the hot gas blower fixed from the top of the capillary as shown in Figure 6.2.

6.3 Results and Discussion

6.3.1 Capillary Testing

Prior to XAFS experiments, we investigated the mechanical strength of the capillary reactor in a fume hood at our home laboratory under the identical experimental configuration. A capillary was filled with the catalyst and the micro-reactor cell was covered with a thick-wall plastic enclosure to make sure that broken pieces of capillary

are not thrown into air. After ensuring all the fittings are properly fastened, the capillary was slowly pressurized with a gas mixture of 8 % CO₂, 82 % H₂ and 10 % Ar at the flow rate of 1 mL/min on syringe pump. When the pressure reached 200 bar, the heating of capillary was initiated at the rate of 10 °C/min up to 280 °C using the coiled heating system. The capillary was gradually pressurized up to 300 bar under the constant temperature of 280 °C. No leakage at the capillary fittings and along the fluid transfer lines was observed. Furthermore, we continued to pressurize the capillary reactor up to 320 bar, at flow rate of 0.5 mL/min. The capillary was found to be intact at pressure of 320 bar and 280 °C with a pressure drop of ca. 4 bar over the catalyst bed even at the rather high flow-rate for the capillary. The choice of performing experiments at 200 bar was for safe operation of the capillary reactor while maintaining higher conversion levels of CO₂ (16-18).

6.3.2 *In Situ* XAFS Spectroscopy

Figure 6.4 shows the X-ray absorption near edge structure (XANES) spectra at the Cu K-edge during the pre-reduction of Cu/ZnO/Al₂O₃ catalyst. The catalyst was reduced during the temperature ramp from 25 to 260 °C using 5 % H₂/He gas mixture at flow rate of 4 μL/min at 70 bar. Due to the highly packed catalyst bed as well as the small inner diameter of the capillary, it was not possible to pass the gas at ambient pressure and therefore the pre-reduction was carried at 70 bar. The pre-edge spectra of the catalyst at 25 °C exhibited a weak absorption in the range of 8978-8980 eV (1s-3d transition), a shoulder at 8985 eV and a strong absorption at 8995 eV. These features indicate that the sample predominantly contains copper in Cu (II) form (19, 20). As the temperature increased up to 260 °C, a change in the oxidation state of copper was observed. The XANES spectrum after reduction at 260 °C was found to be very similar

to that of Cu foil thus to the Cu (0) state. In agreement with the study by Kim et al., copper in the catalyst was directly reduced to metallic copper without formation of an intermediate or sub-oxide (21).

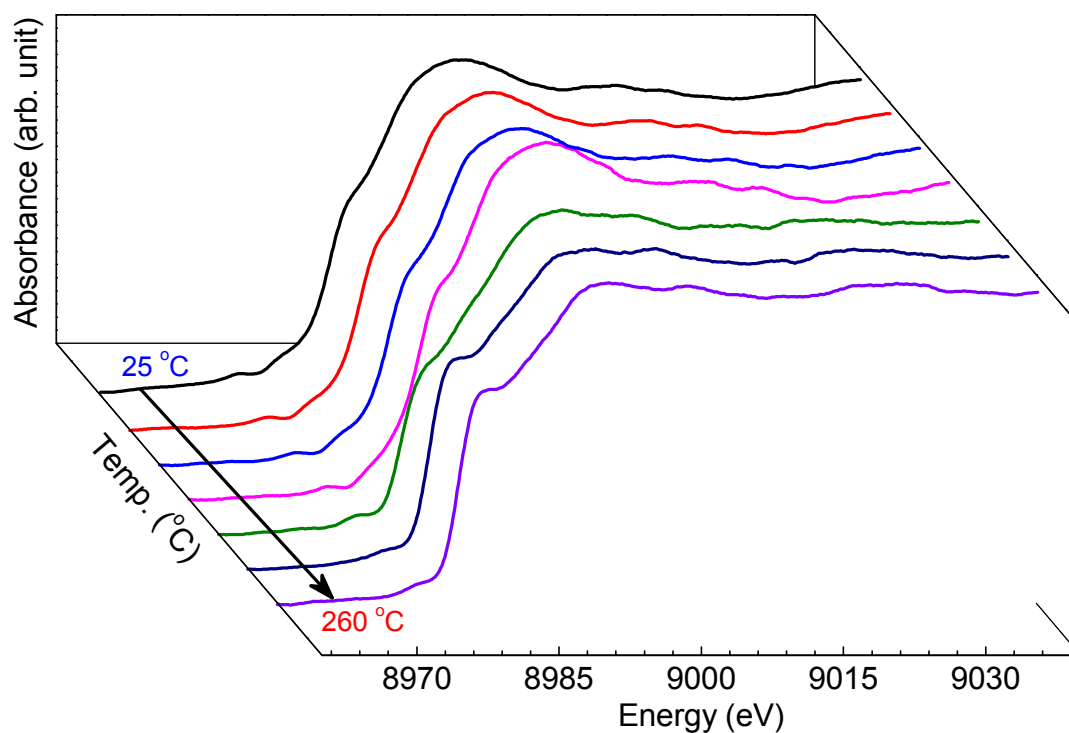


Figure 6.4 XANES spectra at the Cu K-edge of Cu/ZnO/Al₂O₃ catalyst during the pre-reduction at 70 bar under the flow of 5% H₂ in He.

After the pre-reduction of catalyst, the reactor was cooled down to room temperature and pressurised up to 200 bar in CO₂/H₂ gas mixture at CO₂:H₂ ratio of 1:3 and the flow rate of 2 μ L/min. Figure 6.5 presents the XANES spectra collected at three different reaction temperatures at 200 bar. The spectral quality was good, clearly showing that the copper remained in Cu (0) state under all the examined conditions. This is in good agreement with the study by Clausen et al. who reported that copper is present in the metallic state at 220 °C and 48 bar. (3) Our study extends the range of reaction conditions for this observation, up to 200 bar and 260 °C. It is important to mention that the reaction product, methanol and carbon monoxide, could be clearly

detected by mass spectrometry (data not shown) and we will discuss the performance of the capillary system as catalytic reactor in the next section.

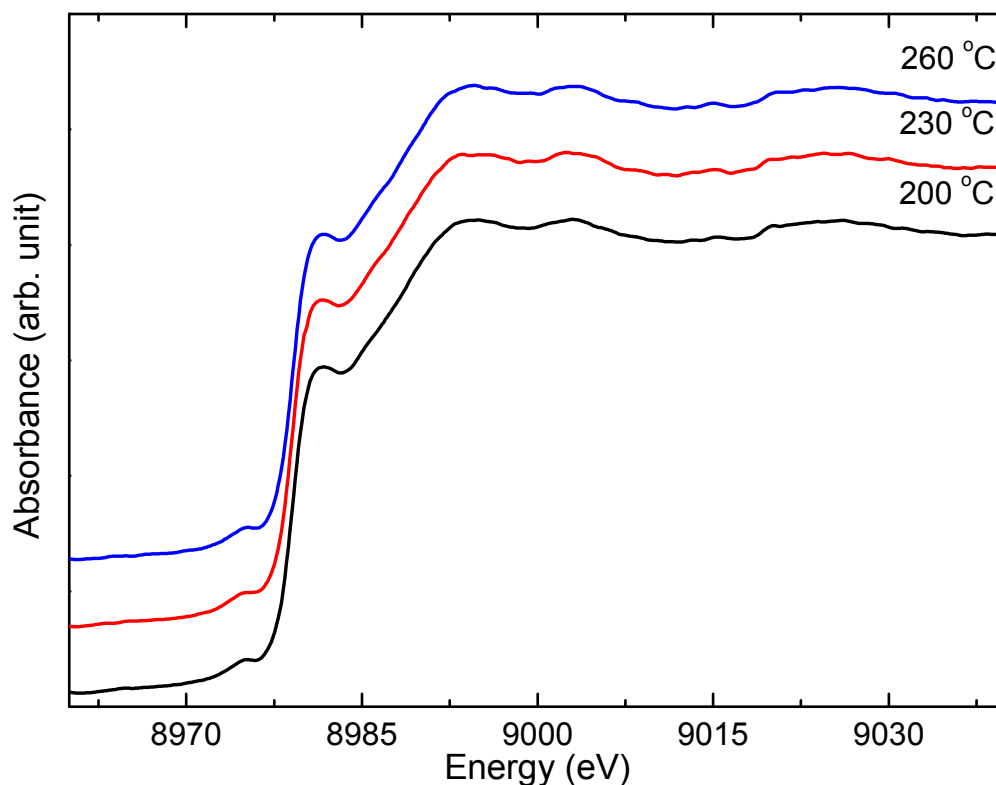


Figure 6.5 XANES spectra collected at three reaction temperatures over Cu/ZnO/Al₂O₃ catalyst at CO₂:H₂ = 1:3 and 200 bar.

6.3.3 Testing of the Capillary Reactor as a Fixed Bed Micro-Reactor

In order to mimic the experimental conditions of laboratory experiments at synchrotron light facilities towards *operando* studies, it is of critical importance to evaluate and compare the performance of the capillary reactor system in CO₂ hydrogenation against that of a laboratory reactor where flow patterns have been proven to be plug flow exhibiting reliable catalytic activities.

For this purpose, high pressure CO₂ hydrogenation was performed in the capillary packed-bed reactor with the coiled heating system (Figure 6.1). 10 mg of Cu/ZnO/Al₂O₃ catalyst was placed inside the capillary and pre-reduced in the stream of

90 % H₂/Ar mixture at 260 °C under pressure of 70 bar for 2 h. The catalyst bed was cooled down to room temperature and pressurized with CO₂:H₂ = 1:3 gas mixture up to 200 bar using the syringe pump. Then the temperature was raised to 260 °C maintaining the GHSV at 26000 h⁻¹ to perform CO₂ hydrogenation. To compare the catalytic performance, the reaction was performed in 1/8" OD laboratory micro-reactor tube (ID: 1.75 mm), maintaining the other experimental conditions identical. The detailed setup of this reactor and product analysis system are described in Chapter 2.

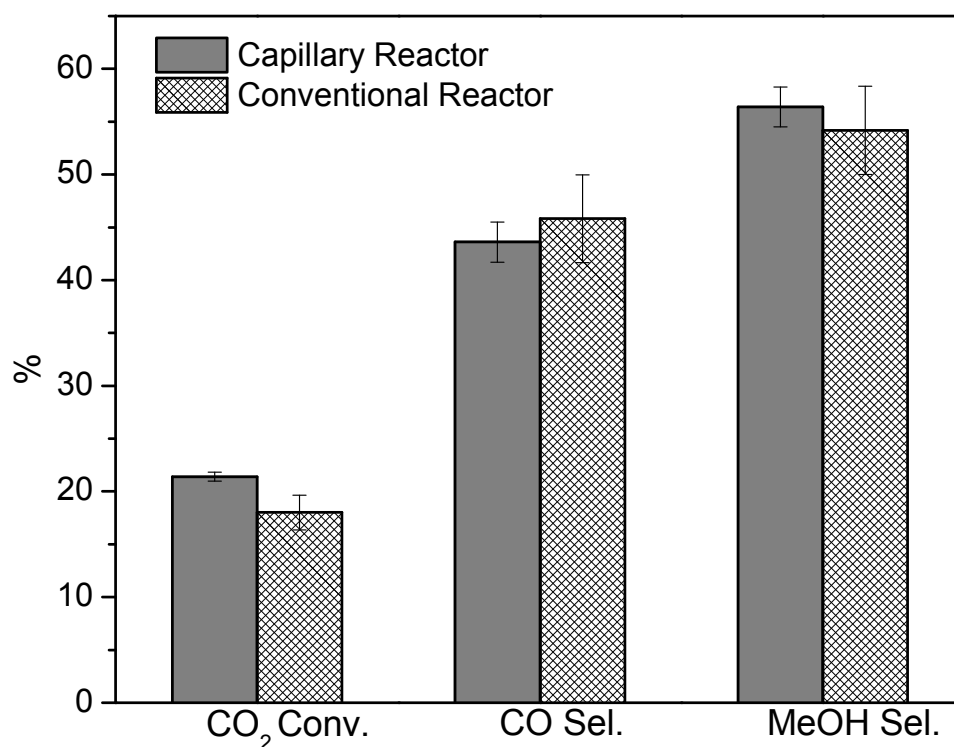


Figure 6.6 Catalytic performance in terms of CO₂ conversion and selectivities to CO and methanol (MeOH) in CO₂ hydrogenation using the capillary reactor and conventional micro-reactor (16) at T = 260 °C, P = 200 bar, CO₂:H₂ = 1:3, and GHSV = 26000 h⁻¹.

Figure 6.6 shows the catalytic performance of the Cu/ZnO/Al₂O₃ catalyst for CO₂ hydrogenation using the two reactors with comparable performance. CO₂ conversion of 18 % and selectivities to methanol and CO of 54.2 and 45.8 %, respectively, were obtained using the conventional reactor, while the capillary reactor achieved a CO₂ conversion of 21 % and selectivities to methanol and CO of 56.2 and 43.5 %, respectively.

respectively, were attained in the conventional micro-reactor. Similar levels of the product selectivities (methanol and CO selectivities were 65.4 and 43.6 %, respectively) were obtained using the capillary reactor at a similar, even a slightly higher level of CO₂ conversion (21.4 %). This slight increase might have been arising from the longer catalyst bed length which may increase the reactants contact time with the catalyst by their back-diffusion. The overall catalytic data was found to be in a very good agreement with the conventional micro-reactor system data and within the confidence limit of error values.

In addition, we calculated the axial dispersion and vessel dispersion number to predict the flow behaviour inside the capillary reactor at the tested reaction condition. The calculated values deviate only by 10 % from the ideal values for plug flow condition in the capillary reactor (22, 23), assuring that the capillary can be used as a reliable reactor at high pressure conditions.

6.3.4 Raman Study

Recently, the availability and versatility of combined, simultaneous multi-probe techniques such as XRD/XAFS-Raman have increased drastically due to their great advantages of complementary information often facilitating to gain deeper insights into chemical and structural states from various angles (24). In particular, Raman spectroscopy has become one of the most popular choices as an additional spectroscopic probe at synchrotron light facilities because of ease in its usage, rich chemical information on local environment and long range ordering and comparably little restrictions for measurements under elevated pressure and temperature. Therefore, it is of great value to evaluate the suitability of the capillary for Raman studies. The polyimide coating of the capillary can be removed by means of hot (ca. 95 °C)

concentrated H_2SO_4 or burning the polyimide coating in flame, rendering it optically transparent for Raman measurements, while maintaining mechanical strength for high pressure studies. Unfortunately, the $\text{Cu}/\text{ZnO}/\text{Al}_2\text{O}_3$ catalyst was not well suited for Raman measurements using the excitation lasers available to us (532 and 785 nm), hence we examined gas-liquid and gas-supercritical transitions of CO_2 at low and pressurized conditions up to 200 bar.

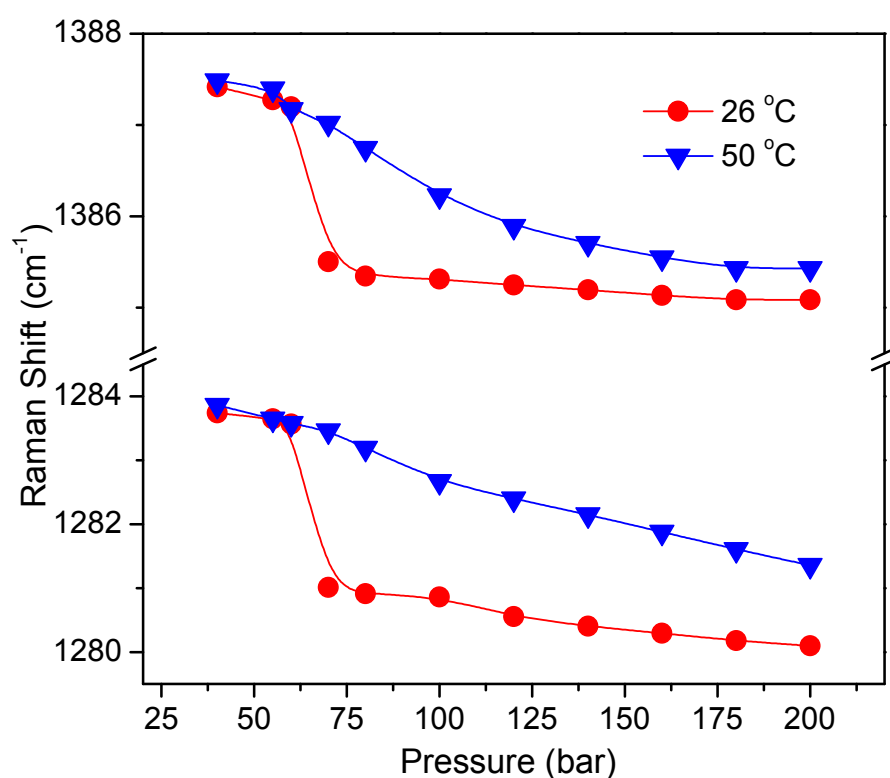


Figure 6.7 Pressure dependent Raman shift of the Fermi dyad band maxima of CO_2 at 26 and 50 °C

Raman spectra along the phase transition of CO_2 were recorded at two different temperatures (26 and 50 °C, the critical temperature of CO_2 is 31.1 °C); one below the critical temperature to observe gas to liquid phase transition and the other above it to observe gas to supercritical phase transitions. Figure 6.7 shows the pressure dependent Raman shift of the two major bands of CO_2 Fermi dyad at ca. 1284 and 1387 cm^{-1} at 40

bar (gas phase). Shifts of the Fermi dyad bands towards lower frequency were clearly observed at increased pressures. At 26 °C there was a sudden drop in their frequencies in the pressure range of 60-80 bar. Considering the critical pressure of CO₂ (74 bar) and the temperature below the critical one, the sudden frequency change can be ascribed to the great variations in intermolecular interactions in the pressure range due to the gas-liquid phase transition.

On the other hand, at 50 °C the frequency shifts of the band maxima were found to be smooth throughout the studied pressure range. This confirms a well-known continuous phase transition of CO₂ in this range from gas to supercritical phase. The observations obtained here are identical to the literature reports (25, 26) clearly demonstrating the feasibility of Raman study and phase behaviour analysis using the capillary micro-reactor cell. It is worth noting that, thanks to the efficient heating system and small volume, the phase behaviour measurements were performed very rapidly, merely taking one hour to complete all the measurements described above.

6.3.5 Effect of Heating Mode on EXAFS Signal

In order to identify the origin of the noise associated with the coiled heating system, several experiments were performed using two different heating modes, (i) a PID controller regulated mode and (ii) a constant current mode. In the former case the current applied to the coil via a tuned PID temperature controller to provide fine control over a set value whereas in the latter case a constant current was maintained in the coil to achieve the desired set value. Figure. 6.8 shows the temperature profiles obtained using the two modes at desired set point of 260 °C. It was observed that in both cases the deviation of the temperature from the set point was well within the acceptable range of ± 4 °C.

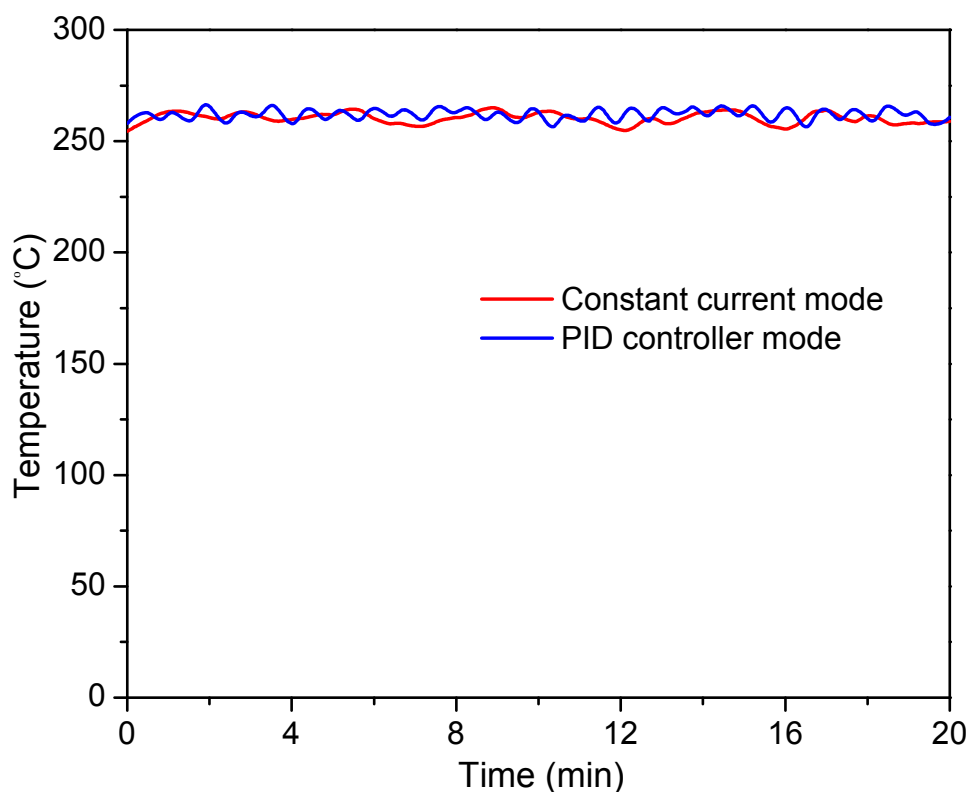


Figure 6.8 Temperature profiles with constant current mode and PID controller mode at the set point of 260 °C.

To reproduce the observed noise during the XAFS measurements with the coiled heating system, a capillary filled with the Cu/Zn/Al₂O₃ catalyst was pressurised up to 197 bar of CO₂ and the temperature of the coil was raised to the 260 °C using the PID temperature controller. For better visualisation of signal instability, the energy was fixed at 8993 eV and the signal intensity was monitored for a long time period. Careful inspection of the signal variations and the power supplied by the controller revealed that the instability in the signal is closely related to the variations in the power regulated by the PID controller and in the current through the coil. Curves (a) and (b) in Figure 6.9 show the variations at the fixed energy of 8993 eV using the constant current mode and the PID controller mode, respectively. In the PID controller mode, the signal intensity was found to be oscillating, at first sight, in response to the power regulated by the PID

controller (curve (c)). However, a closer look into the profiles of the power fluctuation (curve (c)) and also the signal fluctuation (curve (b)) shows a mismatch between the two oscillation frequencies and therefore uncorrelated nature between the two parameters. When a similar experiment was performed with constant current mode, it was observed that the signal (curve (a)) at the fixed energy was exceptionally stable over the measured period and free from signal variation. Clearly, the signal instability using PID controller was mainly caused by the discontinuous nature of the current through the coil and eventually by the variations in temperature. Actually, Figure 6.8 shows the deviation of temperature from the set point was well within the range of ± 4 °C using both heating modes.

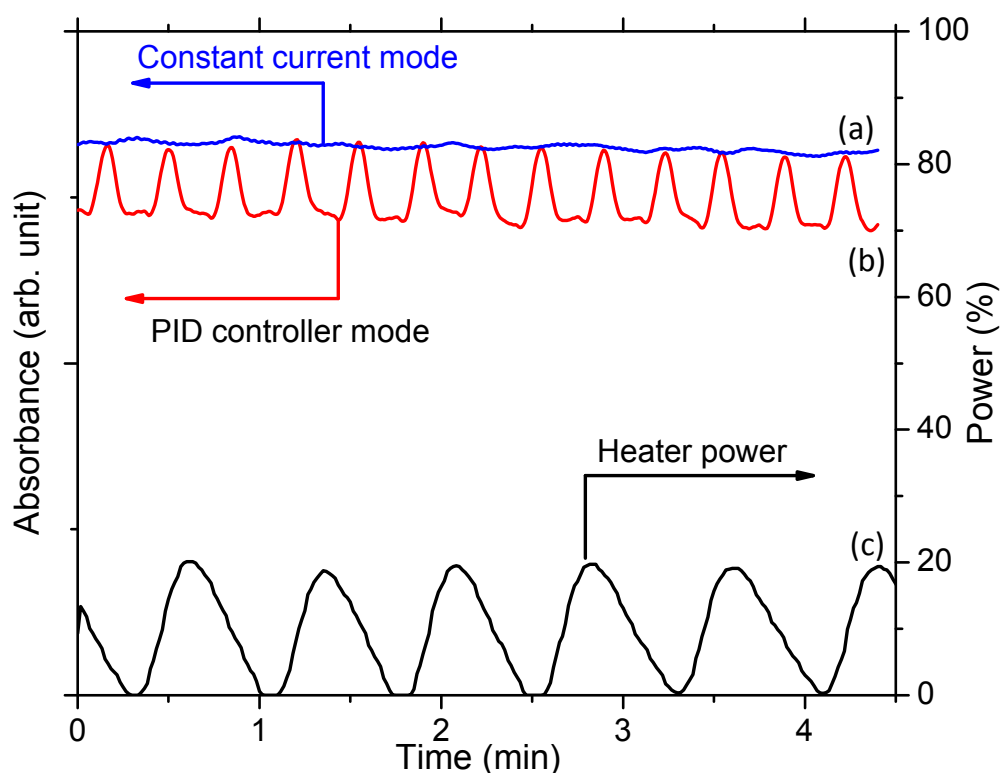


Figure 6.9 Temporal variation of signal intensity at the detector at 8993 eV at 260 °C using (a) constant current mode and (b) PID controller regulated mode. The profiles (c) shows the heater power output (%) using the PID regulation.

It was worth noting that in case of the PID controller regulated mode, the temperature followed a regular oscillating pattern at the same frequency as the power output fluctuation shown in Figure 6.9. This can be explained that, as soon as the temperature deviates from the set point, the PID controller responds to this change by applying or removing the power to the heater results in abrupt, however subtle change in the temperature generating small periodic oscillations in the signal. Whereas, in the constant current mode the temperature variations are dependent only on external parameters such as convection of heat to the surrounding or vice versa and hence more stable.

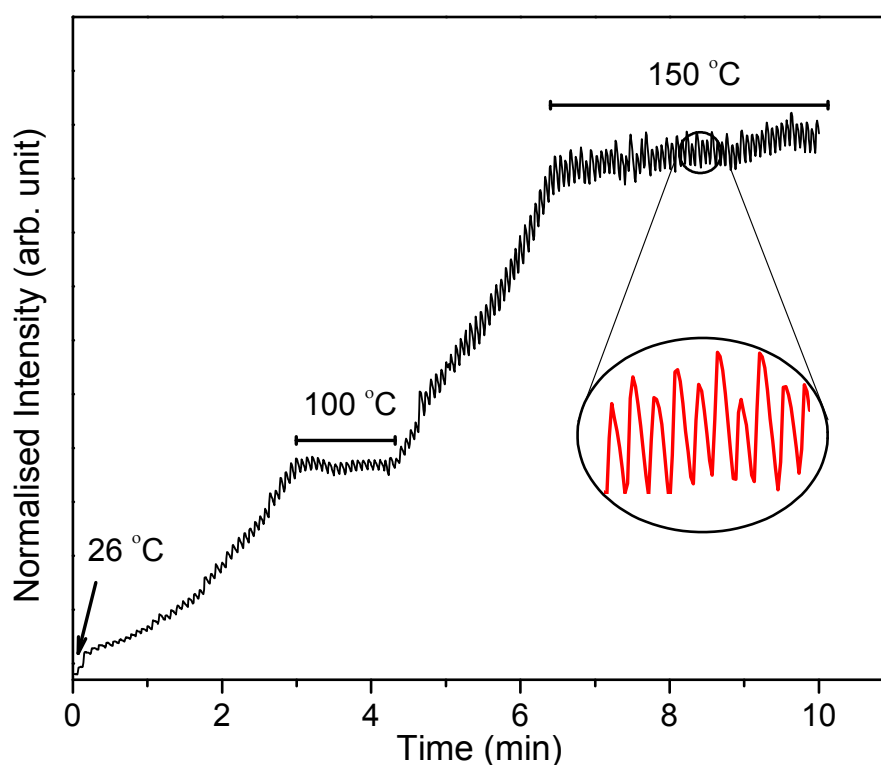


Figure 6.10 Effect of increase in temperature on the signal profile. The inset shows oscillating nature of signal identical to Figure 6.9 (b)

Instigated by the oscillation of temperature and signal intensity and (un)correlation between the two parameters, another experiment was performed to see

the effect of temperature on the signal stability. Figure 6.10 shows a continuous signal scan performed at a fixed energy of 8993 eV upon heating from ambient temperature to 150 °C. As soon as the temperature was increased to 100 °C, the signal level was found increasing. Further rise in temperature up to 150 °C resulted in further increase in the signal intensity. It is interesting to note that holding the temperature at a constant value stabilised the signal at the particular level. The inset in Figure 6.10 shows the magnified image of the signal at 150 °C. To our great surprise, it was found that the signal was composed of periodic oscillations identical to those shown in Figure 6.9 (b). These oscillations were present throughout the measured temperatures and found to be more pronounced at higher temperatures.

Although it was suggested that the signal level and its fluctuation are caused by the effect of temperature and that its fluctuation was induced by the PID regulation, it was not clear why and how it was happening. To understand the origin of signal fluctuations, a 2D X-ray camera was placed after the capillary to identify the causes for the changes in beam intensity. With this setup the capillary was heated up to 150 °C using the PID controller mode. Figure 6.11 shows the images taken by the X-ray camera at four different temperatures. Image (a) taken at room temperature shows that the beam is well focused onto the capillary and therefore the bright spot of the beam is hidden by the capillary and catalyst inside. Increasing the temperature to 80 °C (image (b)) resulted in the appearance of the beam spot from the downside of the capillary. This observation was more pronounced at 100 °C (image (c)) where more beam spot could be observed. Further increase in temperature up to 150 °C (image (d)) evidenced that the beam was almost out of the capillary. The position of the capillary actually changed relative to the encircled area which indicates the position of a square reference point on

the camera. This is a clear evidence that the capillary actually moved upwards as temperature was raised from 26 to 150 °C. Considering the positioning stability of the mounting stage and optical bench at synchrotron facility, bending of capillary by temperature effect can be the only explanation for this observation.

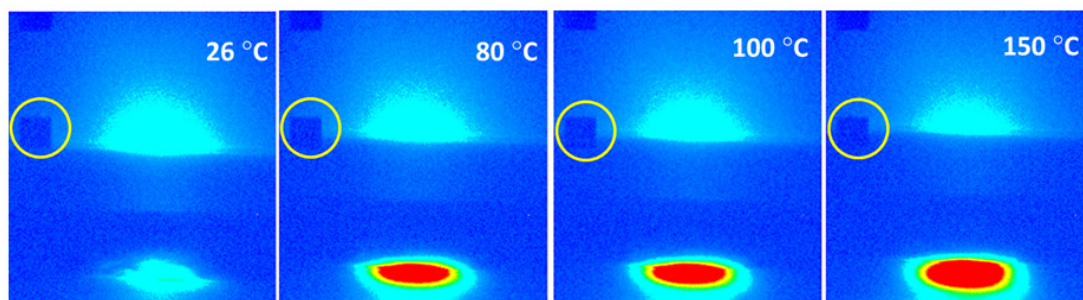


Figure 6.11 Movement of capillary with increase in temperature, (a) 26 °C, (b) 80 °C, (c) 100 °C, and (d) 150 °C. There was no pressure given in the capillary.

It is striking to observe the shift in capillary position induced by the temperature effect which can indeed explain the increased signal intensity as shown in Figure 6.10. Moreover, the 2D images were recorded continuously and quickly, and the signal brightness detected by the X-ray camera of each image was integrated to yield representative X-ray intensity at the detector at certain point in time. Fourier transform of this temporal profile of the X-ray intensity was analysed and it showed clearly one peak corresponding to the characteristic frequency of the small signal fluctuations shown in Figures 6.10. These results indicate that the capillary moves greatly by the large temperature change and the position gets stabilized; however, the capillary position is subject to smaller fluctuations. It should be reminded that the frequency of this small fluctuation of the detected signal was different from that of power output (Figure 6.9). The frequency of the small positional fluctuations seems determined by the characteristic frequency determined by the length of the capillary and the thermal effect

inducing capillary expansion and bending. The power fluctuation likely serves as the driving force for the movement but it does not determine the frequency at which the capillary oscillates. This is similar to playing the guitar where a force is given by the power given by finger, corresponding to the power fluctuation, while the pitch of the sound is determined by the length and strength of a string, corresponding to the length and the mechanical strength and/or expansion of the capillary.

Although the thermal expansion coefficient of fused silica is rather small, the expansion can become significant considering the dimensions of capillary (667 μm OD and ca. 15 cm length), especially in the direction along the capillary because of the much longer length with respect to the OD. The capillary was held firmly using fittings on the cell holder. When heated throughout its whole length, the only possibility for expansion is through the bending of the capillary. This also explains the good quality EXAFS spectra obtained when the gas blower mode was used, since the capillary was heated locally and the expansion occurred only for 1 cm of its length.

Use of the constant current mode to heat the coil can be a simple and economical solution to suppress the small positional fluctuation of the capillary, although the temperature of the capillary has to be measured and set manually. Focusing X-ray at stabilized temperatures allow recording good quality *in situ* spectra. Another option is to use a highly tuned PID controller which can supply constant current to maintain the desired temperature however this can be quite expensive and complex in nature.

6.4 Conclusions

This chapter describes a high pressure micro-reactor XAFS cell fabricated from the polyimide coated fused silica capillary. The XAFS cell was easy to assemble and handle and its operation was demonstrated up to 200 bar and 260 °C in methanol

synthesis by catalytic CO₂ hydrogenation. Due to the high pressure and effectively small flow rate of fluids in the cell, the action of plug flow reactor is assured. Under *operando* conditions good quality XAFS spectra were acquired. During the pre-reduction, the state of copper of the methanol synthesis catalyst changed from Cu (II) to Cu (0) directly without any intermediates. Under the high pressure reaction condition of methanol synthesis, the copper component remained in metallic state. Furthermore, the testing of this capillary cell as a fixed-bed micro-reactor for CO₂ hydrogenation reaction yielded reliable catalytic data, comparable to those obtained by a laboratory reactor system. Thermal expansion of the capillary materials can cause bending movements of the capillary and hence affecting signal to noise upon sample detection. Use of constant current mode and refocusing the X-ray beam spot at a measurement temperature allow stabilizing the capillary movement and recording high-quality XAFS spectra. Alternatively, hot gas blower can be used to record high quality spectra, although the sample heating will be local and most of material in the capillary remain cold and inactive. Also, the well-suitability of the capillary reactor for Raman studies has been demonstrated by monitoring CO₂ phase-transition between gas, liquid, and supercritical phases. These capabilities open up a wide range of possible applications at synchrotron light facilities for combined XAFS-Raman experiments under continuous-flow high pressure conditions.

References

1. D. C. Koningsberger, R. Prins, *X-ray absorption: Principles, applications, techniques of EXAFS, SEXAFS and XANES*. (1987), pp. 624.
2. Y. Iwasawa, Ed., *X-ray Absorption Fine Structure for Catalysts and Surfaces*, (World Scientific, Singapore, 1996).
3. B. S. Clausen, H. Topsøe, *Catal. Today*. **9**, 189 (1991).
4. J.-D. Grunwaldt, B. Clausen, *Top. Catal.* **18**, 37 (2002).

5. E. Kleymentov *et al.*, *Catal. Sci. Technol.* **2**, 373 (2012).
6. S. R. Bare, T. Ressler, in *Advances in Catalysis*, C. G. Bruce, K. Helmut, Eds. (Academic Press, 2009), vol. 52, pp. 339-465.
7. J. Als-Nielsen, G. Grübel, B. S. Clausen, *Nucl. Instrum. Methods Phys. Res., Sect. B* **97**, 522 (1995).
8. G. Sankar, J. M. Thomas, F. Rey, G. N. Greaves, *J. Chem. Soc., Chem. Commun.*, 2549 (1995).
9. G. Sankar, J. Thomas, *Top. Catal.* **8**, 1 (1999).
10. M. M. Hoffmann, J. G. Darab, S. M. Heald, C. R. Yonker, J. L. Fulton, *Chem. Geol.* **167**, 89 (2000).
11. B. S. Clausen *et al.*, *J. Catal.* **132**, 524 (1991).
12. S. L. Wallen *et al.*, *Rev. Sci. Instrum.* **67**, 2843 (1996).
13. J. D. Grunwaldt, M. Caravati, S. Hannemann, A. Baiker, *Phys. Chem. Chem. Phys.* **6**, 3037 (2004).
14. S. D. M. Jacques *et al.*, *Catal. Today.* **145**, 204 (2009).
15. J.-D. Grunwaldt, M. Caravati, M. Ramin, A. Baiker, *Catal. Lett.* **90**, 221 (2003).
16. A. Bansode, B. Tidona, P. R. von Rohr, A. Urakawa, *Catal. Sci. Technol.* **3**, 767 (2013).
17. A. Bansode, A. Urakawa, *J. Catal.* **309**, 66 (2014).
18. B. Tidona, C. Koppold, A. Bansode, A. Urakawa, P. Rudolf von Rohr, *J. Supercrit. Fluids* **78**, 70 (2013).
19. S. H. Liu, H. P. Wang, H. C. Wang, Y. W. Yang, *J. Electron. Spectrosc. Relat. Phenom.* **144–147**, 373 (2005).
20. L. S. Kau, K. O. Hodgson, E. I. Solomon, *J. Am. Chem. Soc.* **111**, 7103 (1989).
21. J. Y. Kim, J. A. Rodriguez, J. C. Hanson, A. I. Frenkel, P. L. Lee, *J. Am. Chem. Soc.* **125**, 10684 (2003).
22. O. Levenspiel, *Chemical reaction engineering*. (Wiley, New York, 1999).
23. D. Tang, A. Jess, X. Ren, B. Bluemich, S. Stapf, *Chem. Eng. Technol.* **27**, 866 (2004).
24. M. A. Newton, W. van Beek, *Chem. Soc. Rev* **39**, 4845 (2010).
25. M. I. Cabaco, S. Longelin, Y. Danten, M. Besnard, *J. Phys. Chem. A* **111**, 12966 (2007).
26. A. Urakawa, F. Trachsel, P. R. von Rohr, A. Baiker, *Analyst* **133**, 1352 (2008).

7

Summary and Outlook

7.1 Summary

A high pressure lab-scale micro-reactor setup for the continuous catalytic hydrogenation of CO₂ at pressures up to 400 bar was successfully designed and constructed, accomplishing the major task of the thesis. Instability in the hydrogen flow was removed by placing two pressure reducing regulators in series. The reaction product analysis was carried out by an online GC system equipped with two parallel detection channels. The GC method for product separation was successfully developed. The long stabilization time of the reactant concentration was mainly due the high reaction pressure and consequent low flow-rate conditions. In-house designed LabVIEW program facilitated the automation of the reactor system to monitor and control the critical parameters of the system remotely. The temperature and flow program feature in LabVIEW program allowed the scanning of various temperatures and flow-rates automatically for a given catalyst. Furthermore, the emergency shutdown function enabled unmanned and safe operation of reactor during the nights and over the weekends.

The reactor setup was used for high pressure CO₂ hydrogenation reaction. First, the impact of pressure and K, Ba promoters on impregnated Cu/Al₂O₃ catalyst in CO₂ hydrogenation reaction was investigated. As expected, reaction temperature had a drastic influence on catalytic performance. It has been demonstrated that low temperatures and high pressures are favourable conditions for methanol synthesis using

the Cu/Al₂O₃ catalyst prepared by the impregnation route of this thesis. The formation of DME over Cu/Al₂O₃ due to dehydration of methanol, mediated by the surface acidity of alumina, was greatly suppressed at 360 bar. This shows that increase in pressure strongly enhances the catalyst activity and it is likely that the amount of water formed as co-product is sufficiently high to inhibit the side dehydration reaction to DME. K and Ba promotion had great influence on selection of the CO₂ hydrogenation pathways. K and Ba promotion enhanced CO and methanol selectivity, respectively, the tendency being particularly prominent at lower temperatures. Promoter effects on the product distribution were found to be consistent with increase in pressure, where effect of K promoter was more prominent than Ba promoter. Both promoters efficiently hindered the formation of DME, which can be correlated with the neutralisation of alumina acidity by the promoters. Further increase in pressure to 360 bar resulted in the observation of good amount of methyl formate along with methanol for Cu-Ba/Al₂O₃, which was explained by the unique combination of the high methanol production and the modified surface acid-base property given by Ba promotion. Promoter effects on the surface species under reaction conditions have been clearly identified by *in situ* DRIFTS study. Both promoters were highly dispersed over the catalyst; the Ba component exists as small crystallites mainly on the alumina support but interacts strongly with Cu and promotes the reducibility of Cu, while the K component exists as nano-crystallites or thin layers covering the surfaces of both the alumina and copper. The high accessibility and enhanced reducibility of the Cu surface of the Ba promoted catalyst was beneficial for the formation of surface formates and further hydrogenation to methanol. On the other hand, for Cu-K/Al₂O₃ the Cu surface was covered by K promoter and the hydrogenation ability of Cu was hindered by the promotion. This effect and enhanced formation of surface formates on the alumina surface by the K promotion likely led to

enhanced probability of surface formate decomposition, as the major path for RWGS reaction.

The impact of high pressure and various reaction parameters was studied over coprecipitated Cu/ZnO/Al₂O₃ catalyst. The results obtained over coprecipitated Cu/ZnO/Al₂O₃ catalyst provides, efficient and highly productive processing strategy for CO₂ conversion at a single step. The high pressure approach using a conventional Cu/ZnO/Al₂O₃ methanol synthesis catalyst under specific reaction conditions for CO₂ hydrogenation remarkably boosted methanol selectivity and productivity by (i) the high H₂ partial pressure to enhance the reaction rate and (ii) thermodynamically favoured high CO₂ conversion and methanol selectivity at high pressure. The preliminary experiments with the commercial catalyst showed extraordinary high methanol productivity at very high GHSVs, possibly justifying the capital and manufacturing costs of high pressure processes. Negligible pressure drops under the examined GHSVs are the advantage of compressive reactants at high pressure. The consumed hydrogen was exclusively utilized for methanol formation at increased hydrogen partial pressure, thereby increasing the efficiency of the process towards methanol synthesis by suppressing chemical and thermal energy consumption for RWGS reaction. Moreover, the excess of hydrogen remaining in stream present under the optimal reaction condition reported in this thesis can be fed directly to another identical or multiples of high-pressure reactors with possible reduction in their sizes, so that compression of hydrogen may only require at initial stage whereas methanol productivity would be multiples of connected reactors. In such configurations, the recycling of H₂ can be minimized or potentially omitted.

The one step transformation of CO₂ to DME by the co-presence of the H-ZSM-5 catalyst was achieved under the optimised process conditions for methanol synthesis

reaction at high CO₂ conversion level. It has been demonstrated that the placement of solid acid catalyst (H-ZSM-5), either in physically mixed state with Cu/ZnO/Al₂O₃ (II) or in the separate reactor connected in series, does not affect the catalytic performance. Furthermore, the methanol-, water-, and H₂-rich, stream from the methanol synthesis reactor can be directly fed to the reactor containing the H-ZSM-5 catalyst and maintained at a higher temperature, and good selectivity to alkane or alkene was attained depending on the operating pressure of the secondary reactor. This encouraging result would instigate further development of CO₂ to olefins and/or gasoline processes via one step hydrogenation process.

A high pressure micro-reactor XAFS cell fabricated from the polyimide coated fused silica capillary has been developed for *in situ* monitoring of methanol synthesis catalyst. The demonstrated XAFS cell was easy to assemble and handle. Its operation was demonstrated up to 200 bar and 260 °C in methanol synthesis by catalytic CO₂ hydrogenation. Due to the high pressure and effectively small flow rate of fluids in the cell, the action of plug flow reactor is assured. Under *operando* conditions good quality XAFS spectra were acquired. During the pre-reduction, the state of copper of the methanol synthesis catalyst changed from Cu (II) to Cu (0) directly without any intermediates. Under the high pressure reaction condition of methanol synthesis, the copper component remained in metallic state. Furthermore, the testing of this capillary cell as a fixed-bed micro-reactor for CO₂ hydrogenation reaction yielded reliable catalytic data, comparable to those obtained by a laboratory reactor system. The well-suitability of the capillary reactor for Raman studies has been demonstrated by monitoring CO₂ phase-transition between gas, liquid, and supercritical phases. These capabilities open up a wide range of possible applications at synchrotron light facilities

for combined XAFS-Raman experiments under continuous-flow high pressure conditions.

7.2 Outlook

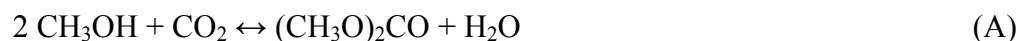
The thesis dealt with the use of high pressure (above 200 bar) in microreactor for the heterogeneously catalysed reactions. For the molecules such as CO₂, which are thermodynamically stable and difficult to activate under normal reaction conditions, this approach was found to be highly beneficial to achieve conversion up to equilibrium. Increasing the hydrogen partial pressure resulted in almost full one-pass CO₂ conversion to methanol. These results are highly important as CO₂ mitigation strategy as well as to utilise the carbon which is “lost” in CO₂. At first glance, one may assume that high pressure CO₂ hydrogenation is an energy demanding process, however as reported in recent literature, the demand of energy is mainly related to the production of hydrogen rather than operating pressure. From the amount of CO₂ which is being currently released to the atmosphere, its very clear that soon the decisive steps for lowering the CO₂ concentration have to be in place irrespective of all the constrains associated with the renewable energy cost for the sustainability of environment. Further, if hydrogen has been envisioned as a main energy carrier of the future fuels then this approach is extremely beneficial to overcome the limitation of transport and storage of hydrogen, by converting it into methanol. The obtained high space time yields of methanol over commercial methanol synthesis catalyst could justify the capital and operating costs for commercial plants considering the present market value of methanol. And there is no doubt that if the future of chemical energy carrier lies in “Methanol Economy” as proposed by George Olah then the demonstrated CO₂ processing strategy can be an integral part of it.

The design and operation of the high pressure plants are rather trivial and common tasks to the modern chemical industry. The first commercialised methanol synthesis process by BASF in 1923 was a high pressure process and for over the next 40 years the chemical industry had practiced it. Besides, over the years the technological advancement led the use of miniaturised devices which are less costly, at the same time highly productive. The use of microreactors for such high pressure hydrogenation reactions is advantageous in terms of safety as well capital cost. Further, the high-throughput reaction technology is proven to be extremely useful to operate high pressure microreactors with great efficiency and flexibility of the reactor operation.

The perspective presented in this thesis is based on the reductive conversion of carbon dioxide, where the cheap and abundant hydrogen sources are assumed to be readily available. Nevertheless, the demonstrated technology can be pursued effectively as of now, since the hydrogen cost could be justified with the higher production rates, although the major source of hydrogen still remain non-renewable. At present, this reductive conversion of carbon dioxide can be viewed as a future technology based on the hydrogen derived from the renewable energy sources.

Another approach is exploring non-reductive conversion of carbon dioxide into target compounds such as organic carbonates; particularly dimethyl carbonate (DMC). The interest in the production of DMC has been growing over the last decade due its several advantageous chemical characteristics. DMC is employed as electrolytes in lithium ion batteries and widely used as aprotic polar solvent (1). Owing to the high octane number, low RVP (Reid vapour pressure), reduced CO and NO_x emissions, DMC as a fuel additive has attracted much attention (2). In addition, DMC can act as methylating and carbonylating agent or as an intermediate in the production of higher carbonates, polyurethanes, isocyanates, and polycarbonates (3). It has been considered

as a promising chemical for greener chemistry processes by its use as a nontoxic substitute for dimethyl sulphate, dimethyl halides and phosgene (4). Currently, DMC is mainly obtained by oxidative carbonylation of methanol in gas- or liquid-phase processes using CuCl or CuCl₂ as catalyst (2). The major drawbacks of the phosgene processes are the high toxicity of phosgene and the disposal of the coproduced hydrogen chloride. The direct synthesis of DMC from methanol and CO₂ (reaction scheme A) is considered to be one of the most promising route for DMC production based on economical and ecological features as well as pathway for the transformation of carbon dioxide.



Both homogeneous and heterogeneous catalysts can catalyse this reaction (5), however due to the obvious advantages, heterogeneous catalysts are preferred. Among the metal oxides catalysts, ZrO₂ and CeO₂ were found to be active in this reaction (6-13), whereas among supported metal catalysts, mainly copper, ruthenium, and nickel are found to be active (14-16). The use of heteropolyacids and their salts as catalyst is also well documented (17-19). In addition to exploring the right catalyst, it is important to realize the thermodynamic equilibrium playing a decisive role in this reaction, typically limiting the reactant conversion much less than 1 %. According to the equation (A), it is necessary to remove water using an adequate drying (dehydrating) agent to boost the catalytic activity or to increase the CO₂ concentration by pressurizing CO₂. Potentially positive impacts of increasing the reaction pressure to achieve the equilibrium conversion have been clearly demonstrated in this thesis. Recently, Tomishige et al. reported catalytic results employing ceria as catalyst and 2-cynopyridine as drying agent for the direct synthesis of DMC from CO₂ and methanol in a batch system (20). The use of 2-cynopyridine as a dehydrating agent resulted in an excellent catalytic activity with

94 % DMC yield with 99 % selectivity. In the absence of dehydrating agents, the yield of DMC based on methanol reaches the equilibrium at a very early stage and is far from the performance considered satisfactory. However, almost all catalytic experiments using dehydrating agents have been carried out in liquid phase because of the batch operation under high pressure conditions. The major disadvantages of batch processes versus continuous flow processes are less control over the process variable, frequent catalyst recovery and associated costs. In a batch system, the reaction needs to be carried out for several hours to achieve the high catalytic activity which reduces the overall productivity against the continuous flow reactions. Furthermore, the longer reaction time could result in secondary reactions thereby reducing the desired product yield.

As a further outlook of possible advantages of high pressure processes, we made an effort to combine the use of dehydrating agent and of high pressure in continuous fixed bed microreactor for the direct synthesis of DMC over ceria from CO₂ and methanol. To enable the injection of methanol, an HPLC pump (Jasco, PU 2080) was connected at the point where CO₂ and H₂ were premixed. To begin with experiment, 300 mg of sieved (300-100 μm) ceria catalyst was charged into the reactor tube. The dehydrating agent, 2-cynopyridine(99 %, Aldrich), was dissolved in methanol (≥99.9 %, Aldrich) with the stoichiometric molar ratio of 1:2 to methanol. First, the reactor was pressurised with liquid CO₂ to the desired reaction pressure and then CO₂ (30 μl/min at 20°C) and methanol (10 μl/min at ambient temperature) were passed over the catalyst bed. For the product analysis, a hot trap (180 °C) was connected to the outlet of BPR where high boiling compounds (2-cynopyridine and 2- picolinamide) were trapped. Following the hot trap, the outlet stream was passed to a water cooled glass condenser (5 °C) filled with 2 mm glass beads to condense methanol and DMC. The collected

liquid products were separated using WCOT fused silica capillary column (BR-5ms, 30 m, i.d. 0.32 μm) connected to the FID channel of GC instrument (Bruker 450). For the analysis, ethanol was used as solvent and 1-hexanol was used as an internal standard. The error in the quantification of methanol and DMC due to the evaporation and condensation was found to be $\pm 10\%$. The product identification was confirmed by injecting the reaction sample on GC-MS (Bruker, Scion Q1).

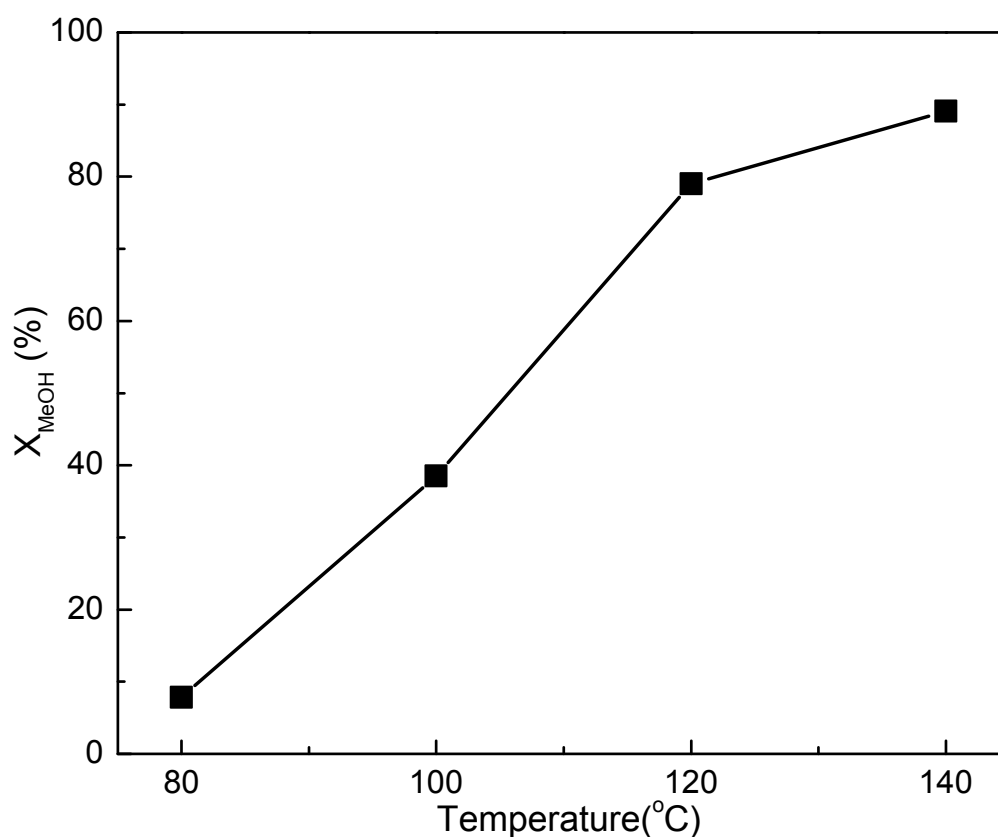


Figure 7.1. Effects of temperature on methanol conversion. Reaction conditions: 200 bar, MeOH:2-Cynopyridine = 1:2 (molar ratio), CO_2 (30 $\mu\text{l}/\text{min}$ at 20 $^\circ\text{C}$), methanol (10 $\mu\text{l}/\text{min}$), and CeO_2 (300 mg)

Figure 7.1 depicts the effect of temperature on methanol conversion at 200 bar pressure and in presence of 2-cynopyridine. With increase in reaction temperature methanol conversion drastically increased. The highest methanol conversion of 89 % was observed at 140 $^\circ\text{C}$, as compared to about 1 % in the absence of the dehydrating

agent. This value is by far the highest among all other reported conversion values over mixed oxide catalysts in direct DMC synthesis from methanol and CO₂ in continuous flow fixed bed reactor. It was striking to note that DMC was the only product formed during the reaction. The reported side-products in this reaction were found to be completely absent making this approach as a highly selective as well as productive due to the continuous flow. With the high conversion values it is clear that the reaction benefits from the enhanced pressure conditions and similar level of contact time could be achieved as that of in the batch system where reactions were performed for much longer duration (ca. 12 h).

The example introduced above shows that the high pressure approach gives new opportunities in heterogeneous catalysis and to investigate reactions in a continuous manner, which are generally performed in batch systems. This approach could form an important part of non-reductive CO₂ mitigation strategy where the CO₂ could be used effectively in the synthesis of valuable products. Finally, it should be remarked that for the effective utilisation of CO₂ into commercially vital chemicals, the use of high pressure and eventually the use of microreactor technology can be paramount.

References

1. A.-A. G. Shaikh, S. Sivaram, *Chem. Rev.* **96**, 951 (1996).
2. M. A. Pacheco, C. L. Marshall, *Energy Fuels* **11**, 2 (1997).
3. Y. Ono, *Catal. Today.* **35**, 15 (1997).
4. T. Sakakura, J.-C. Choi, H. Yasuda, *Chem. Rev.* **107**, 2365 (2007).
5. Y. Cao, H. Cheng, L. Ma, F. Liu, Z. Liu, *Catal. Surv. Asia.* **16**, 138 (2012).
6. K. Tomishige, T. Sakaihorii, Y. Ikeda, K. Fujimoto, *Catal. Lett.* **58**, 225 (1999).
7. K. Tomishige, Y. Furusawa, Y. Ikeda, M. Asadullah, K. Fujimoto, *Catal. Lett.* **76**, 71 (2001).
8. K. Tomishige, K. Kunimori, *Appl. Catal. A-Gen.* **237**, 103 (2002).
9. K. Jung, A. Bell, *Top. Catal.* **20**, 97 (2002).

10. K. T. Jung, A. T. Bell, *J. Catal.* **204**, 339 (2001).
11. H. Lee, S. Park, I. Song, J. Jung, *Catal. Lett.* **141**, 531 (2011).
12. Z.-F. Zhang, Z.-W. Liu, J. Lu, Z.-T. Liu, *Ind. Eng. Chem. Res.* **50**, 1981 (2011).
13. S. Xie, A. Bell, *Catal. Lett.* **70**, 137 (2000).
14. K. Almusaiter, *Catal. Commun.* **10**, 1127 (2009).
15. J. Bian *et al.*, *Chem. Eng. J.* **147**, 287 (2009).
16. X. L. Wu, Y. Z. Meng, M. Xiao, Y. X. Lu, *J. Mol. Catal. A: Chem* **249**, 93 (2006).
17. A. Aouissi, S. S. Al-Deyab, A. Al-Owais, A. Al-Amro, *Int. J. Mol. Sci.* **11**, 2770 (2010).
18. A. Aouissi, Z. A. Al-Othman, A. Al-Amro, *Int. J. Mol. Sci.* **11**, 1343 (2010).
19. A. Aouissi, A. Apblett, Z. Al-Othman, A. Al-Amro, *Transition Met. Chem.* **35**, 927 (2010).
20. M. Honda *et al.*, *ChemSusChem* **6**, 1341 (2013).

Appendix

A

Supplementary Information of Chapter 3

Table A.1 CO₂ conversion, selectivity, and yield for Cu/Al₂O₃ catalyst under different conditions of temperature and pressure at GHSV = 4000 h⁻¹, CO₂:H₂ = 1:3.8.

Temp. (°C)	Press. (bar)	Conv. (%)	Selectivity (%)				Yield (mg·g _{cat} ⁻¹ ·h ⁻¹)			
			CO	DMF	MeO	DME	CO	DMF	MeO	DME
170	4	0.5*	87.9	-	11.2	0.9	12.6	-	1.8	0.2
200	4	0.7*	64.7	-	14.8	20.5	12.7	-	3.3	6.6
230	4	2.2	73.9	-	10.5	15.6	43.2	-	7.0	15.0
260	4	4.0	86.1	-	6.0	7.9	92.2	-	7.4	13.9
280	4	7.6	92.0	-	3.9	4.0	185.8	-	9.0	13.3
170	30	0.7*	35.5	0.8	60.3	3.3	6.8	0.3	13.2	1.0
200	30	1.2	46.7	0.2	42.6	10.5	14.2	0.1	14.9	5.3
230	30	4.0	62.2	0.0	18.8	18.9	65.4	0.1	22.6	32.8
260	30	11.3	79.3	-	6.0	14.7	238.1	-	20.5	72.6
280	30	21.3	86.2	-	3.6	10.2	486.0	-	23.1	94.9
170	100	0.8*	15.9	2.1	80.0	2.1	3.4	1.0	19.5	0.7
200	100	2.4	45.3	0.7	46.2	7.8	29.9	0.9	33.7	8.2
230	100	12.1	76.6	0.1	11.9	11.4	245.7	0.8	43.5	60.1
260	100	16.3	85.2	-	4.5	10.3	368.5	-	22.2	73.2
280	100	22.4	83.6	-	3.0	13.4	495.2	-	20.1	130.9
170	360	3.6	26.9	3.1	69.5	0.5	25.3	6.2	75.0	0.8
200	360	8.4	60.1	2.0	37.3	0.6	121.5	8.6	103.4	2.0
230	360	13.1	85.6	0.2	13.4	0.7	297.9	1.8	53.4	4.2
260	360	20.3	92.7	0.1	5.7	1.6	497.5	0.6	35.2	13.8
280	360	29.6	91.7	0.0	4.5	3.8	718.2	0.6	39.9	48.7

“-“ signifies that no product was observed. The condition, where “*” is placed in CO₂ conversion, denotes that product concentration and/or CO₂ conversion are close to the detection limit

Table A.2 CO₂ conversion, selectivity, and yield for Cu-K/Al₂O₃ catalyst under different conditions of temperature and pressure at GHSV = 4000 h⁻¹, CO₂:H₂ = 1:3.8.

Temp. (°C)	Press. (bar)	Conv. (%)	Selectivity (%)				Yield (mg·g _{cat} ⁻¹ ·h ⁻¹)			
			CO	DMF	MeOH	DME	CO	DMF	MeOH	DME
170	4	0.4*	70.2	-	29.8	-	7.9	-	3.9	-
200	4	1.4	84.7	-	15.3	-	32.1	-	6.6	-
230	4	2.6	95.3	-	4.7	-	64.9	-	3.7	-
260	4	5.0	98.8	-	1.2	-	129.5	-	1.8	-
280	4	10.7	99.0	-	1.0	-	280.6	-	3.1	-
170	30	0.9*	75.2	-	24.8	-	17.5	-	6.6	-
200	30	2.2	89.2	-	10.8	-	52.2	-	7.3	-
230	30	4.2	97.4	-	2.6	-	107.3	-	3.3	-
260	30	10.3	98.1	-	1.9	-	268.5	-	5.8	-
280	30	13.7	99.0	-	1.0	-	357.9	-	4.3	-
170	100	1.7	94.8	-	5.2	-	42.0	-	2.7	-
200	100	3.6	95.8	-	4.2	-	91.3	-	4.6	-
230	100	7.4	97.2	-	2.8	-	191.1	-	6.3	-
260	100	14.1	99.0	-	1.0	-	367.9	-	4.4	-
280	100	20.7	99.1	-	0.9	-	543.0	-	5.5	-
170	360	2.2	91.7	-	8.3	-	52.2	-	5.4	-
200	360	8.9	95.9	-	4.1	-	225.5	-	11.0	-
230	360	14.9	98.5	-	1.5	-	387.5	-	6.9	-
260	360	22.8	98.5	-	1.5	-	595.0	-	10.6	-
280	360	28.6	97.9	-	2.1	-	739.6	-	18.2	-

“-“ signifies that no product was observed. The condition, where “*” is placed in CO₂ conversion, denotes that product concentration and/or CO₂ conversion are close to the detection limit

Table A.3 CO₂ conversion, selectivity, and yield for Cu-Ba/Al₂O₃ catalyst under different conditions of temperature and pressure at GHSV = 4000 h⁻¹, CO₂:H₂ = 1:3.8.

Temp. (°C)	Press. (bar)	Conv. (%)	Selectivity (%)				Yield (mg·g _{cat} ⁻¹ ·h ⁻¹)			
			CO	DMF	MeOH	DME	CO	DMF	MeOH	DME
170	4	0.1*	72.5	-	27.8	0.0	2.3	-	1.0	0.0
200	4	1.3	70.3	-	29.3	0.4	24.6	-	11.8	0.2
230	4	2.7	88.6	-	11.2	0.1	64.4	-	9.4	0.2
260	4	9.3	95.5	-	4.4	0.0	234.	-	12.6	0.2
280	4	16.2	98.1	-	1.9	0.0	419. 0	-	9.3	0.1
170	30	0.4*	22.4	0.5	77.1	0.0	2.5	0.1	9.8	0.0
200	30	1.6	36.4	0.4	62.8	0.0	15.2	0.3	30.0	0.3
230	30	4.7	69.6	0.1	29.7	0.0	87.1	0.2	42.5	1.2
260	30	11.8	89.6	0.0	10.0	0.0	279.	0.1	35.5	2.0
280	30	18.2	93.4	-	6.4	0.0	449. 0	0.0	35.0	1.9
170	100	0.6*	26.0	2.1	71.9	0.0	4.3	0.7	13.7	0.0
200	100	2.8	36.8	0.7	62.2	0.4	26.8	1.0	51.9	0.5
230	100	7.4	80.2	0.2	19.0	0.6	156.	0.7	42.4	2.0
260	100	17.1	92.9	0.1	6.5	0.5	420. ?	0.5	33.5	4.0
280	100	25.2	89.6	0.1	9.3	1.0	598. ?	1.1	70.7	11.4
170	360	1.7	17.4	10.3	72.3	0.0	7.8	9.9	37.1	0.0
200	360	4.3	38.3	4.3	57.2	0.1	43.4	10.5	74.1	0.2
230	360	12.4	84.0	0.9	15.1	0.2	274.	6.0	56.5	1.0
260	360	22.9	93.8	0.1	5.8	0.2	567. 0	1.6	40.2	2.4
280	360	33.7	95.4	0.1	4.1	0.4	850. 6 8	1.5	41.9	5.7

“-“ signifies that no product was observed. The condition, where “*” is placed in CO₂ conversion, denotes that product concentration and/or CO₂ conversion are close to the detection limit.

Appendix

B

Supplementary Information of Chapter 4

Table B.1

Table B.1 Effect of feed composition on CO₂ conversion, product selectivity and weight time yield at P = 360 bar, T = 260 °C and GHSV = 10,471 h⁻¹ over Cu/ZnO/Al₂O₃ (I) catalyst.

Feed Ratio CO ₂ :H ₂	CO ₂ Conv. (%)	Selectivity (%)			Yield (mg·g _{cat} ⁻¹ ·h ⁻¹)		
		CO	CH ₄	CH ₃ OH	CO	CH ₄	CH ₃ OH
1:12	96.2	1.1	0.1	98.8	9.8	0.4	1013.8
1:14	95.9	0.8	0.0	99.1	6.3	0.2	878.5
1:16	96.5	0.9	0.0	99.1	6.0	0.0	878.5
1:18	96.9	0.7	0.0	99.3	4.1	0.0	702.3
1:20	96.5	0.7	0.0	99.2	4.0	0.1	630.3

Table B.1 represents the effect of low CO₂/H₂ feed ratio on CO₂ hydrogenation reaction. Increase in the partial pressure of H₂ did not improve the CO₂ conversion. Methanol selectivity was found to be improved slightly and, as expected, an opposite trend was observed for CO selectivity. As mentioned in the main text, the methanol yield was found to be decreased at the smaller ratios, since the amount of CO₂ in the feed stream (i.e. CO₂ mass flow rate) was lowered. This shows that 1:10 feed ratio of

CO₂:H₂ is an optimum, with the high weight time yields of methanol together with the high CO₂ conversion and the high selectivity to methanol.

Figure B.1

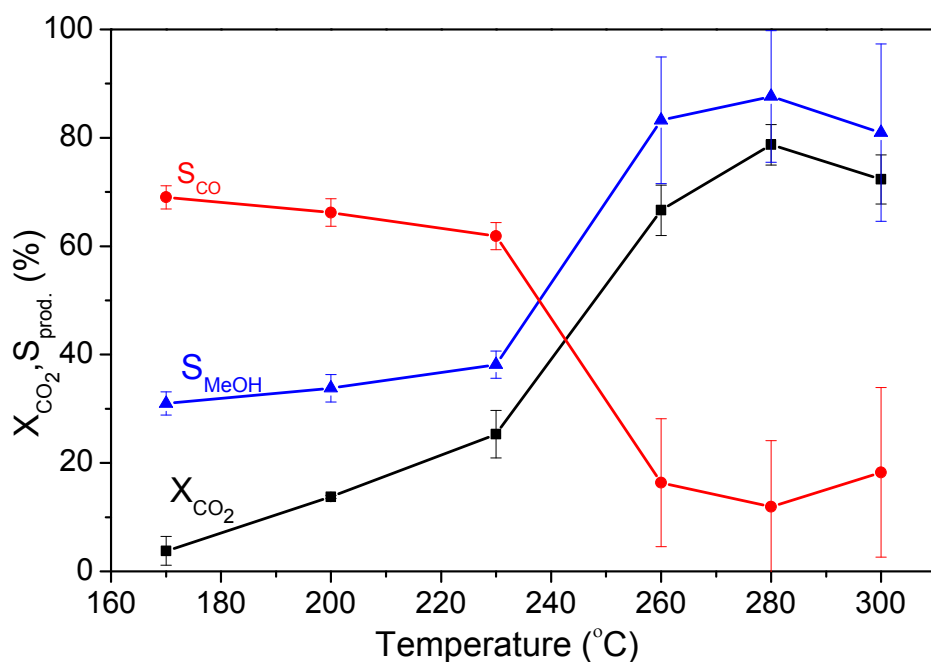


Figure B.1 Effect of temperature on CO₂ conversion (X_{CO_2}) and product selectivity in CO₂ hydrogenation reaction over the Cu/ZnO/Al₂O₃ (I) catalyst. Reaction conditions: P = 200 bar, GHSV = 10,471 h⁻¹, CO₂:H₂ = 1:10.

Figure B.1 shows the effect of temperature on catalytic performance at 200 bar, the CO₂:H₂ feed ratio of 1:10, and the GHSV of 10,471 h⁻¹. Starting from 170 °C, the rise in temperature greatly enhanced the CO₂ conversion, reaching a maximum of 79 % at 280 °C with good selectivity of 88 % towards methanol. Similar to the reaction at 360 bar, the methanol productivity, clearly visible from methanol selectivity and CO₂ conversion, increased with temperature and showed a maximum at 280 °C, slightly higher than that observed at 360 bar (the maximum at 260 °C, Figure 4.3). Under both 360 and 200 bar pressure conditions, the CO selectivity was found to be decreasing up

to certain temperature and above which it was observed to be increasing, implying the reaction path for methanol synthesis via CO. At 200 bar, the drastic change in the methanol productivity occurred between 230 and 260 °C, whereas such a change was prominent already at 170 °C at 360 bar.

List of Publications

Journal Publications

“Impact of K and Ba promoters on CO₂ hydrogenation over Cu/Al₂O₃ catalysts at high pressure”.

Atul Bansode, Bruno Tidona, Philipp Rudolf von Rohr and Atsushi Urakawa, *Catalysis Science & Technology*, **2013**, 3, 767.

“CO₂ hydrogenation to methanol at pressures up to 950 bar”

Bruno Tidona, Clemens Koppold, Atul Bansode, Atsushi Urakawa and Philipp Rudolf von Rohr, *The Journal of Supercritical Fluids*, **2013**, 78, 70.

“Towards full one-pass conversion of carbon dioxide to methanol and methanol-derived products”

Atul Bansode and Atsushi Urakawa, *Journal of Catalysis*, **2014**, 309, 66.

“High pressure, high temperature capillary cell for operando/in-situ X-ray absorption spectroscopy: Observation of methanol synthesis catalyst in catalytic CO₂ hydrogenation at 200 bar”

Atul Bansode, Gemma Guilera, Vera Cuartero, Laura Simonelli, Marta Avila and Atsushi Urakawa, *manuscript in preparation*.

Conference Contributions

“High pressure fixed bed micro-reactor for heterogeneously catalysed chemical reactions”

Atul Bansode, Bertram Kimmmerle and Atsushi Urakawa, Spanish Catalysis Society Conference, Zaragoza (**Spain**), Jul-2011

“Impact of high pressure and K and Ba promoters on CO₂ hydrogenation over Cu/Al₂O₃ catalysts”

Atul Bansode, Antonio Bazzo and Atsushi Urakawa, 15th International Congress on Catalysis, Munich (**Germany**), *Jul-2012*

“CO₂ hydrogenation to methanol at supercritical reaction conditions”

Bruno Tidona, Helena Reymond, Atul Bansode, Atsushi Urakawa and Philipp Rudolf von Rohr, 9th World Congress of Chemical Engineering, Seoul (**Korea**), *Aug-2013*

“Towards full one-pass conversion of CO₂ to methanol & methanol-derived products”

Atul Bansode and Atsushi Urakawa, International Conference on Hydrogen Production, Fukuoka (**Japan**), *FEB-2014*

“Towards full one-pass conversion of CO₂ to methanol & methanol-derived products”

Atul Bansode and Atsushi Urakawa, The Netherlands Catalysis and Chemistry Conference, Noordwijkerhout (**The Netherlands**), *Mar-2014*

Curriculum Vitae

Name	Atul Bansode
Date of Birth	7 th July 1984
Place of Birth	Wavarhire, Maharashtra, India
Nationality	Indian
2010-2014	Doctoral studies at the Institute of Chemical Research of Catalonia, Tarragona, Spain (Supervisor: Dr. Atsushi Urakawa)
2008-2010	Research Technician at Dow Chemical International Pvt. Ltd, Pune, India
2007-2008	Technical Service Officer at AsianPPG Industries, Pune, India
2006-2007	Project assistant at National Chemical Laboratory, Pune, India
2004-2006	M.Sc. study in Physical Chemistry at Department of Chemistry, University of Pune, India
2001-2004	B.Sc. study in Chemistry, T.C. College, Baramati University of Pune, India
1999-2001	Higher Secondary School Maharashtra State Board of Higher Secondary Education, India
1989-1999	Primary and Secondary School Maharashtra State Board of Primary and Secondary Education, India

